MINISTRY OF EDUCATION AND RESEARCH

"VALAHIA" UNIVERSITY OF TARGOVIŞTE

THE ANNALS
OF "VALAHIA" UNIVERSITY

SECTION SCIENCES

NR. 16
2006

SUMMARY

A. PHYSICS SECTION

B. CHEMISTRY SECTION

C. MATHEMATICS SECTION

A. PHYSICS SECTION

C. OROS[1]

S. JIPA[1],

R. SETNESCU[1]

T. ZAHARESCU[2]

CALCULATION OF TRAP DEPTH PARAMETERS FROM GLOW CURVES OF GAMMA IRRADIATED ALKALI HALIDES

[1]Valahia University, Faculty of Sciences and Arts, Carol I Av., Targoviste
[2] INCDIE, ICPE CA, 313 Splaiul Unirii, Bucharest

Abstract: Alkali halides polycrystalline powders, which were colored by high energy irradiation at room temperature display a tendency to thermoluminescence (TL). Several analysis methods were previously proposed [1 - 8] in order to obtain the parameters that characterize the electron traps formed during exposure. However, for these substances, there is considerable disagreement between the results reported by various authors regarding the activation energy of traps. It was, therefore, of special interest to focus the present work on the evaluation of the trap depth of gamma irradiated NaCl, NaI, KCl, KBr and KI.

Keywords: thermoluminescence, color centers, alkali halides

1. Experimental

The alkali halide samples were of analytical grade purity. Before the start of high energy exposure, the studied salts were freshly powdered at room temperature. The samples were gamma irradiated at room temperature at a dose rate of 0.4 kG/h. for irradiation a ^{137}Cs GAMMATOR M-38-2 (USA) equipment was employed.

The glow curves recorded using a laboratory-made Chemiluminograph OL-94 with linear heating rate of 0.7 ^{0}C/s [8].

2. Results and discussion

The color centers of F type form the most important lattice defects in the irradiated alkali halides. They are defined as halide ion vacancies, which have captured an electron. The observed colours due to the presence of F center induced by gamma irradiation are as follows: yellow (NaCl), brown (NaI), magenta (KCl), blue (KBr) and blue-green (KI).

The thermoluminescence phenomenon is known to be due to radiative recombination of thermally released electrons by trapping levels with holes bound to luminescent centers.

Figures 1 and 2 show the glow curves for the studied halides. These samples had been exposed to a dose of 0.8 kGy of 137Cs gamma rays prior the recording of the glow curve. As it can be seen, the NaCl samples presents a glow curve with two peaks located at 78^{0}C and 180^{0}C, while KBr samples show glow curves with a large peak al 87^{0}C and 52^{0}C,

respectively. NaI sample exhibits a glow curve with three peaks placed at 76^{0}C, 118^{0}C and 128^{0}C, while a single peak (at 71^{0}C) glow curve has been evidenced for KI.

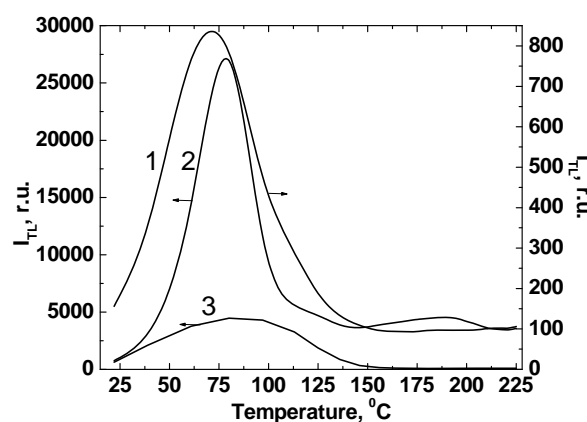**Figure 1**. Thermoluminescence glow curves of γ-irradiated NaCl (1), KCl (2) and KBr (3).
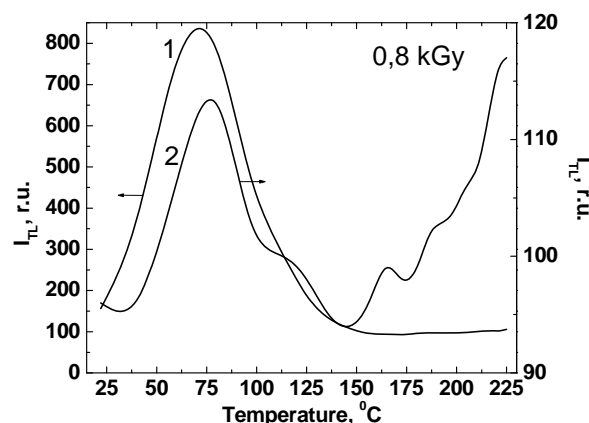

Figure 2. Thermoluminescence glow curves of γ-irradiated KI (1), NaI (2).

TL signals were not observed, when γ-irradiated samples were heated again in the same temperature range after the registration of the above-mentioned glow curves.

The thermal activation energy (E) for emission of thermoluminescence is equivalent to the energy needed to release the charge carriers from the involved trapping levels. For the determination of the trap depth starting from the experimental glow curves, it was necessary to establish firstly the kinetic order of the thermostimulated recombination of the opposite charge carriers. For this purpose, the geometrical factor (μ'_g) method [10] has been used. According to this method, the μ'_g parameter can be obtained by the relation:

$$\mu'_g = \frac{T_2 - T_m}{T_2 - T_1} \qquad (1)$$

where T_m is the temperature of the maximum emission intensity, whereas T_1 and T_2 are the temperatures for which the intensity reaches half of its maximum value at the ascending and descending parts of the peak, respectively.

On this way, we obtained for all samples μ'_g parameters larger than 0.42, which denotes the second order process [10].

For the determination of the trap depth, the methods depending on both shape of the curve and T_m has been used.

For the second order kinetics, Lushchik [11] has shown that E is given by the equation (2):

$$E = \frac{2.K.T_m^2}{T_2 - T_m} \qquad (2)$$

The above formula was empirically modified by Chen [12] by multiplying of 0.853 times for the second order kinetics. This yields activation energy with better accuracy.

Very closed results from this paper to the data reported earlier by Kelly and Laubitz [13] confirm the accuracy of our determinations. For the second order kinetics, they proposed the following equation:

$$E = 1.762 \frac{k.T_m.T_1}{T_2 - T_m} \qquad (3)$$

The method suggested by Chen [12] for determination of activation energy required for recombination according to the second order kinetics is given by:

$$E = 3.54 \frac{k.T_m^2}{T_2 - T_1} - 2.k.T_m \qquad (4)$$

In this equation, the numerical constants are chosen empirically to give a good estimation of activation energy.

The obtained values of the trap depth calculated by the above mentioned methods are given in table 1.

Table 1. The trap depth for the prominent glow peaks of the studied alkali halides, evaluated from the second order kinetics

Method and references	Activation energy, E (eV)				
	NaCl	KCl	KBr	KI	NaI
Lushchik [11]	1.18	0.47	0.62	0.75	0.87
Lushchik modified by Chen [12]	1.01	0.40	0.53	0.64	0.74
Kelly-Laubitz [13]	0.98	0.38	0.48	0.61	0.72
Chen [12]	0.95	0.43	0.43	0.61	0.73
Mean	1.03	0.73	0.52	0.65	0.77

The experimental results described in the present paper show a relative good agreement between the activation energies determined by several methods based on the symmetry of glow curve and T_m. The intensity of the prominent glow peak for NaCl, KBr and KI was plotted against the radiation dose and the resulting graph (figure 3) is convex upward.
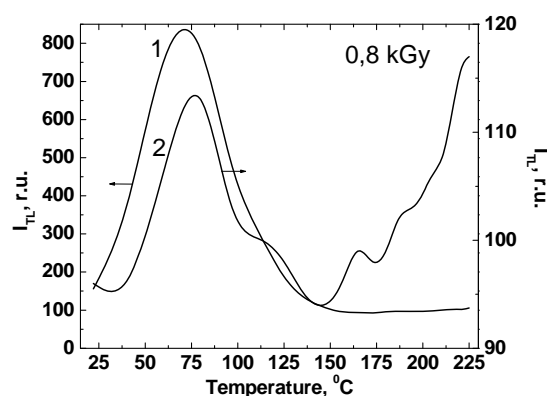
Figure 3. Dependence of TL intensity on γ-radiation dose for NaCl (1), KI (2) and KBr (3).

From this graph it is apparent that even at the largest radiation dose, thermoluminescence saturation is nor reached, It is calculated that γ-radiation causes the filling of electron traps, but it does not create new traps. According to Kristianpoller and collaborators [14] the first order kinetics is characterized by a strictly linear dose dependence of glow peak intensity.

For all the examined alkali halides, the probability for retrapping was found to be larger in comparison with the probability of recombination, which is equivalent to a second order process. One possible mechanism consists of the thermal activation of an electron from a trap to the conduction band followed by its retrapping before combination with a hole resulting in the emission of light (figure 4).

Figure 4. TL model for γ-irradiated alkali halides.
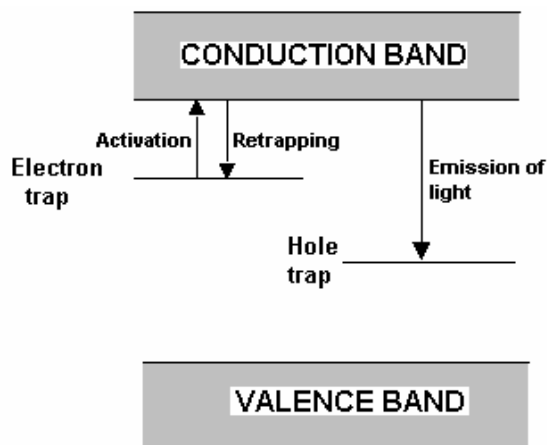
The utility of thermoluminescence studies on the behaviour of ionic crystals under high energy irradiation has generates an extension of investigation areas to other procedures based on luminescence emission. The lyoluminescence (LL) method became an alternative way in the studying of γ-induced defects in ionic crystals [15].

3. Conclusion

The present paper studies the formation and the existence of color centers during high energy irradiation in five alkali halides. It may be remark:

- the recombination kinetics of charge carriers follows the second order law;
- the trap depth were evaluated using different calculation methods based on the shape of glow curves;

.

- the TL intensity was studied as function of irradiation dose emphasizing the occurring of retrapping phenomenon.

References

1. SHALGAOKAR, C. S., NARLIKAR, A. V., J. Mater. Sci., **7**, 1972, p. 1465.
2. KANTOROVICH, L. N., LIVSHICZ, A. I. FOGEL, G. M., J. Phys.-Condensed Matter, **5**, 1993, 7503.
3. LIN, S. W., WENG, P. S., Appl. Rad. Isotop. **46**, 1995, 1369.
4. RASHEEDY, M. S., J. Phys.-Condensed Matter, **8**, 1996, 1291.
5. RASHEEDY, M. S., Japan. J. Appl. Phys. Part 1, **35**, 1996, 634.
6. SINGH, W. S., SINGH, S. D., MAZUMDAR, P. S., J. Phys.-Condensed Matter, **10**, 1998, 4937.
7. FURETTA, C., Riv. Nuovo Cim., **21**, 1998, 1.
8. FURETTA, C., J. Mater. Sci., **39**, 2004, 1.
9. JIPA, S., CONSTANTINESCU, V., SETNESCU, R., SETNESCU, T., Roum. Patent 110367/1996.
10. HALPERIN, A., BRANER, A. A., Phys. Rev., **117**, 1960, 408.
11. LUSHCHIK, C. B., Dokl. Akad. Nauk. SSSR, **101**, 1955, 641.
12. CHEN, R., J. Appl. Phys., **40**, 1969, 570.
13. KELLY, P. J., LAUBITZ, M. J., Can. J. Phys. **45**, 1967, 311.
14. KRISTIANPOLLER, N., CHEN, R., ISRAELI, M., J. Phys. D: Appl. Phys., **7**, 1974, 1063.
15. JIPA, S., MIHALCEA, I., KAPPEL, W., ZAHARESCU, T., SETNESCU, R., Revista de Chimie, in press.

DAN GABRIEL GHIŢĂ*
CONSTANTIN GHIŢĂ**

A UNIQUENESS RESULT FOR A NONLINEAR PROBLEM OF PLASMA PHYSICS

*National Institute of Physics and Nuclear Engineering, Bucharest
** Valahia University, Targoviste

Abstract:We give a variational problem on a Sobolev space to a problem of eingevalue for a magnetic flux, characteriying the gvasi-static equilibrium of plasma. We obtain the existence and regularity results, of a weak solution. Topological arguments – topological degree, ensure the control o f a unique solution depending on a parameter – magnetic permeability of a total ionized gas and on the eigenvalue of an associate Dirichlet problem. The control on a technological parameter to the process initiation ensures equilibrum stabilization functionality of the machine.

1. Introduction

In a technological process of producing a plasma jet inside a burner and confined on the median axis of the burning chamber, according to a nonlinear mathematical model of quasi-static equilibrium of the jet, it is introduced a state function of metallic plasma-vacuum-chamber. We consider the system state function to characterize the domain stability occupied by the ionized gas jet. We will indicate the magnitude and the direction of the magnetic field induction, applied in addition to confine the jet on the median direction of the burner chamber towards the ejection hole. The equations that we study, in a general context of the finite dimensional Euclidean spaces, generalize the MHD equations of a process of producing and stabilization of the plasma field in a tri dimensional chamber.

A parameter, with technological signification which characterizes magnetic permeability of total ionized gas, allows the stating of an eigenvalue problem for an elliptic operator, defined by a magnetic flux potential. The variational formulation on a *Sobolev* space of the nonlinear problem, which governs the phenomenon and topological arguments, ensures the existence results and the smoothness of the solutions [3], even uniqueness in the case of satisfying the quasi linear conditions. For similar problems we refer to [1], [5], [10]. Other results on the solution existence for some problems in plasma physics are found in [3], [7], [10], [12], [19], the regularity results of the solution in [8], [18], of non uniqueness in [14], [15], [16], of uniqueness [4].

The structure of the work is organized as follows: in the first section it is introduced the nonlinear problem of the quasi-static equilibrium of plasma and the conditions for the general state function, having a polynomial asymptotic behavior. Various formulations: variational and critical point problems allow the identification of some weak solutions with classical solutions. The second and the last section cover the study of a uniqueness general result, concerning a quasi-linear behavior of the state function, controlled by the bound of a technological parameter according to the first two eigenvalue for a certain Dirichlet problem, associated to the elliptic operator of the plasma jet equilibrium problem.

From the previous papers: Technological model, existence and regularity results.
2. Technological premises adapted to a stability study of plasma jet. For the elaboration of the steel in an electric arc furnace the heat exchange is made by the *Joule* effect, less through radiation and convection, which creates a deficiency in the process, through uneven heating in areas of interior surface, with consequences in refracting material erosion of the wall. The plasma burner is a device which produce a hot gas, totally ionized, the jet geometry depending on the electric potential, on the current discharge, on the pressure and the working gas flux, the discharge chamber geometry, the ejection hole size. Simplistically, a burner has the following components: the burner head, the isolator and the burner body with electrode. The head and the body of the plasmatron are made of cupper with cooling chamber and the electrode is made of wolfram. It is applied a potential difference by connecting the burner body to the cathode and the head to the anode, so that between the electrode and the burner head it is formed an electric arc. The heat in the arc is transferred to the plasma gas and the totally ionized gas jet is stabilized in the auxiliary magnetic field.
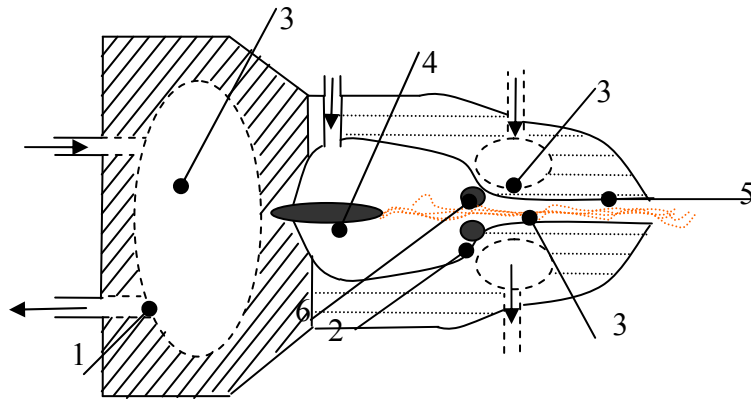
Figure 1
Schema of Plasmatron

1- body, 2- head, 3- cooling chamber, 4- electrode, 5- jet
6 anodic ring.

The plasmatron used in the technology of metal melting ensures the heat transfer from the plasma jet to the metallic load by radiation and a small part dissipated in the anode area of the equipment by conduction. For a homogeneous irradiation of the metallic bath, in the ceiling of the electric furnace are placed three plasmatrons at 120^0, each of them producing a jet of 500 to 1400 mm length, which completely covers by spreading the loading surface. The control of the functioning process, with the possibility of changing the power level, without the interruption danger, due to the confined plasma flow self maintained, is governed by the modification of the radiation parameter while the metal is melted.
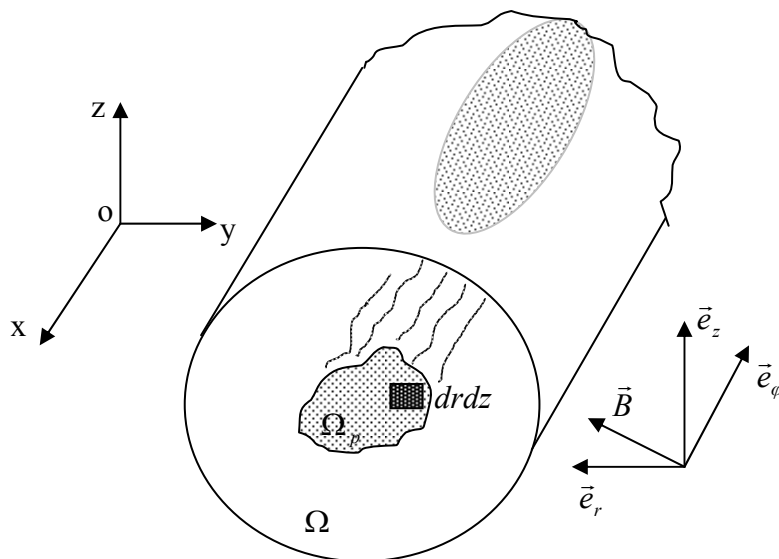
Fig. 2 Cartesian *system of reference placed locally at the conjunction of the chamber with the ejection hole*

From the mathematical point of view, we are interested in the stability of the ionized gas jet on the median line, controlling a magnetic field potential. The equipotential surfaces of the magnetic induction field $\vec{B}$, include the free boundary surface of the plasma jet and also the chamber surface, which allows the control of the jet confinement.

There are made simplified hypotheses on the phenomenon occurrence: the inertial forces, the hydrodynamic pressure of the ionized gas are neglected in contrast to the electromagnetic pressure p, which develops in plasma.

It is considered the electromagnetic forces field, perpendicular to the magnetic induction field $\vec{B}$ and to the electric current $\vec{j}$, $\vec{f} = grad p = \dfrac{1}{C} \vec{j} \times \vec{B}$.

An electromagnetic force variation from the surface $p = ct.$ to the surface $p + dp = ct.$ indicates the direction $\vec{e}_r$, that is $\vec{e}_r = \dfrac{grad p}{\|grad p\|}$, as direction of the force field. The direction of the magnetic induction field defines $\vec{e}_z$ and $\vec{e}_\varphi = \vec{e}_r \times \vec{e}_z$.

In our reference system, the process of production, of stability and plasma flow present a translation invariant along the plasma jet. We keep in mind the equations of the electromagnetic field disturbed by plasma,

$$- grad p + \frac{1}{4\pi} rot \vec{B} \times \vec{B} = 0, \quad div \vec{B} = 0,$$

$rot \vec{B} = \dfrac{4\pi}{C} \vec{j}, \quad div \vec{j} = 0$.

The equipotential surface, on which the field $\vec{B}$ is tangent, has the equation $\dfrac{dx}{B_x} = \dfrac{dy}{B_y} = \dfrac{dz}{B_z}$.

We realize the vector product of the field $\vec{f}$ with $\vec{B}$, on the left $\vec{B} \times \vec{f} = \vec{B} \times grad p =$ $\dfrac{1}{C} \vec{B} \times (\vec{j} \times \vec{B}) + \dfrac{1}{C} \left(-(\vec{B}.\vec{j})\vec{B} + |\vec{B}|^2 \vec{j}\right)$, from here

$$\vec{j} = \frac{C}{B^2}(\vec{B} \times grad p) + \frac{1}{B^2}(\vec{B}.\vec{j})\vec{B}$$

$$= \frac{C}{B^2}(\vec{B} \times grad p) + + \frac{1}{4\pi}(\vec{B}.rot \vec{B})\vec{B},$$

expression which will be used on the calculation of the total current which crosses Ω. We keep in mind that $\vec{B}$ is a field in the plan $(\vec{e}_r, \vec{e}_z)$ and the plan $(\vec{e}_r, \vec{e}_z)$ determines the transversal section Ω. The position of the field $\vec{B}$ referred to the system $(\vec{e}_r, \vec{e}_\varphi, \vec{e}_z)$ leads to the relation $\vec{B}.(d\vec{e}_r \times d\vec{e}_z) = 0$.

With the dot product for the field $\vec{j}$ with $d\vec{e}_r \times d\vec{e}_z$, we have

$$\vec{j}.(d\vec{e}_r \times d\vec{e}_z) = \frac{C}{B^2}(\vec{B} \times grad p)(d\vec{e}_r \times d\vec{e}_z) =$$

$$\frac{C}{B^2} \begin{vmatrix} \vec{B}.d\vec{e}_r & \vec{B}.d\vec{e}_z \\ grad p.d\vec{e}_r & grad p.d\vec{e}_z \end{vmatrix} =$$

$$= \frac{C}{B^2} \begin{vmatrix} 0 & Bdz \\ grad p dr & 0 \end{vmatrix} = -\frac{C}{B} grad p(r,z) dr dz.$$

When crossing the surface Ω, the current density in the domain between the equipotential surfaces $p = ct., p + dp = ct.$, produces a quantity of current $dI = \iint_\Omega \vec{j} d\vec{e}_r \times d\vec{e}_z =$

$$-C \iint_\Omega \frac{1}{B} grad p dr dz \text{ (but } grad p dr = dp \text{)}$$

$$= -C dp \int_\gamma \frac{1}{B} dz < 0, \text{ where } \gamma \text{ is a loop of a force}$$

line.

We admit as a working hypotheses: the specific flux volume of magnetic induction between two equipotential surfaces is constant, than

$$U = \int_\gamma \frac{1}{B} dz = = \iiint_V \frac{1}{(\vec{B}, d\vec{e}_r, d\vec{e}_\varphi)} dV \text{ is}$$

constant along the equipotential surfaces of the magnetic field; we can take as a parametric representation of the equipotential magnetic surfaces the equation $U(x, y, z) = ct.$ A consequence of this hypotheses is just the unchanged total current which crosses Ω_p, $dI = \iint_{\Omega_p} j_\varphi dr dz$, where

$d\vec{S} = d\vec{e}_r \times d\vec{e}_z$, $dS = dr dz$ an area element on the section surface Ω.

3. Quasi-static equilibrium problem. We are able to set the problem which governs the quasi-static equilibrium of the confined plasma.

Problem 3.1: Let Ω be a domain in the rectangular system $(\vec{e}_r, \vec{e}_z)$, closed domain in a boundary band $0 < r_1 \le r \le r_2 < +\infty$, $\Gamma_p = \partial \Omega_p$ is a curve sufficiently smooth. Determine $u \in C^2(\Omega) \cap C^3(\overline{\Omega})$, $\gamma_u \in R$, which satisfies the equation:

$$\mathrm{A}u(r,z) = -\frac{\partial}{\partial r}\left(\frac{1}{r}\frac{\partial u}{\partial r}(r,z)\right)$$

$$-\frac{\partial}{\partial z}\left(\frac{1}{r}\frac{\partial u}{\partial z}(r,z)\right) = \frac{1}{2r}g'(u) + \mu_0 Crf'(u),$$

$$(\forall)(r,z)\in\Omega_p,$$

$$\mathrm{A}u(r,z) = 0, (\forall)(r,y)\in\Omega-\Omega_p,$$

and the boundary conditions: $u_{|\Gamma_p} = 0$,

$\int_{\Gamma_p}\frac{1}{r}\frac{\partial u}{\partial n}ds = \mu_0 I = ct. > 0$, $u_{|\Gamma} = \gamma_u > 0$, u do

not go to zero on Ω_p, $\frac{\partial u}{\partial n}$ is continuous in crossing

the boundary Γ_p, where the arbitrary functions f, g

satisfy the relations $f(0) = f'(0) = g'(0) = 0$.

Remark 3.3: The functions f and g are introduced with the idea of identifying the equipotential surfaces of the magnetic induction field, of the electric current field and even with the level surfaces of the hydrodynamic potential of the totally ionized gas. Indeed, we consider the equipotential

surface of the electric current $\frac{dx}{j_x} = \frac{dy}{j_y} = \frac{dz}{j_z}$, which

rewritten in the Cartesian coordinate $(\vec{e}_r, \vec{e}_\varphi, \vec{e}_z)$ is

$\dfrac{rdr}{-\dfrac{\partial\psi}{\partial z}} = \dfrac{rd\varphi}{-Au(r,z)} = \dfrac{rdz}{\dfrac{\partial\psi}{\partial r}}$. From the first and the

last fraction we deduce $r\left(\dfrac{\partial\psi}{\partial r}dr + \dfrac{\partial\psi}{\partial z}dz\right) = 0$,

that is $d\psi(r,z) = 0$, so $\psi(r,z) = ct.$ on the surface on which $\vec{j}$ is tangent field. On such surfaces we have $j_r = j_z = 0$, $j_\varphi \neq 0$.

Remark 3.4: On the level surface $u = ct.$ it also results $\psi = ct.$, so that the surfaces on which $\vec{B}$ and $\vec{j}$ are tangent, are part of the same family and the

functions $u, \dfrac{\partial u}{\partial n}$ are continuous when crossing any

level surface. Alone, the component j_φ is nonempty on the level surfaces from Ω_p, it is the only component which contributes to the total current in the jet, current which is observed at the free boundary

through $I\mu_0 = \int_{\Gamma_p}\frac{1}{r}\frac{\partial u}{\partial n}ds$. The quadratic functions

case f, g, it was study by *Temam* [17].

Following, there will be showed the relaxing ways, or generalizing the results regarding the

nonlinearity of functions f, g. We will refer to the general treating from *C. Ghiță* [3], [4].

For the particular case showed above, in order to realize a unitary and coherent treatment, we have introduced the state function of the system

$$h : R_- \times R^2 \to R,$$

$$h(r,z;u(r,z)) = \begin{cases} \dfrac{1}{2r}g'(u(r,z)) + rf'(u(r,z)), (r,z)\in\Omega_p \\ 0, (r,z)\in\Omega-\Omega_p \end{cases}$$

and the controlled parameter $\lambda = C\mu_0 \in R_+$, in agreement to which the equilibrium equation of the plasma jet is written $\mathrm{A}u(r,z) = \lambda h(r,z;u(r,z))$, as a nonlinear eigenvalue equation for the operator A.

4. An equilibrium generalized problem. We realize an abstract setting of the equilibrium problem for the confined plasma in the *Hilbert* space. For the study of the week solutions as critical points, for an operational equation we realize the operational writing, defined in a Banach space, equivalent to a variational problem.

Let $\Omega \subset R^n$, be a bounded and measurable sub domain, $\Gamma = \partial\Omega$ its regular boundary; we introduce *Sobolev* spaces $W^{2,p}(\Omega) = \{u\in L^2(\Omega)/D^\alpha u\in L^p(\Omega), |\alpha|\leq 2\}$, D^α is the derivate along the space $\mathrm{D}'(\Omega)$ (of the distributions), with the norm

$$\|u\|_{2,p} = \left(\sum_{|\alpha|\leq 2}\int_\Omega |D^\alpha u(x)|^p dx\right)^p, \text{ the Hölder}$$

function space

$$C^{1+\alpha}(\Omega) = \left\{u\in C^1(\Omega)/\frac{|D^\sigma u(x) - D^\sigma u(y)|}{|x-y|^\alpha} < +\infty, |\sigma| = 1, \forall x, y\in\Omega\right\}$$

with the norm $\|u\|_{1,\alpha} = \sum_{|\sigma|=1}\max|D^\sigma u(x)| +$

$\max_{|\sigma|=1}\dfrac{|D^\sigma u(x) - D^\sigma u(y)|}{|x-y|^\alpha}$, the differential

operator $\mathrm{L} : H^1(\Omega) := W^{2,1}(\Omega) \to L^2(\Omega)$,

$\mathrm{L}u(x) = -\dfrac{\partial}{\partial x_i}\left(a_{ij}(x)\dfrac{\partial u}{\partial x_j}(x)\right) + a_0(x)u(x)$, with

a_{ij} derivable functions, with $D^\sigma a_{ij} \in C^{1+\alpha}(\Omega)$, symmetric, with $|\sigma| = 1$, a_0 a continuous *Hölder*

function, L elliptical uniform, or it exist $\eta \in R_+$, so that

$$a_{ij}(x)\xi_i\xi_j + a_0(x)\xi_0^2 \geq \eta\left(|\xi|^2 + \xi_0^2\right),$$
$$(\forall)\xi \in R^n, \xi_0 \in R.$$

Remark 4.1: The operator L from $H^1(\Omega)$ to $L^2\Omega$ is a linear operator, bounded and uniform elliptic.

We consider $h : \Omega \times R \to R$, a nonlinear function, satisfying the *Caratheodory* condition, derivable in t, with $\dfrac{\partial h}{\partial t}(.,.)$ a Lipschitz, function

satisfying: $\dfrac{\partial h}{\partial t}(x,t) > 0$, for $t < 0$ (positively),

$\dfrac{\partial h}{\partial t}(x,t) = 0 \Leftrightarrow t \geq 0$ (a.e.) on R (zero on semi ax R_+), $(\exists) b_1, b_2 \in R_+, \beta > 1$, for $n \leq 2$;

$\beta = \dfrac{n}{n-2}$, for $n > 2$, so that

$b_1\left(|t|^\beta - 1\right) \leq \dfrac{\partial h}{\partial t}(x,t) \leq b_2\left(|t|^\beta + 1\right)$ (asymptotic behavior).

Remark 4.2: The estate function h allows the stating of an operator, which under conditions of an asymptotic behavior, is an operator of overlapping $B : H^1(\Omega) \to L^2(\Omega)$,

$Bu(x) = \dfrac{\partial h}{\partial u}(x, u(x)) = F(x, u(x))$. Indeed, we

have $H^1(\Omega) \subset L^\delta(\Omega)$, with continuous inclusion, with a relation between parameters : $\dfrac{1}{\delta} = \dfrac{1}{2} - \dfrac{1}{n} = \dfrac{n-2}{2n}$, and $F(x, u(x)) \in L^2(\Omega)$, since $u \in L^\delta(\Omega)$ (even $u \in H^1(\Omega)$).

We introduce the eigenvalue problem,

Problem 4.1: Determine $\Omega_p \subset \Omega$, $u \in H^1(\Omega)$, $\lambda \in R_+$, so that the equation L $u(x) =$

$$= \begin{cases} \lambda Bu(x), x \in \Omega_p \\ 0, x \in \Omega - \Omega_p \end{cases}$$ and the boundary conditions

$u = 0$ on Γ_p, $u = \gamma_u$ on Γ, $I = -\int_{\Gamma_p} \dfrac{\partial u}{\partial v} d\Gamma > 0$ be

satisfied, and u and $\dfrac{\partial u}{\partial v}$ are continuous on Γ_p, cu

$\dfrac{\partial .}{\partial v}$ co normal derivative associated to the operator

L, $\dfrac{\partial .}{\partial v} = a_{ij}\dfrac{\partial .}{\partial x_i}.v_j$.

For treating the Problem 4.1 we will realize an operational formulation, equivalent to the variational formulation in *Sobolev* space. We consider the real function $F : R^n \times R \to R$,

$F(x;t) = \int_0^t \dfrac{\partial h}{\partial t}(x;\tau)d\tau$, for whose realization in

space $L^2(\Omega)$ we find a functional

$$F_2 : L^2(\Omega) \to R,$$
$$F_2(v) = \int_\Omega \{h(x; -u_-(x)) - h(x;0)\}dx,$$

which proves to be *Gâteaux* differentiable on space $H^1(\Omega)$, [13], with the differential

$\left(F_2'(u), v\right) = \int_\Omega \dfrac{\partial h}{\partial u}(x; -u_-(x))v(x)dx$

$= \left(B(-u_-), v\right)$, differential F_2' must be understand from $H^1(\Omega)$ la $H^{-1}(\Omega)$, because $L^\infty(\Omega) \subset H^{-1}(\Omega)$. Functional F_2 is weak continuous on W, indeed, let $\{v_n\}_{n \in N} \subset W$, be weak convergent $v \in W$, submerge theorem [11] for Ω bounded domain, with $\Gamma \in C^1$, ensure $H^1(\Omega) \subset L^p(\Omega)$, with compact inclusion for $1 \leq p \leq \dfrac{2n}{n-2}$, which is strong convergence $v_n \to v$ in $L^p(\Omega)$. Since the function h is continuous in the variable t, with the hypothesis of asymptotic comportment, we have

$\left|F(x; u(x))\right| \leq C_1 +$

$< C_2|u(x)|^{\beta+1}, \beta = \dfrac{n}{n-1} < \dfrac{2n}{n-2}$,

it results that *F*, similar to the defined in the bi-dimensional case, has a continuous realization from $L^{\beta+1}(\Omega)$ to $L^1(\Omega)$, in particular from $H^1(\Omega)$ la $L^1(\Omega)$, so that $F(x, v_n(x)) \to F(x, v(x))$ in $L^1(\Omega)$. In consequence $F_2(v_n) \to F_2(v)$. We note the working space in the study of the Problem 4.1 with $W = \{v \in H^1(\Omega) / \gamma_0 v = \gamma_v = ct.pe \ \Gamma\}$, having the norm of the space $H^1(\Omega)$, we define the bilinear form $a(.,.)$, bounded, symmetric and differentiable on W, nonlinear form $b(.,.)$,

$$a(u,v) = \frac{1}{2}\int_\Omega \left\{ a_{ij}(x)\frac{\partial u}{\partial x_i}(x)\frac{\partial v}{\partial x_j}(x) + a_0(x)u(x)v(x) \right\} dx$$

$$, \; b(u,v) = \int_\Omega Bu(x)v(x)dx \;,$$

which allows us the writing of the variation equation: determine $(\lambda, u(\lambda)) \in R_* \times W$, so that

$(PV) \qquad a(u,v) - \gamma_v I = \lambda b(-u_-, v), (\forall)v \in W$.

We consider in the same time the quadratic functional $F_1(v) = \frac{1}{2}a(v,v) - \gamma_v I$,

Fréchet differentiable, with the differential given by $(F_1'(u), v) = a(u,v) - I\gamma_v$, the product $(.,.)$ being understand in the duality of spaces $H^1(\Omega), H^{-1}(\Omega)$, so it is continuous on W. From variational formulation (PV) of the quasi-static equilibrium of the plasma, it is derived a weak formulation of the critical point: determine $\{\lambda, u(\lambda)\} \in R_+ \times W$, so that

$(PPC) \qquad F_1'(u) = \lambda F_2'(u)$, in $D'(\Omega)$.

Relating to the existence of the critical point u and to the corresponding critical value λ to the equation (PPC), we underline the following result (example [11]):

Theorem 4.1: Let S the level subset determined by the functional F_2 on W, $S = \{v \in W / F_2(v) = C = ct.\}$. The element $u \in W$ is a critical point of the problem (PPC), or it exist $\lambda \in R_+$ and $F_2(u) \neq 0$, so that $F_1'(u) \equiv \lambda F_2'(u)$, if and only if u is a point of minim of the functional $F_1(v) = \frac{1}{2}a(v,v) - \gamma_v I$ on the subset S.

5. Variational formulation and the existence results. With the help of this result the problem of determining the weak solution would be reduced to $\inf\limits_{v \in S} F_1(v)$.

Theorem 5.1: Functional F_1 is inferior bounded on the surface *S,* for the norm in *W* and it reaches the minimum al least in a point $u \in W$, for which $F_2^t(u) \neq 0$.

How much regularity does the solution of the problem (PPC) has and which is the relation between the weak solution of the variational equation and the classical solution of the eigenvalue problem? We will find in the following result an extension for the similar result from *Temam* [17], for n = 2.

Theorem 5.2: Let $u \in W$ a solution of the problem (PPC), or for the variational equation (PV), then $u \in W^{3,\beta+1}(\Omega)$, $\beta > 1$ and $u \in C^{2+\alpha}, 0 \leq \alpha < 1$. If we note $\Omega_- = \Omega_p = \{x \in \Omega / u(x) < 0\}$, $\Omega_+ = \Omega - \Omega_p = \{x \in \Omega / u(x) > 0\}$, the domain occupied by the jet, the empty domain, then u is the solution of Problem 4.1. The subset $\Gamma_p \cap \Omega$ has empty inside in R^n, and if $a_{ij}(x)\frac{\partial u}{\partial x_j}(x)\vec{e}_i \neq \vec{0}$, in a neighborhood of the point $x \in \Gamma_p$, and then the variety Γ_p is a surface defined by a function of class $C^2(\Omega)$ and $\frac{\partial u}{\partial \nu}$ is continuous on Γ_p. More, if $\Gamma_p \in C^1(\Omega)$, then u is not zero in Ω_p and $I = \int_{\Gamma_p} \frac{\partial u}{\partial \nu}(x)d\Gamma > 0$.

6. Comments on results. The result of the last theorem, demonstrated in *Temam* [17], for n= =2, is extended to $n > 2$, $\beta = \frac{2n}{n-2}$, less the analytical function character for *u,* example [7], n = 2. Essential arguments which lead to the result are there related to the ellipticity property of operator L, the properties of the asymptotic behavior of the state operator B. The regularity assured by the emerge theorems allowed us to obtain the identification of the weak solution with the classic solution, and also a good regularity for the free boundary Γ_p.

The character of the eigenvalue problem was eliminated by equivalence with the problem of optimum on level surface determined by the state function of the ionized gas jet. In *Temam* [16] it is obtained the result even through a optimum problem without restriction, introducing a nonlinear functional

$$J: W \to R,$$

$$J(v) = \frac{1}{2}a(v,v) - \gamma_v I + \int_\Omega F(x; \vartheta(v))dx \;, \text{ with}$$

$$\vartheta(v) = -v_-.$$

For a similar problem, using variational formulations in duality, the topological methods and a fixed point argument were obtained existence results in [2].

Actual contribution: Uniqueness result.

2. The control made by the λ parameter upon the free boundary existence and a reduced operator equation. We introduce an eigenvalue problem associated to the operator L :

L $v(x) = \lambda v(x)$ in Ω, $v(x) = 0$ on Γ,

and the modified eigenvalue problem,

$\mathtt{L}\ v(x) = b_1 \lambda v(x)$ in Ω, $v(x) = 0$ on Γ,

with b_1 the constant value from the asymptotic behavior of the state function h and λ_1 the first eigenvalue, v_1 the corresponding eigenvector.

We will show that the weak solutions for the variation problem (PV) are in (1-1) correspondence with the solutions of an operator equation, the new operational formulation will be better adapted to the topologic argument which we will apply in finding the uniqueness of Problem 1.1 (4.1)

We consider the *Dirichlet* problem on Ω: $\mathtt{L}$ $\xi + \xi = w$ $\mathtt{in}\,\Omega$, $\xi = \gamma_u$ on Γ, which has unique solution in space $W \subset H^1(\Omega)$, for any $w \in W^* \subset H^{-1}(\Omega)$. We note with $J: W^* \to W$, the operator which defines the dual isomorphism of the pair (W, W^*), which is $Jw = \xi \Leftrightarrow \xi$ is solution for the problem $\mathtt{L}$ $\xi + \xi = w$ $\mathtt{in}\,\Omega$, $\xi = \gamma_u$ on Γ. The linear form $l(u) = \gamma_u I$ defines in the (W, W^*) duality the element $m \in W$, unique, $m = Jl$, which verifies on Ω the problem with the boundary condition: $m \in W$, $\mathtt{L}\, m(x) + m(x) = 0$ in Ω, $-\dfrac{\partial m}{\partial \nu} = I$ on Γ. The second order elliptic problem theory ensures for m the following steadiness $m \in W \cap H^2(\Omega)$, ([6]). Problem 1.1 (4.1) is equivalent to the operator equation:

(2.1) $\quad u \in W$, $u(x) = m(x) + J(u(x) - \lambda B u(x))$.

The characteristic of free boundary problem is kept in the nonlinear term $n = J(u - \lambda Bu)$. For certain rational premises which we will develop, since $H^1(\Omega) \subset L^{\beta+1}(\Omega)$, with the compact inclusion, J will be extended as an operator from $L^{\beta+1}(\Omega)$ to $L^{\frac{\beta+1}{\beta}}(\Omega)$, and then function n verifies the nonlinear problem:

(2.2) $\quad n \in W$, $\mathtt{L}$ $n(x) + n(x) = u(x) - \lambda Bu(x)$

$$\text{in } \Omega, \frac{\partial n}{\partial \nu}(x) = 0, x \in \Gamma.$$

There exists n, so that $n \in W \cap H^2(\Omega)$, which verifies the problem with the boundary conditions. We are able to present a decomposing result.

Proposition 2.1: If u is the weak solution for the problem (PV) of the nonlinear equilibrium for the plasma jet, then $u = m + n$, with $m, n \in W \cap H^2(\Omega)$, solutions for the problems (2.1), (2.2).

This regularity result can be compared with *Theorem* 3.2, section 3 from [4].

It is defined the application $T: W \times [0, +\infty) \to W \cap H^2(\Omega)$ using the relation $T(\lambda, u) = = m + J(u - \lambda Bu)$, then the variational equation (PV), or the operator equation (PPC), is equivalent to the reduced operator equation,

(2.3) $\quad u \in W \cap H^2(\Omega)$, $u = T(\lambda, u)$.

The problem defined by the mapping T is also a nonlinear problem, with eigenvalue. Under restrictive conditions, but more general than others mentioned in the literature, the problem (2.3) has a unique solution. We will detail first some technical results. On a first step, we will see that the smoothness of the state function reaches the differentiability properties for the multivalent application T.

Lemma 2.1: Let $h: \Omega \times R \to R$ a Caratheodory function, twice differentiable continuous in t, then the mapping $T: [0, +\infty) \times W \to W \cap H^2(\Omega)$ is Frechet-differentiable, with the differential

$$dT(\lambda, u_0)v = Jv - J\left(\frac{\partial^2 h}{\partial u^2}(x, -u_{0-})\right)(H(-u_0)v),$$

where H is a maximal monotone graph, with $0 \in H(0)$, defined by the *Heaviside* function.

Denote by $S(\lambda, u) = u - T(\lambda, u)$ the *Fredholm* application associated to the map T (reduced nonlinear problem (2.3)). As a remark, we mention that the mapping S is *Frechet*- differentiable, with the differential $dS(\lambda, u_0) = I - dT(\lambda, u_0)$.

What conditions on the map S guarantee a local reversibility, in this way the solutions for the equation $S(\lambda, u) = 0$ can have analytical representation, in agreement with the implicit functions Theorem, will be explained (in greater detail) in the following result.

Lemma 2.2: Suppose that the parameter λ from the (PV) formulation satisfies the condition $0 < \lambda_1 < \lambda < \lambda_2$, where λ_1 and λ_2 are the first two positive eigenvalue for the modified eigenvalue problem $\mathtt{L}$ $v(x) = b_1 \lambda v(x)$ in Ω, $v(x) = 0$ on Γ. Let u_0 be a weak solution of the (PV) variational problem, which exists and the state function is concave on R, that is $\dfrac{\partial^2 h}{\partial t^2}(., t) < 0, (\forall) t \in R$, then $dS(\lambda, u_0)$ is an isomorphism on a subspace of W.

Furthermore, if $0 < \lambda \leq \lambda_1$ and the bilinear form $a(.,.)$ satisfies the norm condition: $a(u_0, v) = 0 \Leftrightarrow v = 0$, then the map $dS(\lambda, u_0)$ is also an isomorphism on a subspace of W.

3. The weak solution uniqueness of the ionized gas jet equilibrium. The important result of the section is a uniqueness theorem, the direct consequence to the variational considerations [4], of the lemma 2.1, 2.2 from the previous section, using the topological arguments of degree theory. Generality will not diminish if we admit $a_0 \equiv 0$, so that, we will use a change of unknown function of translation type. We state

Theorem 3.1: Let λ_1, λ_2 the first two eigenvalue of the modified eigenvalue problem, $\mathrm{L}\, v(x) = b_1 \lambda v(x)$ in Ω, $v(x) = 0$ on Γ. If the state function satisfies the conditions: $\frac{\partial h}{\partial t}(x,t) > 0$, for $t < 0$ (positivism), $\frac{\partial h}{\partial t}(x,t) = 0 \Leftrightarrow t \geq 0$ a.e. on R (null on semi-axis R_+), $(\exists) b_1, b_2 \in R_+, \beta > 1$, for $n \leq 2$; $\beta = \frac{n}{n-2}$, for $n > 2$, so that $b_1 \left(|t|^\beta - 1 \right) \leq \frac{\partial h}{\partial t}(x,t) \leq b_2 \left(|t|^\beta + 1 \right)$ (asymptotic increase), $\frac{\partial^2 h}{\partial t^2}(.,t) < 0, (\forall) t \in R$, in addition the local linear behavior: $(\exists)\varepsilon > 0$, so that on $B(0,\varepsilon) \subset R$, the function $t \to \frac{\partial h}{\partial t}(.,t)$ is linear, that is $\frac{\partial h}{\partial t}(.,t)_{B(0,\varepsilon)} = Ct$, with C>0. The bilinear form $a(.,.)$ satisfies the norm condition $a(u_0, v) = 0 \Leftrightarrow v = 0$, then for $0 < \lambda < \lambda_2$, there exist a unique solution for the variational problem (PV).

Remark 3.1: In [3] it was obtained a uniqueness result for the plasma equilibrium solution considering the state function a *Lipschitz* continuous function, with the *Lipschitz* constant smaller than the eigenvalue λ_2. In our case, an affine local behavior ensures the uniqueness. This thing is in agreement with the possibility of initiating the download in gas of the infinitesimal parameter, which ensures a linear characteristic for the potential function of the magnetic field.

The results concerning the uniqueness of the solution of the equilibrium problem were obtained in particular cases. Considering the bi-dimensional problem: determine $u \in C^2(\Omega) \cap C^3(\overline{\Omega})$, $\gamma_u \in R$, which satisfies the equations:

$$\mathrm{A}\, u(r,z) = -\frac{\partial}{\partial r}\left(\frac{1}{r} \frac{\partial u}{\partial r}(r,z) \right)$$

$$-\frac{\partial}{\partial z}\left(\frac{1}{r} \frac{\partial u}{\partial z}(r,z) \right) = \frac{1}{2r} g'(u) + \mu_0 C r f'(u),$$

$$(\forall)(r,z) \in \Omega_p,$$

$$\mathrm{A}\, u(r,z) = 0, (\forall)(r,y) \in \Omega - \Omega_p,$$

and the boundary conditions: $u_{|\Gamma_p} = 0$,

$$\int_{\Gamma_p} \frac{1}{r} \frac{\partial u}{\partial n} ds = \mu_0 I = ct. > 0, \quad u_{|\Gamma} = \gamma_u > 0, \, u \text{ is not}$$

vanished on Ω_p, $\frac{\partial u}{\partial n}$ is continuous across the free boundary Γ_p, where the functions f, g satisfy the relations $f(0) = f'(0) = g'(0) = 0$, were treated as a eigenvalue problem in [18], supposing B of the form $Bu(r,z) = b(r)u(r,z)$, with $b(r) = 2a_0 t + \frac{a_2}{\mu_0 C r}, a_0, a_2, C > 0$. In accordance with the nonlinear second term $\frac{\partial h}{\partial u}(r,y;u(r,z)) = g(r,z;u(r,z)) = \lambda u^+(r,z)$ in [13] is obtained a uniqueness result. For the nonlinear problem having the nonlinear function $g(.,.;t)$ Lipschiz continuous in t, the uniqueness is controlled by the parameter λ in [2].

7. References

[1] A. Arabagiu, *Cuptor de elaborare a oțelurilor speciale și aliajelor greu fuzibile, echipat cu arzătoare cu plasmă*, Certificat de inovator nr. 327/1977 MIM-DT.

[2] H. Berestycki & *H*. Brezis, On *a free boundary problem arising in plasma physics*, Nonlinear Analysis, Theory & Appl., 4 (3), (1980), 415-436.

[3] M. Berger & M. Berger, *Perspectives in Nonlinearity. An Introduction to Nonlinear Analysis*, W.A. Benjamin, Inc., New York, 1968

[4] C. Ghiță, *Asupra soluțiilor unei probleme neliniare din fizica plasmei. Un rezultat de unicitate*, Stud. Cerc. Mat. Tom 34, nr.5 (1982), 425-448,

[5] C. Ghiță, Metalurgie Matematică. *Analiza nestandard a proceselor metalurgice, Ed. Academiei Române*, 1995

[6] D. Gilbarg & N.S. Trudinger, *Elliptic Partial Differential Equations of Second Order*, Springer-Verlag, Berlin, 1977.

[7] D. Kinderlehrer, *Variational inequalities and free boundary problems*, Bull. A.M.S., 84 (1978), 7-27.

[8] D. Kinderlehrer & J. Spruck, *The shape and smoothness of stable plasma configurations*, Ann. Sc. Norm. Sup. 5 (1), (1978), 131-149

[9] J. Laminie & R. Temam, *Determination numerique de la configuration d'equilibre du plasma, dans un Tokomak*, Computing Methods in Appl. Sciences, Lect. Notes Phys., 58 (1976), 497-509.

[10] A. Lemoine, *Contribution à l`étude de transferts de matiére, de chaleur et de quantité de mouvement dans un jet atmosphérique de plasma d`argon*, Thése.

[11] J. Mossimo & R. Temam, *Certains problemes non-lineaires de la physique des plasmas*, Mathematical Aspects of finite Element Methods, Lect. Notes Math., 606 (1975) 237-260.

[12] D. Pascali & S. Sburlan, *Nonlinear Mapping of Monotone Type*, Ed. Academiei & Sijthoff &Noordhoff in. Publ., 1978.

[13] J. P. Puel, *Sur un probleme de valeur propre nonlineaire et de frontiere libre*, C.R. Acad., 484 (1977), 861-863.

[14] D. Schaeffer, *Non uniqueness in the equilibrium shape of a confined plasma*, Comm. Part. Diff. Eqs., 2 (1977), 587-600.

[15] J. Sijbrand, *Bifurcation analysis for a class of problem with a free boundary*, Nonlinear Anal., Methods & Appl., 3(6) (1979), 723-753.

[16] J. Sijbrand, *Bifurcation analysis of a nonlinear free boundary problem from plasma physics. Asymptotic analysis from theory to application*, Lect. Notes Math., 711 (1979), 76-93.

[17] R. Temam, *Application de l'analyse convexe au calcul des variations*, Nonlinear Operators and Calculus of Variations, Lect. Notes Math., 543 (1975).

[18] R. Temam, *Remarks on a free boundary value problem arising in plasma physics*, Comm. Part. Diff. Eqs., 2 (1977), 563-585.

[19] R. Temam, *A nonlinear eigenvalue problems: the shape at equilibrium of a confined plasma*, Arch. Rat. Mech. Anal., 60 (1976), 51-73.

CLAUDIA STIHI
SIMONA APOSTOL
GABRIEL DIMA
CALIN OROS
GHEORGHE VLAICU
SERGIU DINU

THE USE OF VEGETAL BIOINDICATORS AND ATOMIC AND NUCLEAR TECHNIQUES FOR MONITORING OF HEAVY METAL ENVIRONMENTAL POLLUTION

Faculty of Sciences, Valahia University of Targoviste ,2 Carol I street, 130024, Targoviste, Romania , e-mail: stihi@valahia.

Abstract: *In the present work the moss biomonitoring technique and the combination of three analytical techniques – Atomic Absorption Spectrometry (AAS), Inductively Coupled Plasma (ICP) and Neutron Activation Analysis (NAA) – are proposed to be apply for monitoring environment concerning the air pollution in the region of Dambovita county. The main sources of air pollutants are industrial processes, thermal power stations, domestic heating systems and motor vehicles. All these sources are present in the territory of the Dambovita County.*

1. Introduction

The main regional polluting industries in Dambovita county are stainless steel works (Targoviste), cement and related materials production (Fieni), glass and lighting sources production (Targoviste, Fieni), chemicals materials production (Targoviste, Doicesti), coal mining and thermal power station (Doicesti), oil exploration (Targoviste, Moreni, Gaiesti). The above mentioned industries are potential sources of such pollutants as: As, Cd, Cr, Cu, Fe, Ni, Pb, Si, Sb and Zn regularly determined in the European moss surveys. The most affected towns are Fieni, Doicesti, Moreni, Gaiesti and Targoviste in decreasing order regarding pollution with sedimentable powder. The cement factory in the town of Fieni is responsible for the third place in the list of the most polluted localities of Romania (Romanian Statistical Yearbook-2001: National Institute of Statistics).

2. Experimentals

2.1. Bioindicators - biomonitoring technique

Vegetal samples can be used as bioindicators for monitoring environment quality, especially air pollution. Mosses, lichens or leaves can be used with good results.

2.1.1. Mosses can indicate the presence of elements and their concentration gradients.

Most methods in heavy metal monitoring employ mosses as bioaccumulators and involve sample

collection followed by laboratory analysis techniques to detect actual levels.

The majority of studies have been multi-element investigations and few have been restricted to a particular metal except where different methods of analysis were required. Since Burton's review in 1986 [1], approaches to moss monitoring of heavy metal deposition have changed little in principle. Refinements have been made in monitoring design, in terms of standardized sampling and reduction of error and variance. As may be expected new developments in chemical analysis have occurred.

A major choice lies between using techniques which employ indigenous species or transplanted species. A successfully series of studies using mosses as bioindicators were initiated in the Steinnes group [2-6]. **2.1.2. Lichens** are also effective biomonitors primarily in relation to gaseous air pollutants as they possess many similar characteristics to mosses. Lichens are slow growing and assimilate metals at a rapid rate but release them at a low rate. Metal concentrations in lichen thalli have been shown to correlate with atmospheric level [1]. Lichens were first used as bioaccumulative indicators in relation to point emission sources, where decreasing metal concentrations in species correlated with increasing distance from the source. Lichens have also been used to assess deposition patterns and heavy metal burdens for larger scale monitoring purposes. Their application as bioaccumulators on large scale is not as established as for mosses. Transplantation techniques are also possible. A comprehensive review of these aspects is provided in [7].

2.1.3. Plants: Higher plants have appeared as indicators in air pollution monitoring in highly polluted areas where lichens and mosses are often absent. Higher plants act as biomonitors in the assessment of aerial heavy metal contamination by means of their bioaccumulative properties. Therefore, mainly analytical approaches are used in monitoring of metals.

Metal aerosols pollute soil and plants. Higher plants not only intercept pollutants from atmospheric deposition but also accumulate aerial metals from the soil. Aerial heavy metal deposit are taken up from the soil by plants via their root system and translocated to other regions of the plant.

Particle deposition on leaf surfaces may be affected by a variety of factors, including particle size

and mass, wind velocity, leaf orientation, size, moisture level and surface characteristics [8]. The deposited particles may be washed by rain into the soil, resuspended or retained on plant foliage. The degree of retention is influenced by weather conditions, nature of pollutant, plant surface characteristics and particle size [9]. These authors demonstrated experimentally the significance of foliar accumulation and translocation of air derived metal pollutants. The foliar route was found to be of similar importance to the soil-root pathway.

Heavy metal absorption is governed by soil characteristics such as pH and organic matter content [10-11]. Thus, high levels of heavy metals in the soil do not always indicate similar high concentrations in plants. The extent of accumulation and toxic level will depend on the plant and heavy metal species under observation. In an investigation of Cd, Cu, Ni and Pb uptake from air and soil by *Achillea millefolium* (milfoil) and *Hordeum vulgare* (barley) in Denmark, [12] concluded that Cu and Pb plant concentrations correlated with aerial deposition but not with soil concentrations. In contrast, Ni and Cd content in the plants correlated with deposition and soil content. The distribution patterns and budgets of heavy metals within forest trees growing at contaminated sites in Germany were investigated by [13].

The interpretation of analytical data is therefore complicated by many factors. However, metal accumulation in plants can reflect the relative extent of the burden and its dispersal.

2.2 Analytical methods

The choice of analytical method will depend on the purpose of the respective survey. Some analytical methods are non-destructive (e.g. neutron activation) and are useful for repetitive surveys such as baseline studies. Samples can also be archived and used at a later date for additional analysis. Destructive techniques include atomic absorption spectrometry and inductively coupled plasma analysis.

2.2.1. Neutron Activation Analysis

Neutron activation analysis (NAA) was discovered in 1936 by Hevesy and Levi. They found that samples containing rare earth elements became radioactive after exposure to a neutron source. From this observation, they quickly recognized the potential of employing nuclear reactions for the determination of elements present in different samples. Neutron activation analysis was soon established as a method of qualitative and quantitative element analysis and can be successful used for environmental samples [14]. The sample material (solid, liquid sample) is irradiated with neutrons in a neutron source. In this process, stable isotopes are converted into radioactive isotopes. While

these isotopes decay, having half-life's varying from seconds to years, they are emitting γ radiation. Each radionuclide emits γ radiation of a certain energy. The γ radiation is measured with a semiconductor detector and an appropriate acquisition system can record the γ-spectra . The γ-spectra give the following information: the γ-radiation energies give information about which elements are in the sample and the γ-radiation intensities give information about amount of the elements present in the sample.

2.2.2. Inductively Coupled Plasma Analysis

Inductively Coupled Plasma (ICP) method is based on the fact that the atoms and ions produced in the plasma are excited and emit light. The intensity of light emitted at wavelengths characteristic of the particular elements of interest is measured and related to the concentration of each element from samples. ICP is a destructive technique which has been applied to a wide range of sample types: metals and wide variety of industrial materials, environmental samples (water streams, airborne particles and coal fly ash), and biological and medical samples [15].The ICP-OES (Inductively Coupled Plasma-Optical Emission Spectroscopy) spectrometer consists in a sample introduction system, a plasma torch, a plasma power supply and an optical measurement system .

The sample must be introduced into a plasma in a form that can be effectively vaporised and atomised (small droplets of solution, small particles of vapour). The plasma torch confines the plasma to a small diameter. Atoms and ions produced in the plasma are excited and emit light. The optical emission spectra are made using a personal computer.

The intensity of light emitted at wavelengths characteristic of the particular elements of interest is measured and related to the concentration of each element from samples.

2.2.3. Atomic Absorption Spectrometry

Atomic Absorption Spectrometry (AAS) like ICP-OES is a destructive technique used for elemental analysis of different samples from different domains, samples which like ICP samples must be vaporised and atomised.

The AAS spectrometer has a hollow cathode lamp (HCL). The atomic spectrometry uses absorption of light of intrinsic wavelength by atoms contains in a sample. Thus, the light absorbed measure the atomic density. The atomic density determines the absorption rate and the Lambert-Beer's law give the value of absorbency from each element of the samples.

The formula of Lambert-Beer's law is:

(1) $$I = I_0 e^{-k \cdot l \cdot c} \text{ , or}$$

(2) $$-\log \frac{I}{I_0} = k \cdot l \cdot c \text{ , where}$$

$\log \dfrac{I}{I_0}$ value is absorbency, formula that indicates that absorbency is proportional to atomic density. Using the calibration curve – absorbency and concentration – when the absorbency of an unknown sample is obtained, the concentration of the element can be obtained.

3.Results

We have checked the areal distribution of species at the county level and we have compared the efficiency of methods using different vegetal samples (moss, lichens and leaves) collected from the same area. Preliminary results let us to think that the use of mosses constitutes an effective method in air pollution monitoring for several reasons:

- Many species are widely distributed and grow in a large range of habitats;
  - Mosses are small and easy to handle;
  - Most of them are evergreen and can be surveyed all year round;
  - Mosses lack a cuticle and a root system and obtain nutrients as particulates and in solution directly from atmospheric deposition. They have good bioaccumulating ability, particularly for heavy metals, where metal concentrations reflect deposition without the complication of additional uptake via a root system;
  - Comparisons of fresh samples with herbarium specimens enable retrospective analysis of metal pollution;
  - The ability of mosses to accumulate elements in very high concentrations aids chemical analyses of the tissues and may facilitate the detection of elements present in very low concentrations in the environment;
  - The annual growth increment is usually easier to detect in mosses than lichens and mosses are often believed more desirable for temporal studies.
  - More then these, we can use selected moss

species for preparing a moss plate that can be placed in specific area allowing us to have the same reference, to control the period of accumulation and the density of our sampling network in order to compute a map with the heavy metal distribution at the county level.

4. Discussions and conclusions

Factors which should be considered in methodology selection include also finance and resources, desired accuracy of results, study time-scales, size of study area, extent and type of pollution. It is important during metal biomonitoring programs that background concentrations are established.

The design of a future monitoring can be involve: sampling locations – pollution sources location, sample collection - mosses, multi-element determination using NAA and complementary: ICP and AAS techniques; data analysis and data interpretation.

Comparison of the results obtained from moss biomonitoring technique using atomic and nuclear analytical methods with the analysis of aerosol filter from several aerosol stations in the Dambovita County can allow to establish direct correlation between concentration of elements-pollutants in air with atmospheric deposition of the same elements.

References

[1] BURTON, M.A.S. Biological monitoring of environmental contaminants (plants). MARC Report Number 32. Monitoring and Assessment Research Centre, King's College London, University of London. 1986.

[2] STEINNES, E., ANDERSSON, E.M. Atmospheric deposition of mercury in Norway: Temporal and spatial trends. Water, Air and Soil Pollution, **56**, 1991 p.391-404.

[3] STEINNES, E, RAMBAEK, J.P., HANSSEN, J.E. Large scale multi-element survey of atmospheric deposition using naturally growing moss as a biomonitor. Chemosphere, **25**, 1992, p.735-752.

[4] STEINNES, E., JOHANSEN, O., ROYSET, O., ODEGARD, M. Comparison of different multi-element techniques for analysis of mosses used as biomonitors. Environmental Monitoring and Assessment, **25**, 2, 1993, p.87-97.

[5] STEINNES, E., HANSSEN, J.E., RAMBAEK, J.P., VOGT, N.B. Atmospheric deposition of trace elements in Norway: Temporal and spatial trends studied by moss analysis. Water, Air and Soil Pollution, **74**, 1-2 1994 p.121-140.

[6] FRONTASYEVA, M.V., NAZAROV, V.M., STEINNES, E. Moss as a monitor of heavy-metal deposition - Comparison of different multi-element analytical techniques. Journal of Radioanalytical and Nuclear Chemistry-Articles, **181**, 2, 1994 p.363-371.

[7] TYLER, G., BALSBERG PAHLSSON, A.M., BENGTSSON, G., BAATH. E. TRANVIK, L. Heavy-metal ecology of terrestrial plants, microorganisms and

invertebrates. Water, Air and Soil Pollution, **47**, 3-4, 1989 p.189.

[8] BACHE, C.A., GUTENMANN, W.H., RUTZKE, M., CHU, G., ELFVING, D.C., LISK, D.J. Concentrations of metals in grasses in the vicinity of a municipal refuse incinerator. Archives of Environmental Contamination and Toxicology, **20**, 4, 1991, p. 538-542.

[9] HARRISON, R.M., CHIRGAWI, M.B. The assessment of air and soil as contributors of some trace metals to vegetable plants. I. Use of a filtered air growth cabinet. Science of the Total Environment, **83**, 1-2, 1989 p.13-34.

[10] CSINTALAN, Z., TUBA, Z. The effect of pollution on the physiological processes in plants. In: Biological indicators in environmental protection, Kovács, M. (ed.), Ellis Horwood, New York. 1992

[11] JONES, K.C. Contamination trends in soils and crops. Environmental Pollution, **69**, 4, 1991 p. 311-326.

[12] PILEGAARD, K., JOHNSEN, I. Heavy metal uptake from air and soil by transplanted plants of *Achillea millefolium* and *Hordeum vulgare*. Ramussen, L. (ed.), Ecological Bulletins (NFR) **36**. (Ecotoxicology: 3rd Oikos conference), 1984 p. 97-102.

[13] TRUBY, P. Distribution patterns of heavy metals in forest trees on contaminated sites in Germany. Angewandte Botanik, **69**, 3-4, 1995, p. 135-139.

[14] FRONTASYEVA, M.V.,STEINNES, E., Epithermal neutron activation analysis for studying the environment. Proc. Int. Symposium on Harmonization of Health Related Environmental Measurements Using Nuclear and Isotopic Techniques (Hyderabad, India, 4-7 November, 1996), IAEA 1997, p. 301-311.
[15] BOUMANS, R.W.J.M. Inductively Coupled Plasma Emission Spectroscopy, John Wiley and Sons, New York, 1987

SIMONA APOSTOL

CLAUDIA STIHI

CALIN OROS

GABRIEL DIMA

SERGIU DINU

"PHOTOELECTRIC EFFECT" –STEP IN THE PHOTOCHEMICAL CONVERSION OF LIGHT ENERGY IN PHOTOSYNTHESIS

Valahia University, Faculty of Sciences and Arts, Physics Department, 24 Bd Unirii Targoviste

Abstract: The main act in the photochemical conversion of light energy in the photosynthesis process is the delivery of electron from special chlorophyll molecule- the reaction center, after the light absorbtion at the antennae level. This light reaction is the driving force of the photosynthesis, that is followed by the electron conduction in a nanoscale-designed molecular circuitry up to the consumer: chemical machinery located in the citoplasma that performed dark reactions of synthesis of organic matter starting from anorganic CO_2. This paper will analyse the photochemical light reactions in photosynthesis from physical point of view, presenting also the characteristics that make this biological process similar to the photoelectric effect explained by Einstein in 1905. We will present also some optical and spectroscopical properties of this very important pigment in the photosynthesis, the chlorophyll.

1. Introduction

Photosynthesis is the process by which plants and bacteria use the energy from sunlight to produce sugar, which cellular respiration converts into ATP, the "fuel" used by all living things. The conversion of unusable sunlight energy into usable chemical energy, is associated with the actions of the green pigment chlorophyll. The photosynthetic process uses water and releases the oxygen that we absolutely must have to stay alive.

We can write the overall reaction of this process as:

$$6H_2O + 6CO_2 ----------> C_6H_{12}O_6 + 6O_2$$
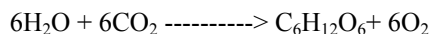
Plants are the only photosynthetic organisms to have leaves (and not all plants have leaves). A leaf may be viewed as a solar collector crammed full of photosynthetic cells, named chloroplasts.

The structure of the chloroplast

The thylakoid is the structural unit of photosynthesis. Both photosynthetic prokaryotes and eukaryotes have these flattened vesicles containing photosynthetic chemicals. Only eukaryotes have chloroplasts with a surrounding membrane.

Thylakoids are stacked like pancakes in stacks known collectively as grana. The areas between grana are referred as stroma. While the mitochondrion has two membrane systems, the chloroplast has three, forming three compartments.
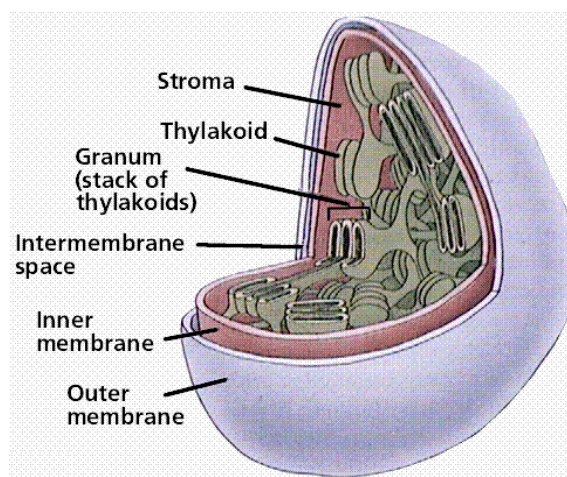
Fig. 1. Structure of a chloroplast.

Photochemical Conversion of light

Photosynthesis is a two stage process. The first process is the Light Dependent Process (Light Reactions), requires the direct energy of light to make energy carrier molecules that are used in the second process. The Light Independent Process (or Dark Reactions) occurs when the products of the Light Reaction are used to form C-C covalent bonds of carbohydrates. The Dark Reactions can usually occur in the dark, if the energy carriers from the light process are present. Recent evidence suggests that a major enzyme of the Dark Reaction is indirectly stimulated by light, thus the term Dark Reaction is somewhat of a misnomer. The Light Reactions occur in the grana and the Dark Reactions take place in the stroma of the chloroplasts.
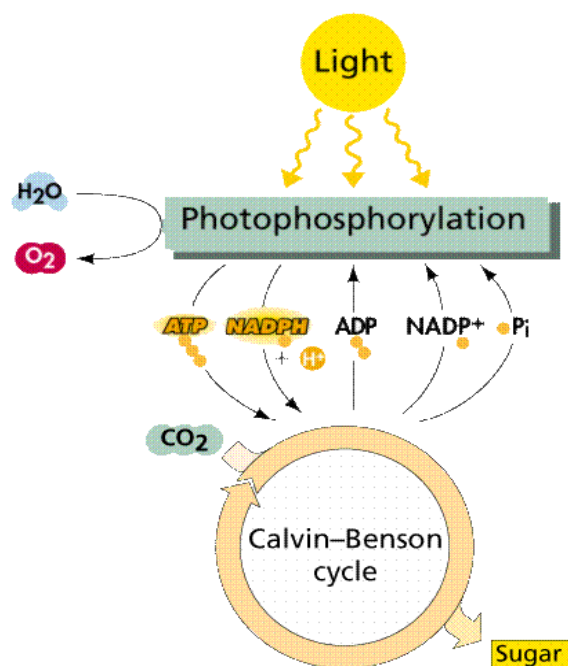
Fig.2. Overview of the two steps in the photosynthesis process.

In the Light Dependent Processes (Light Reactions) light strikes chlorophyll a in such a way as to excite electrons to a higher energy state. In a series of reactions the energy is converted (along an electron transport process) into energetic carriers ATP and NADPH molecules, used further in the Dark Reactions to reduce the carbon dioxide from the atmosphere (or water for aquatic/marine organisms) to carbohydrates $[CH_2O]_n$ process call carbon fixation. In the light reactions water is split providing electrons in the process of electron transport, releasing oxygen as a by-product of the reaction.

Photosystems are arrangements of chlorophyll and other pigments packed into thylakoids. Many prokaryotes have only one photosystem, Photosystem II (so numbered because, while it was most likely the first to evolve, it was the second one discovered). Eukaryotes have Photosystem II plus Photosystem I. Photosystem I uses chlorophyll a, in the form referred to as P700. Photosystem II uses a form of chlorophyll a known as P680. Both "active" forms of chlorophyll a function in photosynthesis due to their association with proteins in the thylakoid membrane.

Light of different collors is efficiently absorbed by leaves at the antennae level by the complex pigment assembly that have differents absorbtion spectra allowing the use of photons of differents wavelength shorter than a threshold of 680 nm in PSII or 700nm in PSI.
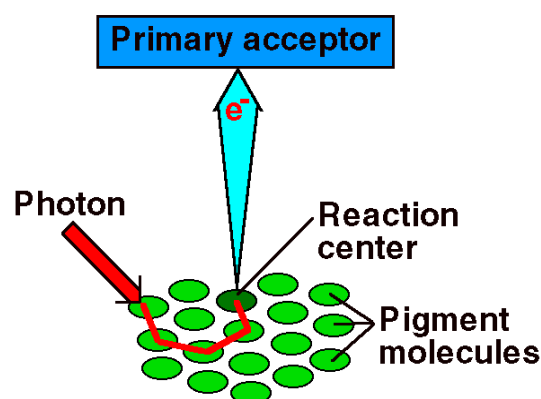
Fig.3. Light collection by antennae and photoelectron ejection in the reaction center

Light energy causes the removal of an electron from a molecule of P680 that is part of Photosystem II. The P680 requires an electron, which is taken from a water molecule, breaking the water into H^+ ions and O^{-2} ions. These O^{-2} ions combine to form the diatomic O_2 that is released. The electron is "boosted" to a higher energy state and attached to a primary electron acceptor, which begins a series of redox reactions, passing the electron through a series of electron carriers, eventually attaching it to a molecule in Photosystem I. Light acts again on a molecule of P700 in Photosystem I, causing an electron to be "boosted" to a still higher potential. The electron is attached to a different primary electron acceptor (that is a different molecule from the one associated with Photosystem II). The electron is passed again through a series of redox reactions, eventually being attached to $NADP^+$ and H^+ to form NADPH, an energy carrier needed in the Light Independent Reaction. The electron from Photosystem II replaces the excited electron in the P700 molecule. There is thus a continuous flow of electrons from water to NADPH, across a potential difference between lowest (P680) and highest energy states (P700*) of about 1.8V. This energy is used in Carbon Fixation.
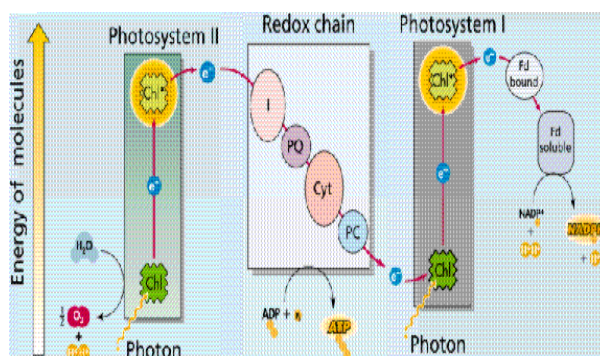
Fig.4. The Z scheme explaining the electron flow in photosynthesis. These processes are better known as the light reactions

The Nature of Light

Visible light is one small part of the electromagnetic spectrum. The light colors is determined by the wavelength of light. The longer the wavelength of visible light, the more red the color. Likewise the shorter wavelengths are towards the violet side of the spectrum. Wavelengths longer than red are referred to as infrared, while those shorter than violet are ultraviolet.

Light behaves both as a wave and a particle. Wave properties of light include the bending of the wave path when passing from one material (medium) into another. The particle properties are demonstrated by the photoelectric effect: light absorbtion in different materials give rise to electrons generation in those materials and can create an electrical current in a circuitry. The critical wavelength is the maximum wavelength of light (visible or invisible) that creates a photoelectric effect. Eintein was the first to demonstate in 1905 the Planck assumption emmited in 1900 that the energy of light is quantified, it is absorbed and emmited as quanta named photons which energy is inversely proportional to the wavelength:

$$\varepsilon = h\nu = hc/\lambda \qquad (1)$$

Consequently, longer wavelengths have less energy than do shorter ones.

2. Materials and Methods

For measuring the photon electron flux we have used variable fluorescence measurements as described by Genty et al 1991, using a FIPAM fluorimeter (Apostol, 2000).

$$ETR = 1/2\ PPFD*fa*\Phi \qquad (2)$$

Where PPFD is the Photosynthetical Active Photon Flux Density, fa is the fraction of absorbed light, usualy around 0.85 depending on leaves, Φ-the quantum yield of photochemistry measured from faximal and stationary fluorescence as

$$\Phi = (F'm - Fs)/F'm \qquad (3)$$

For measuring spectroscopic properties of photosynthetic pigments we have extracted pigments from fresh spinach leaves using column chromatography according to the methods descriebed by Tugulea and Gazdaru 2003. Spectra are registred in differents solvents using a SPECORD spectrophotometer.

3. Results and Discussion

Light reactions–"Photoelectric effect"

The photochemical reaction acting in living cells conducting to the generation of an electron flow in photosynthesis have several similitudes with the photoelectric effect taking place in anorganic matter:

1) It require the absorbtion of light of a certain energy (wavelength threshold around 680-700 nm)
2) A photoelectric current appear in the molecular circuitry if the consumer exist for closing molecular circuitry.
3) The maximal values of current depend on the light intensity but not on the wavelength
4) Intensity of current (measured as ETR) for a given irradiation increase as the potential of them use is higher and attend a saturation when all electrons are used

There are also specific feature of the biological "photoelectric effect"

1)electrons generated by shorter wavelengths have not higher velocity; the energy in excess is lost as heat. All the photoelectrons have similar properties, they are ejected from special Chlorophyll only if the molecular acceptor is ready to accept them (closed molecular circuitry)

2)the electrical voltage across the molecular electron transport chain is fixed, around 1,8 V, allowing electron flow by redox reactions from a carrier to another. Even at this level, regulation mechanisms can occur impeding electron flow.

3)discussing the dependence of photoelectron current on light irradiation it must be put into advance that it is highly regulated by complex mechanisms, depending on the chemical need of electrons in the Calvin cycle, so is difficult to quantify this "potential=need"

4)maximal electron flow is linearly increasing with intensity of light (flux of photons) but up to a certain level (around 2000 μmol photons $m^{-2}s^{-1}$, for plants cultivated in full sun, but it depends on plants). If the light intensity is to high, photoinhibition can occur and photosynthetic machinery can be damaged.

Spectroscopic Properties of Chlorophyll from leaves

A pigment is any substance that absorbs light. The color of the pigment comes from the wavelengths of reflected light (in other words, those not absorbed). Chlorophyll, the green pigment common to all photosynthetic cells, absorbs all wavelengths of visible light except green, which it reflects. Black pigments absorb all of the wavelengths that strike them. White pigments/lighter colors reflect all or almost all of the energy striking them. Pigments have their own characteristic absorption spectra (see fig) ensuring a very efficient absorbtion of visible light at the leaf level. Then, the excitation is rapidly transferred to the reaction center where photochemical act take place.

Chlorophyll is a complex molecule. Several modifications of chlorophyll occur among plants and other photosynthetic organisms. All photosynthetic organisms (plants, prochlorobacteria, and cyanobacteria) have chlorophyll a. Accessory pigments absorb energy that chlorophyll a does not absorb. Accessory pigments include chlorophyll b (also c, d, and e in algae), xanthophylls, and carotenoids (such as beta-carotene). Chlorophyll a absorbs its energy from the Violet-Blue and Reddish orange-Red wavelengths, and little from the intermediate (Green-Yellow-Orange) wavelengths.

Carotenoids and chlorophyll b absorb some of the energy in the green wavelength. Why not so much in the orange and yellow wavelengths? Both chlorophylls also absorb in the orange-red end of the spectrum (with longer wavelengths and lower energy). The origins of photosynthetic organisms in the sea may account for this. Shorter wavelengths (with more energy) do not penetrate much below 5 meters deep in sea water. The ability to absorb some energy from the longer (hence more penetrating) wavelengths might have been an advantage to early photosynthetic algae that were not able to be in the upper zone of the sea all the time.
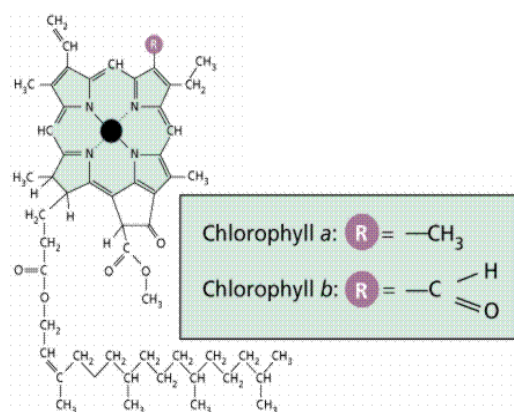
Fig. 6. The molecular structure of chlorophylls *a* and *b*
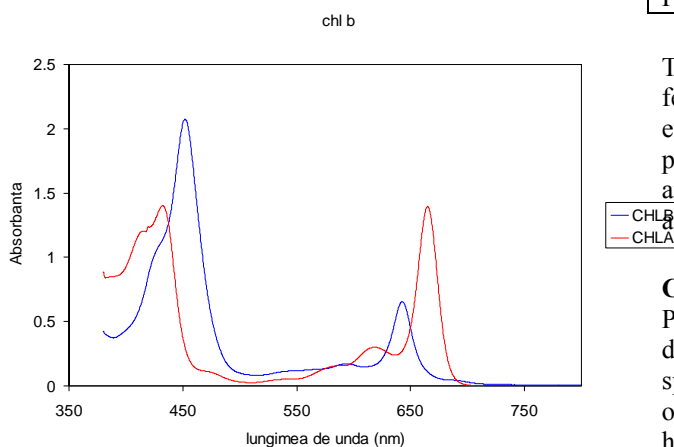
Fig.7. Absorption spectrum of Chlorophyll a and b
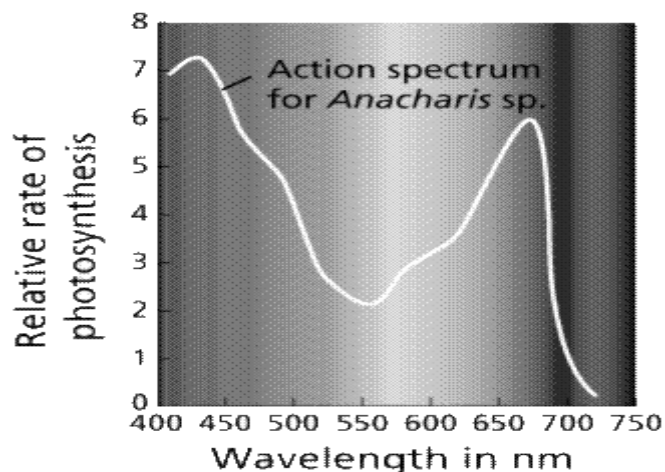
Fig. 8. The action spectrum of plants

The action spectrum of photosynthesis is the relative effectiveness of different wavelengths of light at generating electrons. If a pigment absorbs light energy, one of three things will occur. Energy is dissipated as heat. The energy may be emitted immediately as a longer wavelength, a phenomenon known as fluorescence. Energy may trigger the electron generation at the reaction center. Chlorophyll only triggers a chemical reaction when it is associated with proteins embedded in a membrane as in a chloroplast. This three process are competitive and the energy balance is deplaced when photosynthesis cannot use photoelectrons, inducing an increase of fluorescence emission as well as of the heat dissipation, as seen in Table1 .

Table 1. Ways of use of photon energy when electron transport is activated or blocked in photosynthesis (Rosema et al 1991)

Mecanism of photon use	electrons transport	
	optimal	blocked
Photosynthesis	84	0
Heat	14	88
Fluorescence	2	12

This behaviour is the base of the existence of this unique feature of chlorophyll fluorescence in vivo, its emmission quantum yield is variable depending on the photochemical activity, making from fluorescence analysis a good tool for monitoring photosynthetic activity in plants.

Conclusions
Photosynthesis is a very complex process, functioning due to a complex molecular machinery containing specialized individual entities interconnected , well optimized in terms of efficiency, self protected against harmfull products of his work (reactive oxygen species) and also self regulated by very complex reaction networks. This process stay on the base of our existence on Terra as is the main source of organic matter (food for human and animal in the trofic chain), of chemical energy finaly, as it is converting the non-limited light

energy provided by the Sun into chemical energy need for living organisms. In addition the same reaction is the source of the molecular oxygen, another requirement for life of aerobic organisms, allowing so our life. To have a measurements of the importance of this process let estimate as: "An average hectare of corn produces enough oxygen per hectare per day in mid summer to meet the respiratory needs of about 325 people. This means that the one million or so hectares of corn grown produce enough oxygen for the annual respiratory needs of 10 million residents in about 11 summer days!" (www.ontariocorn.org/envt/envphoto.htlm).

This source of oxygen, is driven by living plants, use only the solar energy and water is a clean process without waste, cost us nothing and allow us to leave! It let us think about the possibilities of manage in our benefit the huge energy source we dispose, the solar light, as the plants do!.

6. References

[1] ApostolS. 2000 Utilisation de la fluorescence chlorophyllienne pour le suivi à distance de la photosynthèse au niveau foliaire, These de doctorat Universite Paris Sud

[2] Genty B, Briantais J and Baker N (1989) The relationship between the quantum yield of photosynthetic electron transport and quenching of chlorophyll fluorescence Biochim Biophys Acta 990: 87-92

[3] Krause GH and Weis E (1991) Chlorophyll fluorescence and photosynthesis: The basics Annu Rev Plant Physiol Plant Mol Biol 42: 313-349

[4] Lawlor D (1993) Photosynthesis: Molecular, Physiological and Environmental Processes, 2nd edition, Longman Scientific&Technical, Harlow

[5] Taiz L and Zeiger E (1991) Plant Physiology, pp 1-565 Redwood City, California: The Benjamin/Cummings Publishing Cie, Inc.

[6] Tugulea L, Gazdaru D (2003) Tehnici si Medode Experimentale in Biofizica, Ed. Universitatii din Bucuresti.

Acknowledgements

T. PETISLEAM [1]

I.V. POPESCU [2]

V. CIUPINA [3]

M. BELC [3]

POLLUTION STUDIES IN MARINE ENVIRONMENTAL SAMPLES OF BLACK - SEA BY ATOMIC ABSORPTION SPECTROMETRY

[1] Physics Department , " Ion Banescu " Industrial Scholar Group , Mangalia , Constantza , Romania , e - mail : mubera_57@yahoo.com
[2] Valahia University of Targoviste, Physics Department, Faculty of Science
[3] Ovidius University of Constanta

Abstract: *Marine pollution was first time observed as a direct result of river mouth and of domestic and industrial waters and wastes discharges into coastal waters .*
I. Pecheanu from " Grigore Antipa " Marine National Research Institute of Constantza , Romania and the research group from " Ovidius " University of Constantza , Romania , we collected marine flora , fauna , seawater and sand samples from the Romanian seacoast of Black - Sea .
The studied zone is located between Mangalia city and a border village with Bulgaria , Vama - Veche.
*The purpose of this paper was a pollution degree comparison between I. Pecheanu ' s obtained results from 1980 untill 1997 and our december 2004 results .The followed heavy metals were Pb , Cu , Cd , Zn and Fe and their concentrations were determined by atomic absorption **spectrometer ATI - UNICAM** , SOLLAR type with Zeeman correction cell from " Grigore Antipa " Institute and by atomic absorption **spectrometer AAS - 6200 SHIMADZU** from " Ovidius " University.*

1. Introduction

Black - Sea has a surface of 432000 km², an 1997 m depth and 537000 km³ volume. Antipa and Wolfe said that Black - Sea is a semi - closed oval marine basin , located in an intramontane depression placed on W - E direction between two mountain ranges which separates Eastern Europe from Asia Minor , [1], [5].

The tectonic movements that formed the depression took place in Tertiary and Quaternary and they are nowadays continuing .

According to Bacescu et al. and to Yucesoy et al. the lower salinity and the poor flora and fauna induce the darken colour of Black - Sea water , [2], [8].

There are two major environmental polluting sources :

- natural sources (such as physical , chemical and biological processes of their upper terrestrial crust rocks) and

- anthropic sources (represented by accelerated human activities), [11], [12].

The natural sources are strongly influenced by the mineralogical composition and the weather forecasts of the studied zone : Mangalia - Vama Veche .

Bonnefouse and Goldberg plead that the anthropic sources appeared after Industrial Revolution and the

scientists discovered their effects in far - off and isolated areas of the Globe, [3], [4].

The heavy metals are the ones that have atomic numbers between 22 - 34 and 40 - 52 , lanthanides and acthinides , inclusively .We must also include the metals with 78 , 80, 82 and 83 atomic numbers (Au , Hg , Pb and Bi) .

The arrival of heavy metals in marine environment produces complex physical , chemical and biological changes , [7].

Only very small quantities of each heavy metal remain in the seawater and the rest lay down on bottom sediments or enter the marine organisms metabolic processes, [9] .

2. MATERIALS AND METHODS
Samples

I.Pecheanu from "Grigore Antipa" Institute of Constantza , Romania collected seawater and marine organisms samples from the studied zone between 1980 - 1997, [10].

The seawater samples were kept in plastic containers and the concentration was made by extraction using APDC (pirolydine - ditio - ammomium - carbamate) as organic reagent and MIBK (methyl - isobuthyl - cetone) as extraction solvent .

The marine organisms samples were represented by :

- fish (hanos and anchovy , scientifically called Gobius Batrachocephalus and Engraulis Encrasicholus Ponticus , respectively) and

-shells (Midia, scientifically named Mytilus Galloprovincialis).

Mytilus Galloprovincialis is an abundant specie along the Romanian seacoast . From the fact that they filter immense water quantities, we conclude that they are natural filters and the best "bioindicator" of areas pollution degree.

They were dried at 20°C, they were mortared and they were kept in the drying stove for two hours at 105°C . From these samples, they took exact shares for mineralization on a sand bath by adding concentrated nitric acid. The dry residue was moisted with nitric acid, 1 N and filtered. The research group from "Ovidius"

University of Constantza, Romania collected seawater, sand, green algae (Cladophora) and marine organisms (hanos, anchovy and Midia shells) samples from mentioned zone in december 2004.

The 500 ml seawater samples were pH - adjusted, prepared with APDC and MIBK and we finally obtained two 25 ml glasses, numbered A1 (Mangalia seawater) and A2 (Vama - Veche seawater) .

The sand, green algae and marine organisms samples were well washed with drinking and distilled water, they were mortared and they were dried in drying stove for three hours at 105°C.

The digestion was made with Hach Germany Digesdahl device by adding concentrated nitric acid and peroxide, [13].Next operating stage, we filtered them into 50 ml glasses and we poured them into photo boxes, numbered as it is shown in table 1.

Table 1 Our december 2004 samples ' details

Sample No .	Sample I.D.	Sample Mass (g)
1	algae	0.66
2	sand	0.60
3	Midia shells	0.60
4	hanos	0.75
5	anchovy	0.68

Atomic absorption spectrometry

All samples were analysed by atomic absorption spectrometry. I. Pecheanu used an ATI - UNICAM spectrometer, SOLLAR type with Zeeman correction cell, [10].

We used an AAS - 6200 SHIMADZU spectrometer with air - acetylene flame.

3. RESULTS AND DISCUSSION

The followed heavy metals were Pb, Cu, Cd, Zn and Fe. The obtained concentration levels for each heavy metal, in I. Pecheanu' s study, [10] and in our study, are shown in tables 2 and 3.

Table 2 I. Pecheanu ' s concentration obtained levels (ppm) for 1980 - 1997 samples, [10]

Heavy Metal / Sample I.D.	Pb	Cu	Cd	Zn	Fe
Hanos Fish	0.24	0.67	0.007	6.39	16.66
Anchovy	0.65	0.15	0.055	15.87	38.30
Midia Shells	< LD	7.09	3.27	189.35	191.04
Mangalia Seawater	1.12	1.55	1.89	12.50	7.08
Vama - Veche	0.50	4.26	1.61	11.54	5.05

These are average values of the obtained concentration levels between 1980 – 1997.

Table 3 Concentration obtained levels (ppm) for our december 2004 samples

Heavy Metal / Sample I.D.	Pb	Cu	Cd	Zn	Fe
1	1.97	< LD	0.04	0.29	20.46
2	0.56	< LD	0.09	0.05	78.83
3	3.14	0.12	0.15	9.66	37.26
4	1.91	< LD	0.09	2.43	28.89
5	2.25	< LD	0.14	1.62	4.74
A1	42.07	< LD	0.08	1.57	0.82
A2	1.99	< LD	0.11	2.42	< LD

where LD = detection limit .
The errors were between 2 - 5 % .

In the tables 4 and 5, we made a comparison between I. Pecheanu's determined concentration levels between 1980 - 1997, [10] and literature's concentration levels, offered by Curi, [6] and between our determined concentration levels for december 2004 samples and international standard concentration values, offered by M.B.H. Analytical, England, [14].

Analyzing Table 4 , we can see that :
- Pb determined concentration levels in all I. Pecheanu ' s collected samples is under literature ' s concentration levels;
- Cu is present in analysed samples, but in concentrations lower than literature ' s values;
- Cd is a very toxic heavy metal but I. Pecheanu ' s determined concentration levels are lower than Curi ' s results;
- Zn presence is important for growth and we notice a major increase of Zn determined concentration level in I. Pecheanu's Midia shells samples , compared to literature's dates; this is a proof that Mytilus Galloprovincialis is a very good natural " bioindicator " of pollution 's degree;
- in all samples, Fe obtained concentration levels exceeds for many times literature ' s concentration numbers.

From Table 5 , we can see that :
- Pb is present in our samples, exceeding for many times the international standard values, excepting sand samples in which determined concentration level is three times lower than international standard concentrations; this is not good for human's health because heavy metals produce disfunctions of the human body;
- Cu is not present in our december 2004 samples, excepting shells, but determined concentration level is lower than international standard value; Cu's lack in algae made them decoloured;
- Cd presence is very harmful for us and we observed that Cd outruns international standard values;
- we found Fe in our samples in concentration that exceeds for many times international standard value.

In table 6 , we made a comparison between I. Pecheanu ' s determined concentration levels from 1980 untill 1997

[10] and our december 2004 determined concentration levels.

Analyzing Table 6, we derived some conclusions about pollution variations between the two studies periods:

- our december 2004 Pb obtained concentration levels are bigger than I. Pecheanu's determined values, showing the increase of human and industrial activities influence over pollution degree;
- we know that Mytilus Galloprovincialis are very good water filters , retaining important amounts of heavy metals, bacteria or suspensions; so, it is not usual that I. Pecheanu found Cu in all samples; but, during the years, pollution degree decreased, so we did not find Cu;

- we observed that Cd concentration in some samples had a major decrease in december 2004, compared to 1997;
-in all analysed samples, 1997's Zn obtained concentration value was many times bigger than 2004;
- Fe was better absorbed by marine plants , organisms and water in I. Pecheanu's study time than it is nowadays .

The main conclusion of these investigations is that the studied zone does not contain high concentrations of heavy metals.

As a general conclusion, we can say that the marine environment along the Romanian seacoast of Black - Sea is not so polluted for beccoming a real danger for the area's human life and activities .

Table 4 Comparison between I. Pecheanu ' s determined concentration levels from 1980 untill 1997, [10] and literature's concentration levels , offered by Curi, [6]

Heavy Metal / Sample	Pb		Cu		Cd		Zn		Fe	
	I.Pecheanu's Determined Concentration (ppm)	Literature's Concentration (ppm)	I.Pecheanu's Determined Concentration (ppm)	Literature's Concentration (ppm)	I.Pecheanu's Determined Concentration (ppm)	Literature's Concentration (ppm)	I.Pecheanu's Determined Concentration (ppm)	Literature's Concentration (ppm)	I.Pecheanu's Determined Concentration (ppm)	Literature's Concentration (ppm)
Hanos Fish Anchovy	0.24 / 0.65	10 - 20	0.67 / 0.15	10 - 20	0.007 / 0.055	10 - 20	6.39 / 15.87	10 - 20	16.96 / 38.30	10 - 20
Midia Shells	< LD	10 - 20	7.09	10 - 20	3.27	10 - 20	189.35	10 - 20	191.04	10 - 20
Mangalia Seawater	1.12	4.00	1.55	1 - 25	1.89	0.003 - 0.006	12.50	7 - 21	7.08	-
Vama - Veche	0.50		4.26		1.61		11.54		5.05	

Table 5 Comparison between our determined concentration levels for our december 2004 samples and international standard concentration values , offered by M.B.H. Analytical , England , [14]

Heavy Metal / Sample	Pb		Cu		Cd		Zn		Fe	
	Determined Concentration (ppm)	International Standard Concentration (ppm)	Determined Concentration (ppm)	International Standard Concentration (ppm)	Determined Concentration (ppm)	International Standard Concentration (ppm)	Determined Concentration (ppm)	International Standard Concentration (ppm)	Determined Concentration (ppm)	International Standard Concentration (ppm)
Hanos Fish Anchovy	1.91 / 2.25	0.60 / 0.54	-	-	0.09 / 0.14	0.05 / 0.05	2.43 / 1.62	16.97 / 15.38	28.89 / 4.74	0.28 / 0.25
Midia Shells	3.14	0.47	0.12	3.56	0.15	0.04	9.66	13.53	37.26	0.22
Mangalia Seawater	42.07	0.02	-	-	0.08	0.04	1.57	6.42	0.82	-
Vama - Veche	1.99	0.02			0.11	0.04	2.42	6.42	-	
Sand	0.56	1.61	-	-	0.09	0.02	0.05	14.17	78.83	0.04

Table 6 Comparison between Pecheanu ' s determined concentration levels from 1980 untill 1997 , [10] and our december 2004 obtained concentration levels

Heavy Metal / Sample	Pb		Cu		Cd		Zn		Fe	
	I.Pecheanu's Determined Concentration (ppm)	Our Obtained Concentration (ppm)	I.Pecheanu's Determined Concentration (ppm)	Our Obtained Concentration (ppm)	I.Pecheanu's Determined Concentration (ppm)	Our Obtained Concentration (ppm)	I.Pecheanu's Determined Concentration (ppm)	Our Obtained Concentration (ppm)	I.Pecheanu's Determined Concentration (ppm)	Our Obtained Concentration (ppm)
Hanos Fish	0.24	1.91	0.67	< LD	0.007	0.09	6.39	2.43	16.96	28.29
Anchovy	0.65	2.25	0.15	< LD	0.14	0.14	15.87	1.62	38.30	4.74
Midia Shells	< LD	3.14	7.09	0,12	3.27	0.15	189.35	9.66	191.04	37.26
Mangalia	1.12	42.07	1.55	< LD	1.89	0.08	12.50	1.57	7.08	0.82
Seawater Vama - Veche	0.50	1.99	4.26	< LD	1.61	0.11	11.54	2.42	5.05	< LD

5.References

[1]. Gr. Antipa, "Marea Neagra", Editura Academiei Romane, Bucuresti , 1941.

[2]. M. Bacescu, Th. Busnita, R. Codreanu, "Ecologie marina", Editura Academiei Romane, Bucuresti, 1969.

[3]. S. Bonnefouse, "Omul sau natura?", Editura Politica, Bucuresti, 1976 .

[4]. E. D. Goldberg, "The health of the oceans", The Unesco Press, Paris, 1976 .

[5]. D. Wolfe, "La toxicite´ et la biacumulation de certaines substances dans les organisms marins", Rapport sur les pêches Nr. 334, Rovinj Yougoslavie, p. 1 - 22 , 1976 .

[6]. Curi, Kriton, "Pollution studies in the Sea of Marmara and the Black - Sea" , Rapp. P - V , CIESM 26, p. 223 - 236, 1978 .

[7]. U. Forstner, G. T. Wittman, " Metal pollution in the aquatic environment ", Heidelberg, Berlin, 1979 .

[8]. F. Yucesoy, M. Ergin, "Heavy metal geochemistry of recent sediments from continental shelf and slope of the southern Black - Sea ", in " Proceedings of the 44 th Geological Congress of Turkey ", Ankara, Turkey, 1991 .

[9]. M. I. Davies, "Guidelines for the use of sediments for marine pollution monitoring programmes", The Scotish agriculture and fisheries, Marine Laboratory, Abardeebn, Scotland, 1994 .

[10]. I. Pecheanu, R. Mihnea, "Distributia concentratiei de cupru in sedimentele superficiale din zona de mica adancime din dreptul litoralului romanesc", IRCM, Constantza, Romania, 1994 .

[11]. A. Cociasu, L. Dorogan, G. Huborg, L. Popa, "Long - term ecological changes in Romanian coastal waters of Black - Sea", Marine Pollution Bulletin 32, p. 32 - 38, 1996 .

[12]. W. R. Fairbridge, "The encyclopedia of oceanography. Encyclopledia of earth sciences series", vol. I, Reinhold Publishing Corporation, New York, 1996 .

[13]. E. Chirila, "Chimie analitica.Aplicatii", Editura Universitatii " Ovidius ", Constantza, Romania, 2000 .

[14]. M.B.H. Analytical, International Standards, England   .

V. GHISA[1]

I.V. POPESCU[2]

V. CIUPINA[3]

M. BELC[3]

STUDY OF GEOLOGICAL - ARCHAEOLOGICAL SAMPLES BY AAS METHOD

[1]Master in Statistical Mathematics , *Transilvania* University of Brasov
[2] Valahia University of Targoviste, Physics Department, Faculty of Science,
[3]Ovidius University of Constanta

Abstract: : In a feasibility study, AAS analysis was performed in an attempt to classify samples obtained at Sinca Veche, an archaeological site in Romania

1. Introduction

One of the most important factors is the scientific examination of antiquities including the application of AAS analysis of the interior composition of an object with ancient symbolic representations. It is in the speed of analysis that AAS has a clear advantage. By example, it is common for NAA to require one or two reactor irradiations followed by cooling periods and then at least 100 min of counting time whereas AAS analysis of a given sample can be performed in about 10-15 min. This paper will present the results of an application of AAS to the study of preroman inscriptions from the ancient site of Sinca Veche.

2. Experimental procedure

There are five different places from where the samples were taken and these elements were observed by AAS method in order to determine the metal concentration of traces. For a proper concentrations determination of the geological solid sample those were taken for a preliminary process of atomisation. The device was given from HACH and it made up in order to realise a complete mineral state in about 3-12 min with a low consume of reactive. The samples were attacked with 8 ml of nitric acid concentrated, a boiling of the mixture followed during 3 minutes.   After a process of cooling (5 min), the sample was ready to be analized in the spectrometer. The samples taken to solvent were observed with a Schimadzu spectrofotometer, present in one of laboratories of Ovidius University of Constanta, which is assisted by a computer having incorporated a AA-6200 soft. After the proper selection of lamp which correspond with the analized element, it`s an initialisation of the programme specific for the element. For emitted radiation was used the next wavelenghts:

$Fe(\lambda=248,3nm)$, $Cu(\lambda=324,8nm)$, $Zn(\lambda=213,9nm)$, $Pb(\lambda=283,3nm)$, $Cd(\lambda=228,8nm)$. From the window of the element the selection operation is automatically don for the wavelenght (the monocromator searches the emitted wavelenght by the lamp) and the collimation system of the hollow cathode lamp, which emitted fascicle. The operation is preceded by the reading of the debits values for the gas mixture by burning, after that the gas is fired. Every chemical element has a characteristic temperature of excitation, which is obtained through the mixture air and acetylene.

The background correction is done through this method. The programme makes 3 or 5 readings and that the meaning value precedes. The value of concentration is calculated by programme and it`s reported after that to the calibration curve. In the end, there obtain different concentrations in (ppm) of Fe, Zn, Pb, Cu, in every sample.

3. Results and discussion

Because of the very point of this analyse is the determination of elements concentrations in taken samples even in the old human activities signs of tackled stones we can observe a comparative sorting of results varying on the importance for every location of the taking samples. We determined the next concentrations of Fe(table 1), Zn(table 2), Pb(table 3), Cu(table 4) on the samples.

In conformity with the value of the analyse there result the next features: The main representations of recess (field 1) the sample was taken from the central domain, and there observe (in the hypothetically presence of a convergence centre of the ritual place) because there exists a lot of raised concentrations of Zn(20.23), Cu(29.55), Fe(100.83) from all other fields focused in the observation. The elements of Cu, Zn can takes from the tools traces with whom the recess was processed, if those are manufactured by brass. A nearly hypothesis is possible for Fe. The location 1 and 4 are also possible to present almost exclusively structural the characteristic features which are independent by the human activity, but this fact could make them attractive and having given special destination points.

Regarding the sample 4 we observe a raised concentration of Pb(45.90), Fe(100.04) and comparatively with the other samples this contains Cd traces, this fact making us consider that the metals which were used here are different by those used in the field 1 and those 1 which has a more recent provenience, the Pb having the quality of higher mechanical properties in the metallic structure, respectively plasticity, mechanical endurance and relative elongation.

As a standard zone regarding the contain of analized element, we can consider the field from where we took the sample 5 and which are characterized by Fe(50.92), Zn(3.98), Cu(1,07) concentration and Pb, Cd traces are not detectable. We also can't observe in this field the human activity signs and just process of natural degradation.

Comparatively we observe that the field 1 and 4 are in the top in order of functional importance.

Table 1

Sample	Mass from the d	Dilution volu	Absorbance	Concentration SA	Standard dev	Concentration fr
S1	0.4733	25	0.0604	0.1909	±0.0002	93.842
S2	0.7365	25	0.0016	0.0725	±0.0008	24.607
S3	0.2413	25	0.0020	0.0810	±0.0007	83.903
S4	0.5135	25	0.0070	0.2055	±0.0014	94.825
S5	0.6726	25	0.0042	0.1370	±0.0016	50.921

Table 2

Sample	Mass from the d	Dilution volu	Absorbance	Concentration SA	Standard dev	Concentration fr
S1	1.3806	50	0.2457	0.5587	±0.0009	20.233
S2	0.8522	50	0.0997	0.1977	±0.0032	11.599
S3	1.1573	50	0.1190	0.2455	±0.0020	10.606
S4	0.5720	25	0.0889	0.1712	±0.0016	7.482
S5	1.4785	50	0.0673	0.1177	±0.0013	3.981

Table 3

Sample	Mass from the d	Dilution volu	Absorbance	Concentration SA	Standard dev	Concentration fr
S1	1.3806	50	0.0091	0.1619	±0.0012	5.863
S2	0.8522	50	0.0122	0.3575	±0.0013	20.957
S3	1.1573	50		undetectable		
S4	0.5720	25	0.0233	1.0503	±0.0006	45.904
S5	1.4785	50		undetectable		

Table 4

Sample	Mass from the d	Dilution volu	Absorbance	Concentration SA	Standard dev	Concentration fr
S1	1.3806	50	0.0974	0.8162	±0.0070	29.559
S2	0.8522	50	0.0136	0.0593	±0.0021	3.479
S3	1.1573	50	0.0104	0.0305	±0.0005	1.317
S4	0.5720	25	0.0248	0.1605	±0.0016	7.014
S5	1.4785	50	0.0106	0.0319	±0.0007	1.078

5.Conclusions

We observe that, indeed, there exist some concentration of characteristic elements from which the antique tools were manufactured in the chiselled representation of sanctuary walls, the tools having the base of alloys by Cu-Zn(brass).

We could make a contrastive study of different fields from location in order to observe the AAS determined concentration for Fe, Zn, Cu, for the analogies to establish the importance of the different fields of location.

The study needs to be improved in future by the determination of the other elements concentration, the area of research being enlarged in order to make a more detailed analyse.

5.References

[1] E.Chirila, S.Birghila, P.Capota: *Biogeochemical characterisation of an ecosystem using ICP-AES*, Ovidius Univ. Constanta 1999.
[2] Shimadzu Corporation Analytical Instrument Division Kyoto Japan: *Instruction manual AA-6200.*

GHEORGHE VALERICA CIMPOCA[1]

NANOGEOSCIENCE

[1]Valahia University of Targoviste, Faculty of Science and Arts, Physics Department, cimpoca@valahia.ro

Abstract: Nanogeoscience addresses a number of issues crucial to the geological sciences: the transport of metals and organics in the near-surface environment; global geochemical and climate cycles (including the carbon cycle); ore genesis and exploitation, soil science; microbial geochemical action; origin of life; space weathering and planetary surfaces; atmospheric particle transport and ice nucleation; and even deep Earth processes. Nanogeoscience also addresses national needs: environmental safety, national security, and human health; mining, minerals, oil, and gas; environmentally friendly manufacturing and new geomimetic materials; and agriculture and food.
The chemical and physical interactions that characterize the interface between a biomolecule and crystal structure can play a major role in natural processes such as, mineral dissolution, biomineralization, bacterial adhesion, and biofilm development, as well as technological advances such as nanolithography, self-assembling reactions, and bioremediation strategies.

1. Introduction

Nanogeoscience is broadly defined to include the study of materials and processes at the nanoscale in their role in geologic processes on the Earth and other planets. Because many nanoscale phenomena are concentrated near the Earth's surface, in the region sometimes referred to as the *critical zone* and comprising land, water, air, and the immediate subsurface environment, these phenomena are of crucial importance to humans. Because processes are intrinsically molecular at the nanoscale, there is an immediate synergy and a diffuse boundary between nanogeoscience and the fields of chemistry, physics, and materials science. Furthermore, geoscientists increasingly recognize the major role played by microorganisms in geologic phenomena. There is an equally fuzzy boundary between nanogeoscience and the life sciences in this realm because microbial processes often proceed by manipulating surface forces at the nanoscale.

Geoscientists have unique skills in aqueous and solid state chemistry, particularly in complex multicomponent systems. They study phenomena occurring on a vast range of scale, both in space (nanometers to thousands of kilometers) and time (nanoseconds to billions of years). Such a multiscale approach to scientific

problems is necessary in monitoring and minimizing the effects of pollution, evaluating the toxicity of materials, and ensuring the safety of water and food supplies. Furthermore, we are just beginning to explore technological applications of the incredibly diverse and functional materials produced by geochemical and biogeochemical processes. In addition, research on processes at the nanoscale accelerates the healthy evolution within Geosciences toward understanding geologic process from the molecular to the global scale. This evolution is important both intellectually and because the nation increasingly needs expert opinions on short-term problems, such as strategies to minimize pollution, the toxicity of materials, the safety of water and food supplies, and the identification of new useful materials for industry.

The Venn diagram below shows how nanoscience is central to many important problems in Earth science and how nanogeoscience links Earth science to other disciplines.

2. The Significance of Nanoscience to the Geoscience

On land, researchers study how nanosized minerals capture toxins such as arsenic, copper, and lead from the soil. Facilitating this process, called soil remediation, is a tricky business. Some toxins weakly adhere to particles through electrostatic forces while others precipitate onto a particle's surface, forming chemical bonds that are more difficult to undo. Even more troublesome is aggregation, in which the precipitated toxin is sandwiched between the grains of a particle. As Waychunas explains, learning how these processes work on the nanoscale could greatly improve the effectiveness of remediation efforts. Another promising soil remediation strategy links nanogeoscience with biomimetics, an equally new field in which researchers design substances that mimic biological processes. For example, researchers are interested in natural processes in which microbes produce minerals that are highly reactive and therefore ideal components of a toxic uptake system. Taking this a step further, they hope to manipulate microbes into producing nanosized minerals of specific sizes and shapes that most efficiently bind with toxins. Other research explores the changing characteristics of particles as they become smaller. At the nanoscale, for example, there are many more atoms associated with the surface of a particle than the interior. This intrigues researchers like Waychunas, because

most chemical reactions occur on the surface of minerals, large and small. But what's true for a fist-sized chunk of quartz doesn't necessarily translate to a particle only a few molecules across. At this minute size, surface properties can change, meaning the nature of these all-important surface reactions also changes.

This paper contains several examples, based on one graphic and a descriptive figure caption. Its purpose is to highlight a few exciting recent developments in nanogeoscience and to demonstrate the breadth and variety of the work done.
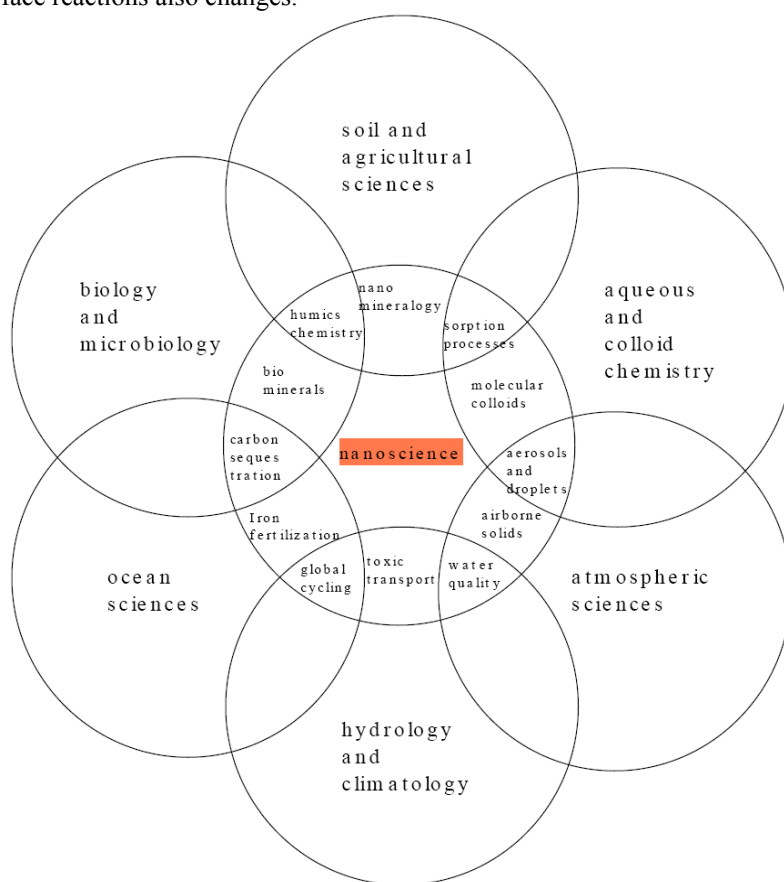

Fig.1 Venn diagram showing overlaps of traditional environmental science s with nanoscience . We suggest that all of such overlaps define Nanogeoscience.

3.1 Mineral surface adsorbates: quartz with iron

We are just beginning to appreciate the complexity of precipitate development on mineral surfaces in response to adsorbate aggregation, drying reactions, surface catalyzed reactions, and redox variations. The AFM image shows a highly polished (0.2 nm rms roughness) m-plane surface of synthetic quartz that has been exposed to a 10^{-4} M solution of Fe^{3+} at low pH (figure 2). Precipitates of Fe hydroxide have formed on the surface, with a significant concentration along the edges of the step structure. The surface topology is that of steps and terraces which look like a corduroy pattern. The individual steps are 0.25 nm high, while the terraces average 80 nm in width. The cartoon crystal structure image shows what this looks like on edge. Clearly, the edge of the steps provide a unique location for initial attachment of sorbed Fe^{3+}, and later formation of oxyhydroxide precipitates

3.2 Uraninite nanocrystals in carbonaceous particles in the atmosphere

There is increasing concern for the health effects of fine particles (less than a micron) inhaled from polluted air. Aerosols collected from Detroit contain very small amounts of uranium. Due to these extremely low concentrations (< 10 ppm), the form of the uranium has been unknown. American scientists identified nanocrystals of uraninite, UO2+x, encapsulated in carbonaceous matter (about 50 nm) with a structure similar to that of fullerene. (a) HRTEM image of U-bearing nanoparticles encapsulated in a "cage" of fullerene. (b) HRTEM of the U-particle. The matrix carbon has lost its structure because of the focused electron. The inset is the Wiener-filtered image of the area outlined by the white square

Fig.2.The AFM image shows a highly polished (0.2 nm rms roughness) m-plane surface of synthetic quartz that has been exposed to a 10^{-4} M solution of Fe^{3+} at low pH.
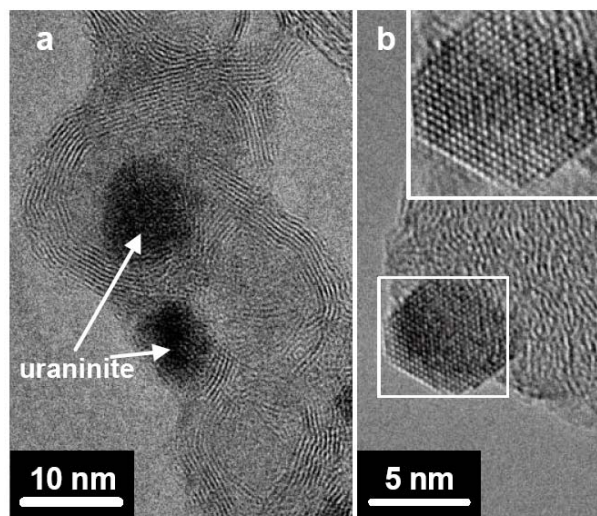

Fig.3. (a) HRTEM image of U-bearing nanoparticles encapsulated in a "cage" of fullerene. (b) HRTEM of the U-particle.

3.3 Nanoscale Bacterial Protein Layers

Recent experiments suggest that the intimacy between the biological and geophysical worlds is preserved in the genetic make- up of microorganisms such that there is a natural affinity or specificity between bacterially produced macromolecules and minerals. Lower et al. are using force microscopy to quantify the natural, inter- and intra-molecular forces between bacterially produced biopolymers and mineral surfaces (Lower et al.,2000; 2001). Force measurements have revealed that dissimilatory metal reducing bacteria command exquisite control of protein synthesis such that specific outer membrane proteins are produced to mediate contact with iron hydroxides as opposed to aluminum hydroxide isostructures (Lower et al., 2001). This information is being used to create a lithographic technique in which a living cell is induced to fabricate various biomolecular patterns on inorganic surfaces, thereby creating nanoscale domains of different structures and functions (see figure 4).
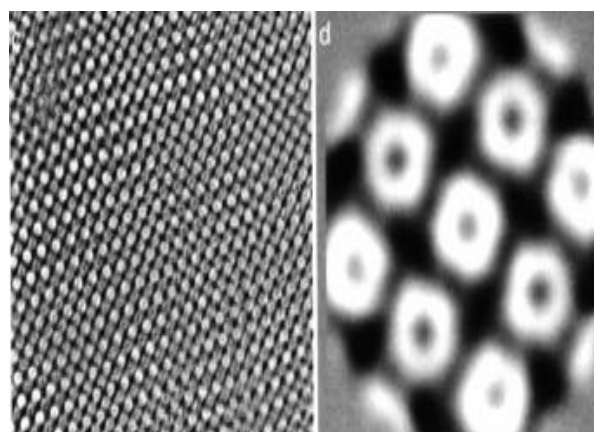
Fig.4. Bacteria produce paracrystalline protein layers on their outer surfaces. The ones shown here have center-tocenter spacing between donuts of 11 nm (b is higher resolution of a). A fundamental goal is to understand how cells modulate intermolecular forces of interaction between these biopolymers and nascent minerals such that bacteria control the growth or dissolution of select mineral phases.
Images courtesy of T. Beveridge.

4. Relevance to National Needs

We decided to commit of the research and development (R&D) of novel nanobiotechnological techniques, available for the industrial extraction and exploitation of georesources: NanoGeoScience.
Targets of R&D are: • Sustainable resource extraction of solid, liquid, and gaseous phases with the focus on high-strength materials in complex multi-component systems. • Non-thermal molecular phase separation and a more effective byproduct mitigation by molecularly tailored catalysts. • Cheap nanofabrication from low-grade georesources by environmental friendly manufacturing governed by the principles of sustainable development.
To integrate more fully into the national nanoscience initiative, the growing nanogeoscience community needs access to specialized techniques and samples and better coordination of scientific and educational activities. We need improved access to major facilities such as synchrotrons and neutron sources with EXAFS, XANES, and related x-ray spectroscopies, including those suitable for light elements, spatially resolved
chemical analytical techniques, diffraction and small angle scattering, and synchrotronbased infrared spectroscopy. We also need user-friendly access to smaller, but still quite specialized, facilities which offer both equipment and expertise in electron microscopy, NMR, thermal analysis and calorimetry, x-ray diffraction, isotopic measurements, uv-visible, infrared, and Raman spectroscopy, Mössbauer spectroscopy, AFM, STM, and other probe microscopy, and other techniques. Even when a technique is relatively well established, its application to nanomaterials offers special challenges.
We need to identify, synthesize, and disseminate reference nanoparticles and porous materials appropriate to the geosciences. We need new techniques for manipulating small samples, for isolating nanoclusters from solution, and for characterizing nanoparticles and nanopores. We need to complement lab studies with large-scale experiments and field trials. We need improved computational methods for molecular modeling and to better integrate theory and experiment.
We need to coordinate graduate education and offer interdisciplinary training in both concepts and techniques. Such experience often transcends the boundaries of any given discipline or institution. We need to attract and prepare graduate students for multifaceted careers in academe, industry, and government. The national laboratories have a great need for American graduates trained in nanogeoscience. We

need to communicate our science to the general public and to provide guidance in policy issues in which nanoparticles are important.
A distributed center in nanogeoscience is an excellent way to serve community needs in science, facilities, education, and outreach.

5. Conclusions

A fundamental goal of the Nanogeoscience community is to understand the properties of nanoparticles that change disproportionately with size and distinguish them from those that simply scale with surface area. We must then understand how both the enhanced surface reactivity and the unique nanoscale properties affect geologic processes. A related subject is to describe the chemistry of very small pores of nanometric dimension and understand how they influence the integral chemistry of the Earth. Two examples illustrate the geologic application of fundamental nanoscale science. The catalytic properties of zeolites relate to how their nanopores constrain the reactants and it is likely that nanopores in sediments and rocks have analogous unique chemistries that we do not yet understand. In oxides developed for magnetic memories and other applications, the ability to maintain magnetization over time decreases as the particle size diminishes. For materials science applications such as compact discs, the concern is about stability of magnetic memory over months to decades. In paleomagnetism, the concern is on a time scale of millions of years. The growing nanogeoscience community needs access to specialized techniques and samples and better coordination of scientific and educational activities. Specifically, the following needs are identified: Shared Facilities and Expertise; Reference Materials; New Methods for Manipulating Small Samples; Isolating Nanoclusters from Solution; *In Situ* Methods of Characterizing Nanoclusters and Nanopores; Large Scale Experiments and Field Trials; Integration with Geomicrobiology; Molecular Modeling;

6. Bibliography

[1].Waychunas, GA, Davis JA and Reitmeyer, R (1999) GIXAFS study of Fe3+ soprtion and precipitation on natural quartz surfaces. J. Synchrotron Rad. 6, 615-617.
[2]. S. Utsunomiya and R. C. Ewing, (2002), Environmental Science & Technology.
[3]. Lower S. K., Hochella M. F., and Beveridge T. J. (2001a) Bacterial recognition of mineral surfaces. Nanoscale interactions between *Shewanella* and ? - FeOOH. *Science* **292**, 1360-1363.
[4]. Report of the Nanogeoscience Workshop, Berkeley CA, June 14-16,2002.
[5]. V.Cimpoca, Nanogeoscience, Workshop, Targoviste, June 2-3, 2005.

GABRIEL DIMA[1]

CLAUDIA STIHI[1]

CALIN OROS[1]

SERGIU DINU[1]

LAUR MANEA[1]

SIMONA APOSTOL[1]

WATER QUALITY ANALYSIS BY ATOMIC ABSORBTION SPECTROSCOPY

[1]Valahia University of Targoviste, 2 Regele Carol blvd., Targoviste, Romania

Abstract: Water is one of the most essential constituents of the human environment. The water resources generate development in socio-economical issues crucial to the society in general and more specifically for industries, agricultural activities and for the public use. Although it is agreed that water is an economic good, it is also a social good, finite, non-substitutable and vital to all forms of life. The last three elements make water not just like any other commodity but a good that should be conserved and treasured. Water is vulnerable to contamination at all points in the hydrologic cycle, and all pathways that transport water can also carry pollutants. Land use activities and wastewater discharges can degrade water quality. Many practices of the past, especially for waste disposal, which were not known at that time to have serious adverse water quality impacts have left behind long lasting contamination problems. Surface water classifications are designations applied to surface water bodies, such as streams, rivers and lakes, which define the best uses to be protected within these waters (for example swimming, fishing, drinking water supply) and carry with them an associated set of water quality standards to protect those uses. Atomic-absorption (AA) spectroscopy uses the absorption of light to measure the concentration of gas-phase atoms. From this reason, AAS is a better tool for water quality analysis.

1. Introduction

Water quality is affected by the many substances water contacts during its movement through the hydrologic cycle. Water dissolves a wide variety of minerals, nutrients, and other substances from soils, rocks, and the atmosphere, and carries them in solution. Lakes, streams, and groundwater accumulate these dissolved substances and reflect the distinctive characteristics of their watershed's soils, geology, and land use. Human activities also can change the composition of surface runoff and groundwater. Water is vulnerable to contamination at all points in the hydrologic cycle, and all pathways that transport water can also carry pollutants. Land use activities and wastewater discharges can degrade water quality. Many practices of the past, especially for waste disposal, which were not known at that time to have serious adverse water quality impacts have left behind long lasting contamination problems.

Some agricultural and forestry practices have had significant impacts on water quality. Soils denuded of protective vegetation have the potential for rapid erosion. Sediment entering lakes and streams from surface runoff reduces water clarity, thus shading aquatic plants, smothering eggs, or interfering with an animal's ability to catch prey or avoid predators. Nutrients, primarily nitrogen and phosphorus, enter water through surface runoff and stimulate plant growth which may become a nuisance and indirectly contribute to periodic reductions in dissolved oxygen, causing fish kills. Many pesticides and herbicides are extremely toxic to aquatic species and may enter surface waters because of over application, wind drift, or surface runoff. Even when these substances are present in nonlethal quantities, they can interfere with fish reproduction and growth or kill aquatic insects, which are a major food source of many game fish. Urban areas also contribute pollution through surface runoff and storm sewers. When the land surface is sealed by concrete and asphalt, very little infiltration occurs. During a storm, rainwater washes over the surface, picking up oils, grease, soil, salt, and anything else in its path. The contamination can enter surface waters through direct surface runoff, or through storm sewers. When storm sewers are separate from sanitary or human waste sewers, the stormwater, often untreated, is released directly into surface waters. When storm and sanitary sewers are combined, street runoff and sewage are treated by the wastewater treatment plant prior to discharge. During a storm, the combined sewer often overflows the capacity of the plant, and untreated sewage is released into the river with the contaminated stormwater.

2. Surface water classifications

Lakes, rivers, reservoirs, ponds, etc., are termed surface waters. They receive water directly from precipitation and surface run-off. These various bodies of water also receive a portion of their total amount from underwater springs connected with the groundwater supply. As we have known, surface waters are generally lower in mineral content. On the other hand, they possess far more contamination and are unsafe to use for human consumption unless properly treated.

Pollution of water comes from many sources. Municipalities and industries sometimes discharge waste materials into bodies of water that are used as public sources of supply. This is a most serious source of contamination. Surface run-off also brings mud, leaves,

decayed vegetation together with human and animal wastes into streams and lakes. In turn, these organic wastes cause algae and bacteria to flourish.

There is a belief that rivers and streams purify themselves in the course of their flowing 20 miles. This action should not be taken for granted, however.

Organic pollution of water is reduced by nature in many ways:

1. Bacteria and algae consume large quantities of organic waste. Larger microorganisms devour the bacteria and algae. In turn, the microorganisms provide food for fish and other higher forms of animal life.

2. Unless the rate of flow is too fast, mud and suspended matter will naturally settle to the bottom and oxidation will render organic matter harmless. Rough bed streams, riffles and spillways speed this process.

3. Due to its ultraviolet rays, sunlight also has some germicidal effect on the water. Sunlight is not constant due to cloudy weather and its unavailability at night.

Rivers and streams also show great variations in their dissolved mineral content.

In general, lakes and reservoirs (especially large ones) show fairly constant dissolved solids content. Because they are relatively more quiet than moving bodies of water, lakes and reservoirs are very efficient settling basins. The result is they possess less turbidity. Large bodies of water are frequently subject to seasonal changes that cause the water to become quite turbid for a period of time. Our definition of water states that it achieves its maximum density at 3.8^0C. As it becomes chilled to this point in the fall or warmed to it in the spring, the denser water cannot stay at the top. As it sinks, it causes convection currents to be set up. Sometimes these become so strong that they lead to a complete overturning of the water and bring about the turbid condition. Heavy storms will also churn up a lake or reservoir and make it turbid.

Surface water classifications are designations applied to surface water bodies, such as streams, rivers and lakes, which define the best uses to be protected within these waters (for example swimming, fishing, drinking water supply) and carry with them an associated set of water quality standards to protect those uses. Surface water classifications are one tool that state and federal agencies use to manage and protect all streams, rivers, lakes, and other surface waters in North Carolina. Classifications and their associated protection rules may be designed to protect water quality, fish and wildlife, the free flowing nature of a stream or river, or other special characteristics.
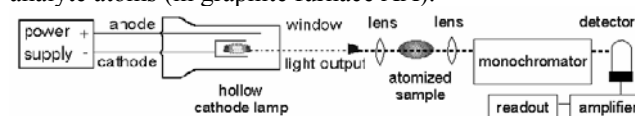
3. Experimental

Atomic-absorption (AA) spectroscopy uses the absorption of light to measure the concentration of gas-phase atoms. When atoms or molecules absorb light, the incoming energy excites a quantified structure to a higher energy level. The type of excitation depends on the wavelength of the light. Electrons are promoted to higher orbitals by ultraviolet or visible light, vibrations are excited by infrared light, and rotations are excited by microwaves.

An absorption spectrum is the absorption of light as a function of wavelength. The spectrum of an atom or molecule depends on its energy level structure, and absorption spectra are useful for identifying of compounds.

Measuring the concentration of an absorbing species in a sample is accomplished by applying the Beer-Lambert Law. Since samples are usually liquids or solids, the analyte atoms or ions must be vaporized in a flame or graphite furnace. The atoms absorb ultraviolet or visible light and make transitions to higher electronic energy levels.

The analyte concentration is determined from the amount of absorption. Applying the Beer-Lambert law directly in AA spectroscopy is difficult due to variations in the atomization efficiency from the sample matrix, and nonuniformity of concentration and path length of analyte atoms (in graphite furnace AA).

Figure 1 The experimental set-up

The light source is usually a hollow-cathode lamp of the element that is being measured. Hollow-cathode lamps are a type of discharge lamp that produce narrow emission from atomic species. They get their name from the cup-shaped cathode, which is made from the element of interest. The electric discharge ionizes rare gas atoms, which are accelerated into the cathode and sputter metal atoms into the gas phase. Collisions with gas atoms or electrons excite the metal atoms to higher energy levels, which decay to lower levels by emitting light.

Lasers are also used in research instruments. Since lasers are intense enough to excite atoms to higher energy levels, they allow AA and atomic fluorescence measurements in a single instrument. The disadvantage of these narrow-band light sources is that only one element is measurable at a time.

AA spectroscopy requires that the analyte atoms be in the gas phase. Ions or atoms in a sample must undergo desolvation and vaporization in a high-temperature source such as a flame or graphite furnace. Flame AA can only analyze solutions, while graphite furnace AA can accept solutions, slurries, or solid samples.

Flame AA uses a slot type burner to increase the path length, and therefore to increase the total absorbance (see Beer-Lambert law). Sample solutions are usually aspirated with the gas flow into a nebulizing/mixing chamber to form small droplets before entering the flame.

The graphite furnace has several advantages over a flame. It is a much more efficient atomizer than a flame and it can directly accept very small absolute quantities of sample. It also provides a reducing environment for easily oxidized elements. Samples are placed directly in the graphite furnace and the furnace is electrically heated in several steps to dry the sample, ash organic matter, and vaporize the analyte atoms.

Light separation and detection

AA spectrometers use monochromators and detectors for uv and visible light. The main purpose of the

monochromator is to isolate the absorption line from background light due to interferences. Simple dedicated AA instruments often replace the monochromator with a bandpass interference filter. Photomultiplier tubes are the most common detectors for AA spectroscopy.

Photomultiplier Tubes (PMTS) are light detectors that are useful in low intensity applications such as fluorescence spectroscopy. Due to high internal gain, PMTs are very sensitive detectors.

PMTs are similar to phototubes. They consist of a photocathode and a series of dynodes in an evacuated glass enclosure. Photons that strikes the photoemissive cathode emits electrons due to the photoelectric effect. Instead of collecting these few electrons (there should not be a lot, since the primarily use for PMT is for very low signal) at an anode like in the phototubes, the electrons are accelerated towards a series of additional electrodes called dynodes. These electrodes are each maintained at a more positive potential. Additional electrons are generated at each dynode. This cascading effect creates 10^5 to 10^7 electrons for each photon hitting the first cathode depending on the number of dynodes and the accelerating voltage. This amplified signal is finally collected at the anode where it can be measured.

The Beer-Lambert law (or Beer's law) is the linear relationship between absorbance and concentration of an absorbing species. The general Beer-Lambert law is usually written as:

$$A = a(\lambda) \cdot b \cdot c$$

where A is the measured absorbance, $a(\lambda)$ is a wavelength-dependent absorptivity coefficient, b is the path length, and c is the analyte concentration. When working in concentration units of molarity, the Beer-Lambert law is written as:

$$A = \varepsilon \cdot b \cdot c$$

where epsilon is the wavelength-dependent molar absorptivity coefficient with units of M^{-1} cm^{-1}.

Experimental measurements are usually made in terms of transmittance (T), which is defined as:

$$T = I / I_o$$

where I is the light intensity after it passes through the sample and I_o is the initial light intensity. The relation between A and T is:

$$A = -\log T = -\log (I / I_o).$$

Modern absorption instruments can usually display the data as either transmittance, %-transmittance, or absorbance. An unknown concentration of an analyte can be determined by measuring the amount of light that a sample absorbs and applying Beer's law. If the absorptivity coefficient is not known, the unknown concentration can be determined using a working curve of absorbance versus concentration derived from standards.
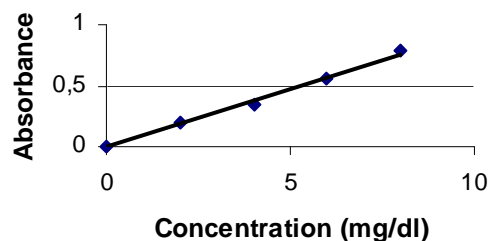
Figure 2 The working curve

The linearity of the Beer-Lambert law is limited by chemical and instrumental factors. Causes of nonlinearity include:

- deviations in absorptivity coefficients at high concentrations (>0.01M) due to electrostatic interactions between molecules in close proximity
- scattering of light due to particulates in the sample
- fluoresecence or phosphorescence of the sample
- changes in refractive index at high analyte concentration
- shifts in chemical equilibrium as a function of concentration
- non-monochromatic radiation, deviations can be minimized by using a relatively flat part of the absorption spectrum such as the maximum of an absorption band
- stray light

4. Results and discussions

We have collected surface water samples from Cricovul Dulce river. The collected samples were analyzed by AAS method at Targoviste Stainless Steel Factory in order to determine the degree of pollution of the Cricovul Dulce river who cross along the important industrial zones from Dambovita region.

Standard Value of Surface Water for Class 1, 2 and 3 are presented in the Table 1:

Table 1
Standard Value of Surface Water for Class 1,2 and 3

	Standard Value (mg/l) of Surface Water for Class:		
Element	**1**	**2**	**3**
Calcium (Ca)	1	3	3
Iron(Fe)	0.3	1	1
Copper (Cu)	0.05	0.05	0.05
Nickel (Ni)	0.1	0.1	0.1
Manganese (Mn)	0.1	0.3	0.8
Zinc (Zn)	0.03	0.03	0.03
Cadmium (Cd)	0.003	0.003	0.003
Cr (hexavalent)	0.5	0.5	0.5
Lead (Pb)	0.05	0.05	0.05
Sodium (Na)	100	200	200

Class 1 means very clean fresh surface water, ecosystem conservation where basic organisms can breed naturally, resources used for:

- Consumption which requires ordinary water treatment processes before use
- Aquatic organism of conservation

- Fisheries
- Recreation

Class 2 means medium clean fresh surface water resources used for:

- Consumption, but passing through an ordinary treatment process before use
- Agriculture

Class 3 means fairly clean fresh surface water resources used for:

- Consumption, but requires special water treatment process before use
- Industry

We can report that for the most of the elements the analyzed surface water were classified in class 2.

5. References

[1] Davies, B. R. and Walker, K. F. The ecology of river systems. 1986, John Wiley & Sons, New York.,75-82
[2] Dix, H.M. (1981). Environmental Pollution. John Wiley, Chichester, 121-124
[3] J. Koski-Vähälä, H. Hartikainen and P. Tallberg Journal of Environmental Quality 30:546-552 (2001)

WAVELETS AND FRACTALS ANALYSIS IN CANCER THERAPY

R.M.ION[1,2]

S.APOSTOL[3]

V.I.R.NICULESCU[4]

1   Valahia University, Faculty of Materials Engineering, Mechathronics and Robotics, Targoviste
2   ICECHIM, Bucharest, Romania;
3   Valahia University of Targoviste, Faculty of Sciences, Physics Departement
4   National Institute for Laser, Plasma and Radiation Physics, Bucharest, Romania

Abstract: The aim of this paper is to analyze TEM images in order to obtain fractal dimensions of 3-dimensional objects and to apply the method to some porphyrins used in cancer therapy. The "mass-radius" relation is used to compute fractal dimension of TEM micrograph.

The computer methods are often based on Fourier transformations, convolution with a filter and deconvolution techniques, polynomial interpolation, so on. In this way, is possible to make more visible the boundaries between tissues.

This paper is based on wavelet transform analysis (WTA) used for the enhancement and delimitation of human tumor area from some micrograms recorded before and after photodynamic (PDT) treatment. The proposed algorithm improves the detection performance through the use of image processing multiresolution analysis with a new type of bidimensional window and wavelet approximation. This paper is based on wavelet transform analysis (WTA) used for the enhancement and delimitation of tumor area from some micrograms recorded before and after photodynamic (PDT) treatment.

1. Introduction

Western culture is obsessed with order, smoothness and symmetry, to the point that we often impose on nature patterns and models derived from classical Greek geometry. Historically this tendency can be traced to Plato, for whom the 'real' world consisted of smooth, Euclidean shapes created by a supreme being. Plato was able to reconcile the inability of classical geometry (as later formulated by Euclid) to describe the world we inhabit.

Fractal theory offers methods for describing the inherent irregularity of natural objects. In fractal analysis, the Euclidean concept of 'length' is viewed as a process.

This process is characterized by a constant parameter D known as the fractal (or fractional) dimension. The fractal dimension can be viewed as a relative measure of complexity, or as an index of the scale-dependency of a pattern. Excellent summaries of basic concepts of fractal geometry can be found in Mandelbrot (1982).

The fractal dimension is a summary statistic measuring overall 'complexity'. Like many summary statistics (e.g. mean), it is obtained by 'averaging' variation in data structure.

Biologists have traditionally modelled nature using Euclidean representations of natural objects or series. Biological systems and processes are typically characterized by many levels of substructure, with the same general pattern being repeated in an ever-decreasing cascade. Most biological processes and structures are decidedly non-Euclidean, displaying discontinuities, jaggedness, and fragmentation. Nonetheless, fractal geometry is far closer to nature than is Euclidean geometry.

Using a fractal approach, the complex surface of tree bark is readily quantified. The higher the fractal dimension D, the greater the perceived rate of increase in length (or surface) with decreasing scale.

Formally, a mathematical fractal is defined as any series for which the Hausdorff dimension (a continuous function) exceeds the discrete topological dimension. Topologically, a line is one-dimensional. The dimension D of a fractal 'trace' on the plane, however, is a continuous function with range $1 \leq D \leq 2$.

A completely differentiable series has a fractal dimension $D = 1$ (the same as the topological dimension), while a Brownian trace completely occupies two-dimensional topological space and therefore has a fractal dimension $D = 2$. Fractal dimensions $1 \leq D \leq 2$ quantify the degree to which a trace 'fills' the plane. In the same way, a planar curved surface is topologically two-dimensional, while a fractal surface has dimension $2 \leq D \leq 3$. Consider estimation of the length of a complex 'coastline'. For a given spatial scale, the total length L is estimated as a set of N straight-line segments of length l. Because small 'peninsulas' and other features not recognized at coarser scales become apparent at finer scales, the measured length L increases as decreases. This dependence of length on measurement scale is a fundamental feature of fractal objects. The relationship between length and measuring scale is summarized by the power law:

$$\delta = \delta^{(1-D)}$$

where K is a constant. The fractal dimension ($1 \leq D \leq 2$) quantifies the degree of coastline complexity. In practice, D can be estimated from the slope of the log-log plot:

$$\log L = \log K + (1 - D)\log$$

Mathematical fractals exhibit exact self-similarity across all spatial scales the Hausdorf dimension D_F of a geometrical that successive magnifications reveal an identical structure. An example is the Koch outline, a fractal object in which a reduction in the measuring scale by one-third measured length by four-thirds $(Ln+1/Ln) = 4/3$. Substituting i

$$(L_{n+1}/Ln) = (n+1/n)^{1-D}$$

$$(4/3) = (1/3)^{1-D}$$

$$4 = 3^D$$

$$D = \log 4/\log 3 = 1.26$$

The fractal dimension D is most commonly estimated from the regression slope of a log-log power law plot. However, the definition of 'independent' and 'dependent' variables (required in least squares or Model I regression analysis) is not straightforward in such applications. This is a serious but largely unrecognized problem, for using least square regression in this way results in a biased slope estimate.

The image fractal dimension characterizes the plane object projection. Therefore, fractal dimension of 3-dimensional object will be greater then TEM micrograph fractal dimension:

$$D = D^{TEM} + D^o$$

Where:

D is powder fractal dimension;

D_{TEM} is image fractal dimension;

Do is a correction factor with fractal dimension behavior.

As we already saw, to compute fractal dimension of a 3-dimensional object, we measure total number of r size boxes that covered the object.

The dimension of a fractal-like structure can be measured using a multiresolution approach, as for instance the merging boxes method. Increasing the size of the box used to explore the structure of a distribution of points in a background space, the number of filled boxes, i.e., of the boxes containing points that belong to the given set, decreases according to a power law with the exponent giving the fractal dimension of the set of points:

$$D_F = \log (N_2/N_1)/\log B_2/B_1$$

where

N_1 and N_2 are the numbers of filled boxes of sizes B_1 and B_2, respectively. The fractal-like structure is revealed by the linearity of the plot $\log(N)$ *vs* $\log (B)$, the slope gives the fractal dimension, and the range over which holds the linearity shows the scales for which the set has the self-similarity property, typical for fractals.

Some signals (objects) possess the self-similar (fractal) properties. It means that by changing the scale one observes at a new scale the features similar to those previously noticed at other scales. This property leads to power-like dependences. The formal definition of a

spatial fractal Hausdorf dimension D_F of a geometrical object is given by the Kolmogorov

$$0 < \lim_{\epsilon \to 0} N(\epsilon)\epsilon^{D_F} < \infty,$$

which states that D_F is the only value for which the product of the minimal number of the (covering this object) hypercubes $N(\epsilon)$ with a linear size $l = \epsilon$ and of the factor ϵ^{D_F} stays constant for ϵ tending to zero. In the common school geometry of homogeneous objects, it coincides with the topological dimension.

The probability $pi(\epsilon)$ to belong to a hypercube $Ni(\epsilon)$ is proportional to ϵ^{D_F}, and the sum of moments is given by

Fractals and multifractals are common among the purely mathematical constructions (the Cantor set, the Serpinsky carpet etc) and in the nature (clouds, lungs etc).

The pointwise Hölder exponents are now determined using wavelet analysis. Since wavelet analysis just consists in studying the signal at various scales by calculating the scalar product of the analyzing wavelet and the signal explored, it is well suited to reveal the fractal peculiarities. In terms of wavelet coefficients it implies that their higher moments behave in a power-like manner with the scale changing. The wavelet coefficients are less sensitive to noise because they measure, at different scales, the average fluctuations of the signal.

Thus the necessary condition for a signal to possess fractal properties is the linear dependence of log $Zq(j)$ on the level number j. If this requirement is fulfilled the dependence of τ on q shows whether the signal is monofractal or multifractal. Monofractal signals are characterized by a single dimension and, therefore, by a linear dependence of τ on q, whereas multifractal ones are described by a set of such dimensions, i.e., by non-linear functions τ (q). Monofractal signals are homogeneous, in the sense that they have the same scaling properties throughout the entire signal.

Multifractal signals, on the other hand, can be decomposed into many subsets characterized by different local dimensions, quantified by a weight function. The wavelet transform removes lowest polynomial trends that could cause the traditional box-counting techniques to fail in quantifying the local scaling of the signal. The function τ (q) can be considered as a scale-independent measure of the fractal signal. It can be further related to the Renyi dimensions, Hurst and Holder (at q = 1 as is clear from the examples in the previous Sections) exponents. The range of validity of the multifractal formalism for functions can be elucidated [35] with the help of the two-microlocal methods generalized to the higher moments of wavelet coefficients.

2. Materials and methods

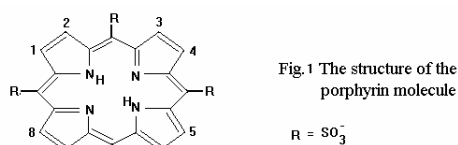H_2TSPP (Figure 1) has been prepared according to the literature [4]:

Fig.1 The structure of the porphyrin molecule

R = SO_3^-

Figure 1. Structural formula of H_2TSPP .

Aggregates were prepared according to the procedure reported in [4] by adding an HCl and/or NaCl solution to a solution of meso-tetrakis(4-sulfonatophenyl)porphine tetrasodium salt (TSPP) (Aldrich), and used within a couple of days.

Values of the fractal dimension, D_f, have been calculated using a box-counting technique where the minimum length of the box edge was equal to the

$$\sum_i p_i^q(\epsilon) \propto \epsilon^{qD_F} .$$

size of the pixel, and the maximum length was taken as the 1/5 of the width of a fractal object.

A direct method to determine fractal dimension is to analyze images obtained from scanning tunneling microscopy, scanning probe microscopy, transmission electron microscopy (TEM). TEM micrographs can provide high-resolution pictures of 3-dimensional objects.

The aim of this paper is to analyze TEM images in order to obtain fractal dimensions of 3-dimensional objects and to apply the method to some porphyrins. The "mass-radius" relation is used to compute fractal dimension of TEM micrograph. Some assumptions are to be made to obtain fractal dimension of 3-dimensional object from TEM micrograph fractal dimension.

This paper is based also, on wavelet transform analysis (WTA) used for the enhancement and delimitation of human tumor area from some micrograms recorded before and after photodynamic (PDT) treatment.

3. Results and discussion

Preliminary measurements of the size of H2TSPP indicate that $N \sim 10^4$-10^5 [15] and aggregate is roughly a hollow cyclinder [16] with a radius corresponding to the radius TPP molecule (0.2 nm) and the length of the aggregate is 16 μM.

Fractal analysis of the images of the typical patterns found on a coverslip which were modified to the binary format was carried out using a box-counting method, and the following values of the fractal dimension were obtained: (i) Df = 1.44; (ii) Df = 1.50; (iii) Df = 1.71. These values characterize the geometry of the observed structures and reflect the complex phenomena which occurred during a crystallization process. From the analysis of the images it is noted that the situation is different from the case with the low porphyrin concentration.

The processing methods are often based on Fourier transformations, convolution with a filter and deconvolution techniques, polynomial interpolation, so

on, very useful in medical diagnosis and therapeutics because they make possible to visualize the boundaries between tissues.

In processing signals and images, apart the well known Fourier methods, a more powerful instrument is offered by the wavelet theory. The advantage of wavelets is given by the orthogonal base on a compact support. The disadvantage is implied by the necessity to pass to a space augmented by one in each direction.

The wavelet can be constructed in many different ways. The approximated delta window is given by eq.1a:

$$f(\varepsilon;t) = \frac{\varepsilon}{\varepsilon^2 + t^2} \frac{1}{\pi} \qquad (1a)$$

Also we have (Mexican hat), eq.1b:

$$f(\varepsilon;t) = \frac{1}{\varepsilon\sqrt{\pi}} \exp\left[-\left(\frac{t}{\varepsilon}\right)^2\right] \qquad (1b)$$

where for ε tending to infinity the limit is the Dirac function $\delta(t)$. Also, was given the approximated delta window, eq.2a:

$$g(\varepsilon,d;t) = \frac{\varepsilon}{\varepsilon^2 + (t-d)^2} \frac{1}{\pi} \qquad (2a)$$

where d represents the window length. An 2D window as sum of two term products of 1D windows like (1a or 2a) can be constructed. The mother wavelet which is the first derivative of the window expression can be evaluated. The set of daughter wavelets from the mother wavelet by shift operations are generated. This type of wavelets satisfy admissibility condition (the Fourier transform and the integral from the wavelet equal zero). The wavelet transform is a correlation operation between the signal f(t) and the shifted and scaled mother wavelet. So the images can be approximated by 1D windows or wavelets sums of products. In figure 2 an Approximated Delta 2D Window constructed in arbitrary units is generated
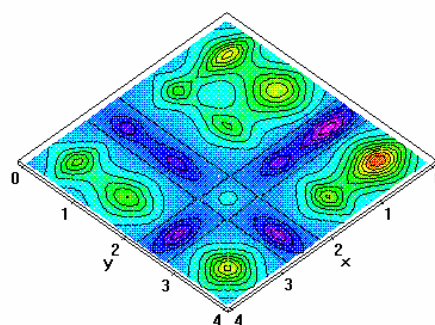

.

Fig.2 An Approximated Delta 2D Window Image

In the window computation only usual arithmetic operations are used. For the same number of parameters less operations in delta wavelet evaluation than for mexican hat one is obtained. So the necessary computing time for these 2D windows and 2D wavelets by the absence of exponential evaluations are reduced. This new type of wavelets are more versatile ones than the Morlet wavelets.

This paper is based on wavelet transform analysis (WTA) used for the enhancement and delimitation of human tumor area from some micrograms recorded before and after photodynamic (PDT) treatment.

The proposed algorithm improves the detection performance through the use of image processing multiresolution analysis with a new type of bidimensional window and wavelet approximation.

The wavelet transform is superior to the Fourier transform first of all due to the locality property of wavelets. The Fourier transform uses sine, cosine or imaginary exponential functions as the main basis. It is spread over the entire real axis whereas wavelet basis is localized. It helps analyze the local properties of a signal using wavelets while the Fourier transform does not provide any information about the location where the scale (frequency) of a signal changes. Decomposition into wavelets allows singularities to be located by observing the places where the wavelet coefficients are (abnormally) large. Once the wavelets have been constructed they perform incredibly well in situations where Fourier series and integrals involve subtle mathematics or heavy numerical calculations. But wavelet analysis cannot entirely replace Fourier analysis, indeed, the latter is often used in constructing the orthonormal bases of wavelet series. Many theorems of wavelet analysis are proven decomposition. The two kinds of analysis are thus complementary.

The Fourier spectrum fω of a one-dimensional signal f(t) having (squareintegrable) is given by

$$f_\omega = \int_{-\infty}^{\infty} f(t) e^{-i\omega t} dt.$$

The inverse transform restores the signal. It is an unitary transformation

$$\int |f(t)|^2 dt = \frac{1}{2\pi} \int |f_\omega|^2 d\omega.$$

This is the so-called Parseval identity which states the conservation of energy between the time and the frequency domains.

The difference between the wavelet and windowed Fourier transforms lies in the shapes of the analyzing functions ψ and g. All g, regardless of the value of ω, have the same width. In contrast the wavelets ψ automatically provide the time (location) resolution window adapted to the problem studied, i.e., to its essential frequencies (scales). It means that the wavelet window resolves both the location and the frequency in fixed proportions to their central values. The wavelet transform cuts up the signal (functions, operators etc) into different frequency components, and then studies each component with a resolution matched to its scale providing a good tool for time-frquency (position-scale) localization. That is why wavelets can zoom in on singularities or transients (an extreme version of very short-lived high-frequency features!) in signals, whereas the windowed Fourier functions cannot. In terms of the traditional signal analysis, the filters associated with the windowed Fourier transform are constant bandwidth filters whereas the wavelets may be seen as constant relative bandwidth filters whose widths in both variables linearly depend on their positions.
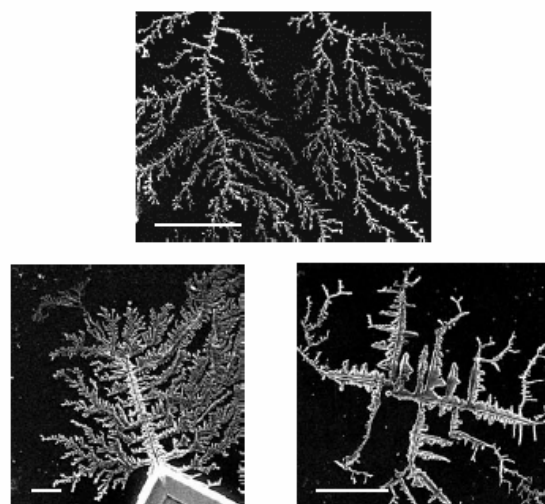
The constant shape of the windowed Fourier transform region and the varying shape (with a constant area) of the wavelet transform region. The density of localization centers is homogeneous for the windowed Fourier transform whereas it changes for the wavelet transform so that at low frequencies the centers are far apart in time and become much denser for high frequencies.

The second lifetime (0.9 - 8 ps) is ascribed to the process of intra aggregate vibrational energy redistribution for the cases (i) and (iii) because its typical value is ~ 1 ps but it is too long for the case (ii), τ_2 = 8 ps, which corresponds to the largest value of fractal dimension. It is noticeable that the lifetimes for the cases of (i) and (iii) are closer to each other as well as the D_f values for these cases, and the

increase in the lifetimes corresponds to the increase in D_f. This is reasonable since the increase in branching will lead to the increase in density of the vibrational states.

The third, large lifetime τ_3 = 10-39 ps) would be obvious to assign to the process of vibrational cooling, i.e. transfer of energy to surrounding solvent molecules. Again, lifetime values are in the reasonable range for the aggregates in the experimental condition. This unusual behavior might be associated with the specificity of localized vibrational states of the self-similar fractals called fractons.

Figure 3. SEM images of the solidification patterns of the solution of H2TPPS4 4- aggregates: (i) 50 μl H2TPPS44-, pH = 0.7, Df = 1.44 (upper); (ii) 50 μM H2TPPS4 4-, pH = 2.8, 0.5 M NaCl, Df = 1.71 (lower left); (iii) 50 μM H2TPPS44-, pH = 0.7, 2 M NaCl, Df = 1.50 (lower right). Bar = 10 μm.

4. Concluding remarks

The lifetime values are in the reasonable range for the aggregates in the experimental condition. This unusual behavior might be associated with the specificity of localized vibrational states of the self-similar fractals called fractons. Dynamic behavior of fractons is described by spectral dimension, ds, which is related to Df, and thus should also correlate with photophysical observations. It is of interest to determine the values of Df for all cases and will be the area of our future research.

5. References

[1] Meyer Y Wavelets and Operators (Cambridge: Cambridge University Press, 1992)

[2] Daubechies I Ten Lectures on Wavelets (Philadelphia: SIAM, 1991)

[4] Meyer Y Wavelets: Algorithms and Applications (Philadelphia: SIAM, 1993)

[5] Chui C K An Introduction to Wavelets (San Diego: Academic Press, 1992)

[6] Hernandez E, Weiss G A First Course on Wavelets (Boca Raton: CRC Press, 1997)

[7] Kaiser G A Friendly Guide to Wavelets (Boston: Birkhauser, 1994)

[8] Wavelets in Medicine and Biology Eds. Aldroubi A, Unser M (Boca Raton: CRC Press, FL, 1994)

[9] Blanco S, Kochen S, Rosso O A et al IEEE Engineering in Medicine and Biology 16 64 (1997)

[10] Antonini M, Barlaud M, Mathieu P, Daubechies I IEEE Transactions on Image Processing 1 205 (1992)

[11] RM. Ion, S Apostol (2003) SPECTROSCOPIC ANALYSIS FOR SOME PORPHYRINIC AGGREGATES, Annals of Valahia University pp 32-37

[12] H.-J.Schneider and M.Wang, Associations with Porphyrins in Water: Quantification by Constant Free Energy Increments, J.Chem.Soc., Chem.Commun, 1994, 413-415.

[13] D.Narayana Rao, S.Venugopal Rao, F.J.Aranda, D.V.G.L.H.Rao, M.Nakashima and J.A.Akkara, Ultrafast relaxation times of matalloporphyrins by time-resolved degenerate four-wave mixing with incoherent light, J.Opt.Soc.Am. B, 14(1997), 2710-2715.

[14] J.Rodriguez, C.Kirmaier and D.Holten, Optical Properties of Metalloporphyrin Excited States, J.Am.Chem.Soc., 111(1989), 6500-6506.

[15] L.Edwards, D.H.Dolphin, M.Gouterman and A.D.Adler, Porphyrins XVII. Vapor Absorption Spectra and Redox Reactions: Thetra phenylporphins and Porphin, J.Mol.Struct., 38(1971), 16-32.

[16] S.R.Gwaltney and R.J.Barlett, Coupled cluster calculations of the electronic excitation spectrum of free base porphin in a polarized basis, J.Chem.Phys., 108(1998), 6790-6798.

SERGIU DINU[1]

GABRIEL DIMA[1]

CALIN OROS[1]

CLAUDIA STIHI[1]

SIMONA APOSTOL[1]

GHEORGH VLAICU[2]

MAXWELL EQUATIONS AND THE OPTICS PROPERTIES OF MATERIALS

[1]Valahia University of Targoviste, 2 Regele Carol blvd., Targoviste, Romania
[2]Special Steel Factory, Targoviste, Romania

Abstract: This issue offers an example of applying Maxwell equations on solid materials. By using the electrical properties of these materials, which are mainly linked with electronic conduction, the most important optical parameters which characterize them have been find out.

1. Introduction

The connection between the refractive index and the properties of the medium of propagation is formally provided by Maxwell's equations. For the case of a nonmagnetic and isotropic material of dielectric constant ε and conductivity σ they may be written as

$$\nabla \cdot \vec{E} = 0, \tag{1}$$

$$\nabla \cdot \vec{H} = 0, \tag{2}$$

$$\nabla \times \vec{E} = -(1/\varepsilon_0 c^2)\partial \vec{H}/\partial t, \tag{3}$$

$$\nabla \times \vec{H} = \varepsilon\varepsilon_0 \partial \vec{E}/\partial t + \sigma\vec{E}. \tag{4}$$

microscopic structure of the material. Let us briefly review the main features of nonmetals (insulators or semiconductors) and metals.

2. Results and discussions

a. Nonmetals

Insulators and semiconductors in the absence of excitation have only bound electrons and are basically transparent, except in the vicinity of what can be thought of as resonances. In the classical Lorentz model the electron is represented as a harmonic oscillator driven by the oscillating force of the wave's electric field .The oscillating electrons produce a macroscopic polarization of the material which superposes on the electric field of the incident wave. The dielectric function is simply the ratio of the total field (wave plus polarization) to the field of the wave alone. In quantum mechanics, a resonance corresponds to the transition of

Taking the curl of (3), recognizing that $\nabla \times (\nabla \times \vec{E}) \equiv \nabla(\nabla \cdot \vec{E}) - \nabla^2 \vec{E}$ and using (1,4) yields the wave equation

$$\nabla^2 \vec{E} = (\varepsilon/c^2)\partial^2 \vec{E}/\partial t^2 + (\sigma/\varepsilon_0 c^2)\partial \vec{E}/\partial t. \tag{5}$$

Insertion of the plane wave ansatz (2.1) and use of (2.2) with the complex index shows that the latter is related to ε and σ by:

$$n^2 = \varepsilon + i\sigma/\varepsilon_0\omega \equiv \varepsilon = \varepsilon_1 + i\varepsilon_2. \tag{6}$$

The quantity ε defined by the right-hand part of (6) is the complex dielectric function which can be regarded as a generalized response function of the material. The real and imaginary parts of **n** and **ε** are related by:

$$\varepsilon_1 = n_1^2 - n_2^2;$$
$$\varepsilon_2 = 2n_1 n_2, \tag{7}$$
$$n_1^2 = (|\varepsilon| + \varepsilon_1)/2;$$
$$n_2^2 = (|\varepsilon| - \varepsilon_1)/2. \tag{8}$$

The dielectric function fully describes the response of a material to weak electromagnetic irradiation. It depends on the light frequency in a manner determined by the

an electron between two states, the energy difference ΔE of which determines the resonance frequency $\omega_0 = \Delta E/h$. The classical and quantum mechanical treatments yield almost identical expressions for the dielectric function. For a nonmetal with N_e bound electrons showing one single resonance we have [2.2]

$$\varepsilon = 1 + (N_e e^2/m_e\varepsilon_0)f_{osc}(\omega^2 - \omega_0^2 + i\Gamma\omega)/[(\omega^2 - \omega_0^2)^2 - \Gamma^2\omega^2] \tag{9}$$

Here f_{osc}, the oscillator strength, is a measure of the probability of the transition, while the damping constant Γ describes the width of the resonance that arises from the finite width of the initial and final electron states.

Real materials have, of course, many resonances, and in their expression for **ε** the resonance term of (2.19) is replaced by a sun over many terms. The most important resonance arises from transitions of valence-band electrons to the conduction band (interband transitions).

b. Metals

The optical response of a metal is dominated by the conduction electrons. Since the electron gas is degenerate, only electrons in states close to the Fermi level, referred to as "free electrons", contribute to the optical properties. There is no resonance frequency for a free electron, and its only interaction whit the lattice is by collisions. The dielectric function of a free-electron metal can be obtained from (9) by formally replacing the damping constant Γ by the inverse collision time $1/\tau_e$ and setting the resonance frequency equal to zero and f_{osc} equal to one. The resulting expression can be written as

$$\varepsilon = 1 + \omega_p^2 (-\tau_e^2 + i\tau_e/\omega)(1+\omega^2\tau_e^2) \qquad (10)$$

where

$$\omega_p = \sqrt{N_e e^2 / m_e \varepsilon_0} \qquad (11)$$

Is the electron plasma frequency. At $\omega = \omega_p$ (which is in the vacuum ultraviolet for most metals) both ε_1 and n_1 vanish. The variation of $\boldsymbol{\varepsilon}$ and the associated quantities with the light frequency is shown in Fig.1. The plasma frequency is seen to separate two regimes of rather different optical properties: Large R and α for $\omega < \omega_p$ and small R and α for $\omega > \omega_p$.
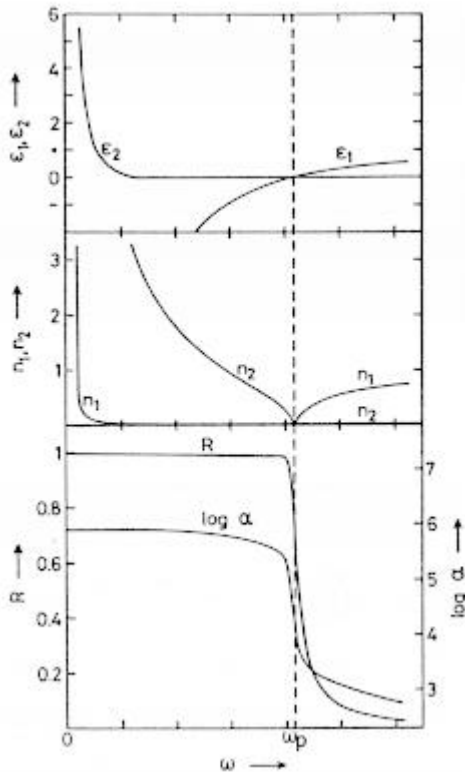
Figure 1. Frequency dependence of the dielectric function, the refractive index, the Fresnel reflectance and the absorption coefficient of a free-electron metal (calculated for $h\omega_p = 8.3$ eV, corresponding to $N_e = 5 \cdot 10^{22}$ cm^{-3}, and $h/\tau_e = 0.02$ eV)

The optical properties of a free-electron metal for $\omega < \omega_p$ are related to its DC conductivity σ_0. Whit the aid of the Drude expression

$$\sigma_0 = N_e e^2 \tau_e / m_e = \omega_p^2 \varepsilon_0 \tau_e, \qquad (12)$$

useful approximate expressions for the optical parameters can be obtained. For the range $\omega \ll 1/\tau_e$ (far-infared region) Eq. (10) gives $\varepsilon_1 \cong -\sigma_0 \tau_e / \varepsilon_0$ and $\varepsilon_2 \cong -\sigma_0 / \varepsilon_0 \omega$, from which follows that $n_1 \cong n_2 \cong \sqrt{\sigma_0 / 2\varepsilon_0 \omega}$.

$$1 - R \cong \sqrt{8\varepsilon_0 \omega / \sigma_0} \qquad (13)$$

and

$$\alpha \cong \sqrt{2\omega\sigma_0 / \varepsilon_0 c^2} . \qquad (14)$$

For the range $1/\tau_e \ll \omega < \omega_p$ (near-infared and visible regions for most metals) we have $n_1 \cong \omega_p / 2\omega^2 \tau_e \cong 0$ and $n_2 \cong \omega_p / \omega$ which gives

$$1 - R \cong 2 / \omega_p \tau_e = 2\varepsilon_0 \omega_p / \sigma_0 \qquad (15)$$

and

$$\alpha \cong 2\omega_p / c . \qquad (16)$$

In real metals the simple free-electron behavior is modified by a number of secondary effects, in particular by interband transitions. As an illustration, we show in Figure 2 the coupling parameters for Al and Au. The curves of both metals show oscillations caused by interband transitions, such as the one at 0.83 µm (1.5 eV) in Al. A comparison with Fig 1 indicates that the plasma frequency for Al is indeed in the vacuum ultraviolet, whereas that of Au appears to be in the visible. The anomalously low apparent plasma frequency of Au (which causes its yellow color) is due to transitions from d-band states which set in at $h\omega \cong 2eV$. The d-electrons make a bound-type contribution to the dielectric function, and since the contribution to ε_1 is positive, the point $\varepsilon_1 = 0$ which defines ω_p is
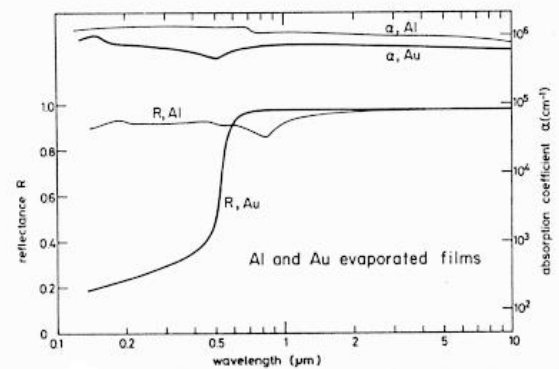
Figure 2. Reflectance and absorption coefficient as a function of wavelength for aluminium and gold

ments tend to reveal an optimum level of irradiance, characteristic of the material, where the momentum transfer per unit laser pulse energy is largest. That there should be an optimum is not surprising: At too low an irradiance a regime of adiabatic evaporation is never reached, and most of the pulse energy is spent in heating the condensed phase. As the irradiance increases, the surface temperature and the molar energy of the vapor

also increase, reducing its efficiency in imparting momentum to the target (a larger number of less energetic particles carry more momentum than a lesser number of more energetic ones). In addition, more energy also goes into internal degrees of freedom of the vapor particles (dissociation, ionization) which do not contribute to the recoil. However, the dependence of momentum transfer on incident irradiance tends to reflect the behavior of the degree of absorption more than evaporation kinetics per se, as we shall discuss in the next section.

The primary target of the vapor recoil is, of course, the evaporating melt layer. The interaction affects the dynamics of evaporation and its response to transients in the irradiation . Net forces onto the melt layer result only from pressure gradients, but lateral pressure gradients are always present, if only because a beam has a finite cross section. These forces invariably result in lateral displacement of liquid, which may range from mere changes in the surface topography of the irradiated material to the formation of holes and deep welds.

3. References

[1] Dieter Bauerle - Laser processing and chemistry (Springer, Berlin, 2000), 150-156

[2] I. Ursu, A. Prokhorov - Interactia radiatiei laser cu substanța , Ed. Academiei, 1986, 15

[3] Martin von Allmen- Laser Beam Interactions with Materials- Physical Principles and applications, 1997, 11

VALENTIN GHISA[1]

ION V. POPESCU[2]

VICTOR CIUPINA[3]
ANCA GHEBOIANU[2]

XRF COMPOSITIONAL ANALYSIS OF SOME ROMAN BROOCHES DISCOVERED AT TOMIS

[1]Master in Statistical Mathematics , *Transilvania* University of Brasov
[2] Valahia University of Targoviste, Physics Department, Faculty of Science
[3]Ovidius University of Constanta

Abstract: XRF method was used in order to determine the concentration of the main compounds in the raw materials and on the other hand to make a clasification of the different types of brooches discovered at Tomis now Constanta city, an arheological site in Dobrudja-Romania..

1. Introduction

The main point of this paper is to study a number of 27 samples of different brooches placed in Dobrudja, more exactly in the antique metropolis of Tomis, by XRF method. The brooches are some small acccessories for clothes extremely used in antiquity. These are a kind of mixture between today`s safety pin and on art object manufactured in order to symbolise a religious imagine. In what regards XRF, the next facts is well known. When a primary x-ray excitation source from an x-ray tube or a radioactive source strikes a sample, the x-ray can either be absorbed by the atom or scattered through the material. The process in which an x-ray is absorbed by the atom by transferring all of its energy to an innermost electron is called the ,,photoeffect". During this process, if the primary x-ray had sufficient energy, electrons are ejected from the inner shells, creating vacancies. These vacancies present an unstable condition for the atom. As the atom returns to its stable condition, electrons from the outer shells are transferred to the inner shells and in the process giving off a characteristic x-ray whose energy is the difference between the two binding energies of the corresponding shells. The emitted x-ray produced from this process is XRF. The XRF method is widely used to measure the elemental composition of materials. Since this method is fast and non-destructive to the sample, it is the method of choice for field applications. Depending on the application, XRF can be produced by using not only x-rays but also other primary excitation sources like alpha particles, protons or high energy electron beams.

2.Experimental procedure

In order to have an accurate result the samples were cleaned before the analise. This operation was used for the elimination of corrosive elements. It was necessary to have a smooth surface in order to avoy the incidental radiation reflexion from the source.The samples were ranged in 2π irradiation geometry, namely, the source in front of the sample, the radiation spreading in all directions. The samples were place about 5 cm from the source. The radioisotope ^{241}Am was here the excitation source, which after the desintegration emits photons gamma heaving the energy of 59,5 keV. The annular source of ^{241}Am has an activity of 10 mCi is by the best eficiency providing the energy which has the values near the biggest absorbtion point in the target. The element which is excited by this method is supposed, after that to be desexcited and to emit the characteristical X-spectrum. The spectrum is achieved in 1000 sec by the detection chain. This will show the all elements from the contain of the sample. The Si (Li) detector used here will receive the caracteristic x-radiation and can determine the elements, if the radiation energy requests it. The attached soft to the detecting chain works out the spectrum and calculates every element concentration directely through the method of interstandardisation. The standard is composed by Cu 99,7%, Pb 0,005%, Fe 0,005%, Zn 0,005%, Sn 0,005% (MERK products). The formula for concentrations determination is:

$$\rho = \frac{RR \cdot CF(RL) \cdot CF(AT)}{K} \qquad (1)$$

Where: ρ is elements concentration, RR is the perturbating rate in x-ray detection, CF(RL) is the correcting factor for losses, CF(AT) is the correcting factor for attenuation and K is the calibration constant. CF(RL) is determined through the radioisotope normalizing by formula:

$$\frac{\Omega}{4\pi} \cdot \frac{\cos\phi}{\cos\theta} \qquad (2)$$

Where: Ω is the solid angle, ϕ, θ is the emergent (incident) radiation angle. CF(AT) has two

components:one for γ exciting radiation and one for x-fluorescence radiation,

$$CF(AT) = -\frac{\ln \alpha}{1-\alpha} \qquad (3)$$

$$CF(AT) = e^{-\left(\frac{\mu_\gamma}{\cos\phi}+\mu_x\right)L} \qquad (4)$$

Where: μ_γ, μ_x is the mass attenuating values and L is the sample average thickness.

3.Results and discussion

The following elements concentrations in the samples were determined:

Table 1 Concentrations for brooches type A

Sample	Zn%	Pb%
P1	21.31	2.11
P2	15.07	1.94
P3	14.82	1.83
P4	14.65	1.69
P5	14.13	2.02
P6	14.02	3.97
P7	12.46	1.79
P8	8.74	1.02

Figure 1 Concentrations for brooches type A
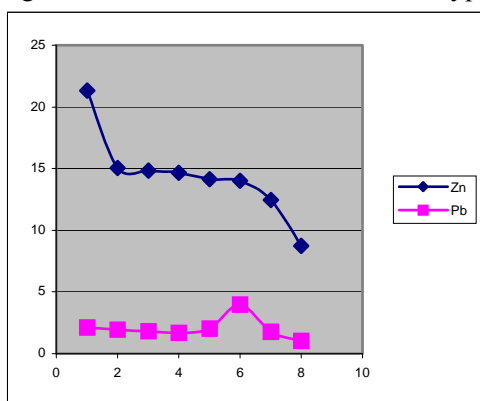
Table 2 Concentrations for brooches type B

Sample	Zn%	Pb%
P1	0.31	1.12
P2	0.22	1.43
P3	0.1	2.62
P4	0.42	3.77
P5	1.55	5.61
P6	1.07	6.13
P7	0.19	6.38
P8	1.81	8.13

Figure 2 Concentrations for brooches type B
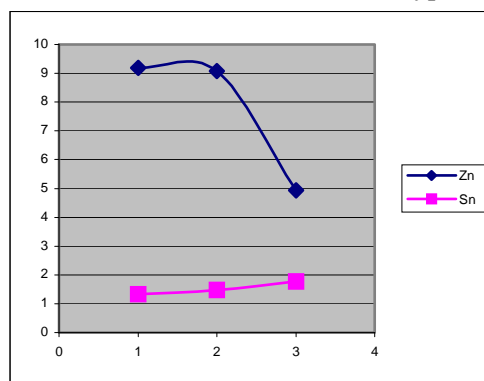
Table 3 Concentrations for brooches type PSP

Sample	Zn%	Sn%
P1	9.18	1.33
P2	9.07	1.48
P3	4.93	1.77

Figure 3 Concentrations for brooches PSP
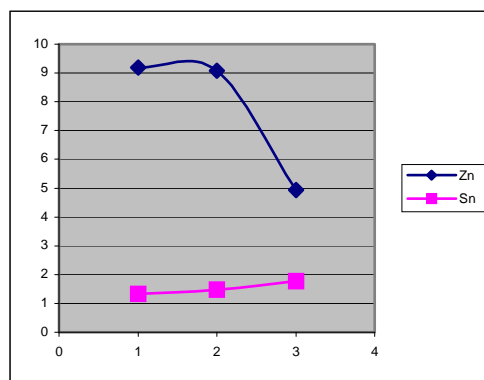
Table 4 Concentrations for brooches type PSC

Sample	Zn%	Sn%
P1	4.05	12.45
P2	3.78	8.23
P3	3.47	5.76
P4	2.62	4.07

Figure 4 Concentrations for brooches PSC
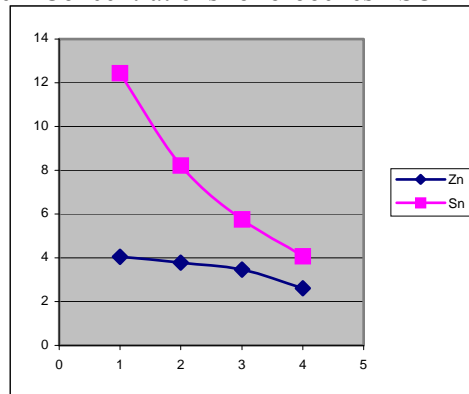
Table 5 Concentrations for brooches type PCf

Sample	Zn%	Sn%
P1	2.15	4.12
P2	3.8	9.64
P3	2.81	9.53
P4	4.46	11.02

Figure 5 Concentrations for brooches PCf
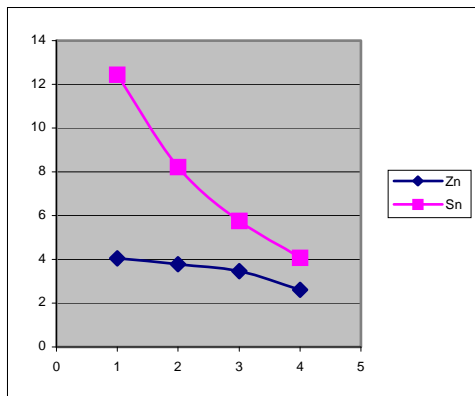
Standard deviations: Zn($\pm0,0028$), Sn($\pm0,0025$), Pb($\pm0,0025$)
Type A: brooches with the shape of spur
Type B: brooches with hasp or articulation
Type PSP: plane simple brooches
Type PSC: brooches with simple circular ornaments
Type PCf: cross- form brooches

After the determination of the concentration through XRF and also through a metallographic study of the structure, we observe that the brooches can be divided in two main types according to the localization in time. The simple brooches, manufactured from a single part, are from the preroman civilization and those manufactured in a complex shapes, rich adorned are from the roman civilization. We also observe that it was a superior technology in roman period, because of functional quality. After researches, we observe that all samples from the Iron Age it was manufactured by alloys of bronze and Si. This type of alloy was often used in that period. The Latene civilization brooches had their origins in the preroman period but same types continued to be produces after the roman conquest. Those are divided in two different categories; the first one contains the samples made by Sn, with insignificant traces of Zn and the others having a composition 10% of Zn, or more. In all the analyzed samples, Pb is absent or present in very small concentrations. Another types of brooches are which those have a lot of ornaments on the main rod. The standard brooches, with no ornaments have arched needle, extremely flexible, being manufactured from relatively reached content of bronze. Types of brooches with oblique prominences on the rod, were manufactured from bronze with a low level of Zn. A lot of the samples with fixed needle are made from bronze with content of Pb (6-7%) in mean. The samples with mobile needle are manufactured by pliant composition: brass or bronze

with a low level of Pb. These can be divided in two small groups based on the methods of manufacture. The plane ones are from brass with Zn (4-10%) and don`t have a significant level of Pb (1%).All brooches which have a special ornamentation contain Pb (4,6%) in mean. The brooches with the shape of spur (type A) can be divided in two groups. The first group are those with discs on the bow, they are manufactured from brass, with 10-20% Zn, with a low level of Sn and small traces of lead. The second group is formed by same samples which are not very different by the others but which have their surfaces better processed in the curved shape. The brooches with hasp or articulation (type B) need to have a rich level of Pb and the bronze present a low concentration of Zn. The cross- form brooches appear in the same time with the other, but they keep on being used to the end of the 3rd century B.Ch. The simplest classification of these brooches would be: plane brooches (PSP), with simple circular ornaments (PSC) and cross- form brooches (PCf). The first type of these samples has a low contain of Zn (4,2%) and of Sn (3,8%) but the last two types have a relatively high contents of Zn (7,7%) respectively very small (0,7%) and a low contain of Sn (1,5%) respectively (8,5%). It was proved in this way that the first two types are very old so the others some to be more recent. The tendency of using small quantities of Zn in the alloys rich in Sn can indicate graduated increase of technologies in the roman civilization.

4. References

Camp, D., Ruther, W.: Nondestructive energy–dispersive X-ray fluorescence. International Atomic Energy Agency Report IAEA-R-1557R, 1977.

Bertin, P.: Principles and practice of X-ray spectrometric analysis. Plenum Press, New York, 1975.

Woldseth, R.: All you ever wanted to know about XES. Kevex Corp., Burlingame, California, 1973.

B.Webster Smith: Sixty Centuries of Copper, http://60centuries. copper.org/right.html

Tylecote, R.F. 1992, A History of Metallurgy Second edition. London: Institute of Materials.

B. CHEMISTRY SECTION

MARIUS BUMBAC[1]
LAURA MONICA GORGHIU[1]
CRINELA DUMITRESCU[1]
SILVIU JIPA[1]
RADU SETNESCU[1]
TRAIAN ZAHARESCU[2]
ION MIHALCEA[3]

# INVESTIGATION OF ROSEMARY EXTRACTS FOR THE PROTECTION OF POLYETHYLENE AGAINST THERMAL OXIDATION

[1]VALAHIA University of Targoviste, B-dul Unirii 12-14,
[2]ICPE C.A. Bucuresti, [3]Universitatea Bucuresti

Abstract: This paper presents the effect of some rosemary extracts on the thermal stabilization of low density polyethylene (LDPE). IR and UV spectra's of these extracts indicates that the major substances are carnosic acid, carnosol and epirosmanol. Chemiluminescence (CL) resulting from the exothermic termination reaction of peroxi radicals was used for the characterization of effectiveness of these extracts for protection of LDPE.

1. Introduction

Rosemary (*Rosmarinus officinalis*) is of a great applicative interest because it exhibits considerable antioxidant properties in comparison to other plants. The main compounds that are responsible for the antioxidant activity of rosemary belong to the phenolic diterpenes [1-3]. Carnosic acid, carnosol, rosmanol and epirosmanol (fig.1) were shown to be the major substances which have been found in leaves of rosemary [4,5].
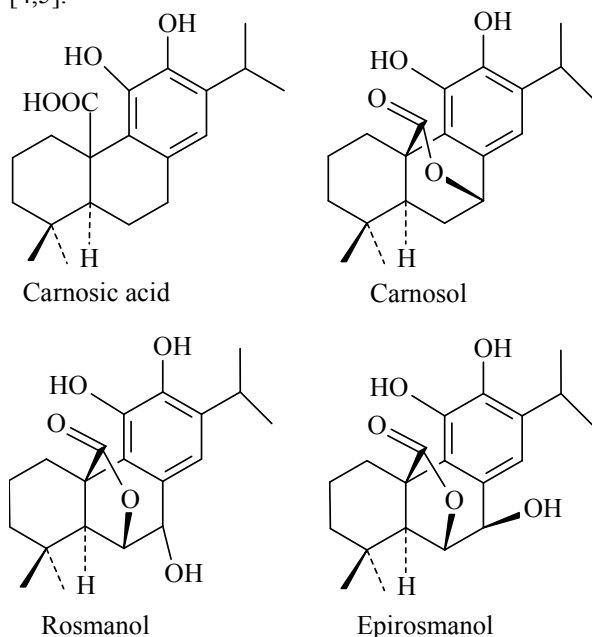
Fig.1 – Antioxidative compounds in rosemary leaves

Wenkert et al [4] reported a concentration of 0,35% carnosic acid in dried leaves. Richheimer et al [6] found a markedly higher concentration of carnosic acid ranging from 1,7% to 3,9%, and the carnosol content amounted to 0,2-0,4% in dried rosemary leaves.

In the presence of oxygen, carnosic acid is converted to carnosol and rosmanol [7].

The problem of stabilizing polyethylene against thermal-oxidative ageing is still of topical interest. Despite the abundance of new stabilizers in the patent literature, further investigation of natural antioxidant compounds have received increasing interest for their use instead of synthetic ones. Interest in employing antioxidants obtained from natural sources is due to the toxic effects of synthetic antioxidants and is connected with the plastic packing for the food industry.

Chemiluminescence (CL) resulting from the exothermic termination reaction of peroxi radicals has proved to be a sensitive technique for antioxidant ranking.

In the present study we have applied the chemiluminescence method for the characterization of the effectiveness of some rosemary extracts for the protection of low density polyethylene (LDPE) against thermal-oxidation.

2.Experimental

Plant material was extracted with methanol, chloroform, acetone and diethyl ether, separately. All the solvents were of analytical grad purity. The extraction precipitates were separated from liquid phase by filtration.

The infra-red absorption spectra of rosemary extraction precipitates were recorded over the range 400 to 4000 cm^{-1} on IR-75 Carl Zeiss Jena spectrophotometer.

Ultra-violet absorption measurements (200 to 300 nm) were made upon a Secomam S-750 spectrophotometer. In these measurements rosemary liquid extracts were examined.

Low density polyethylene (LDPE) provided by the Brazi Chemical Company as K322® type was used as polymeric support. LDPE was purified by precipitation with methanol from hot o-xylene solution. After the removal of remaining solvent, LDPE mass was dried at room temperature.

The rosemary extracts were added to LDPE by intimate grinding of polymer wet ($CHCl_3$) powder. The compounded (0,25 % w/w) samples were dried in a dessiccator at room temperature for 24 h.
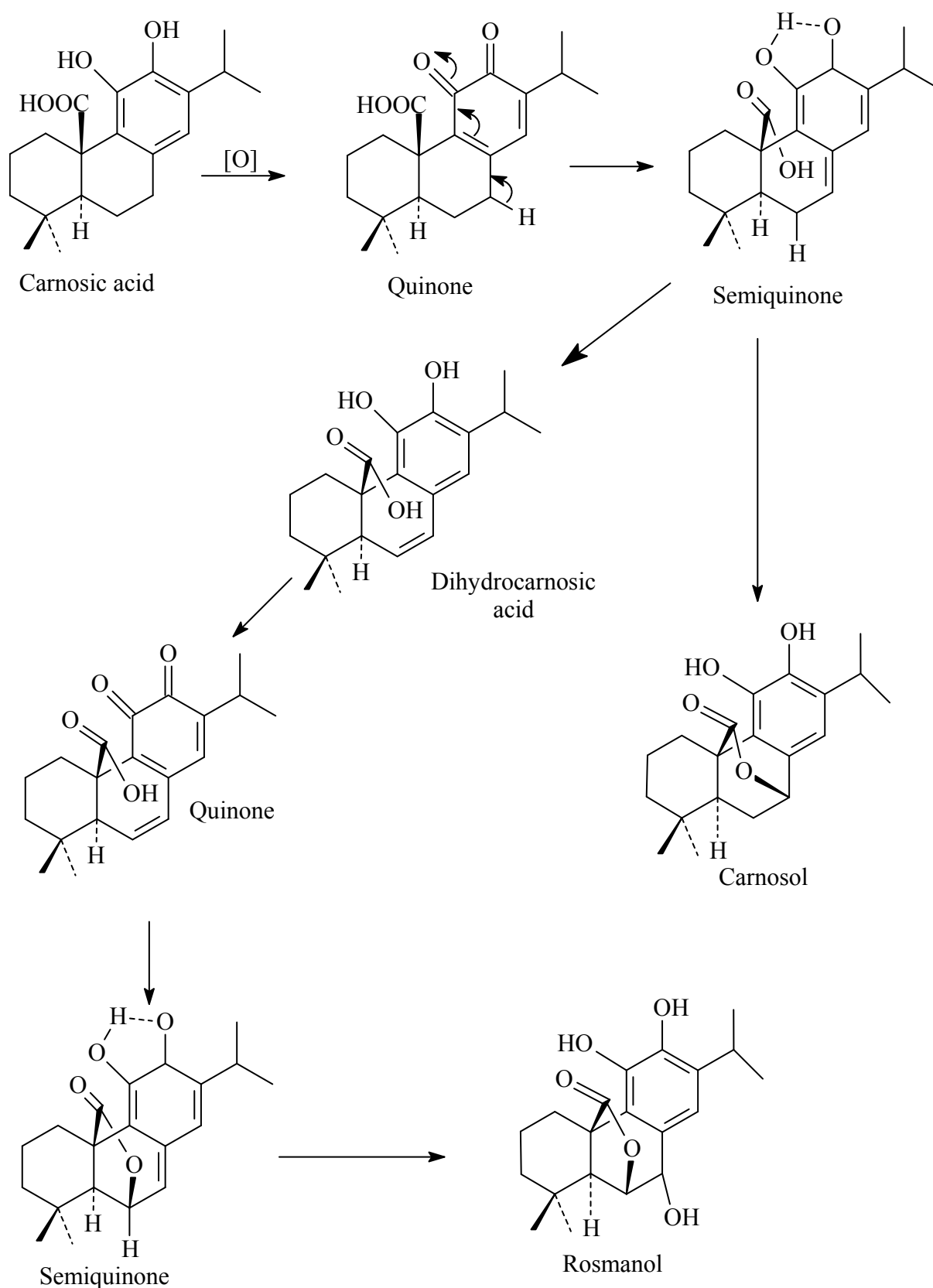
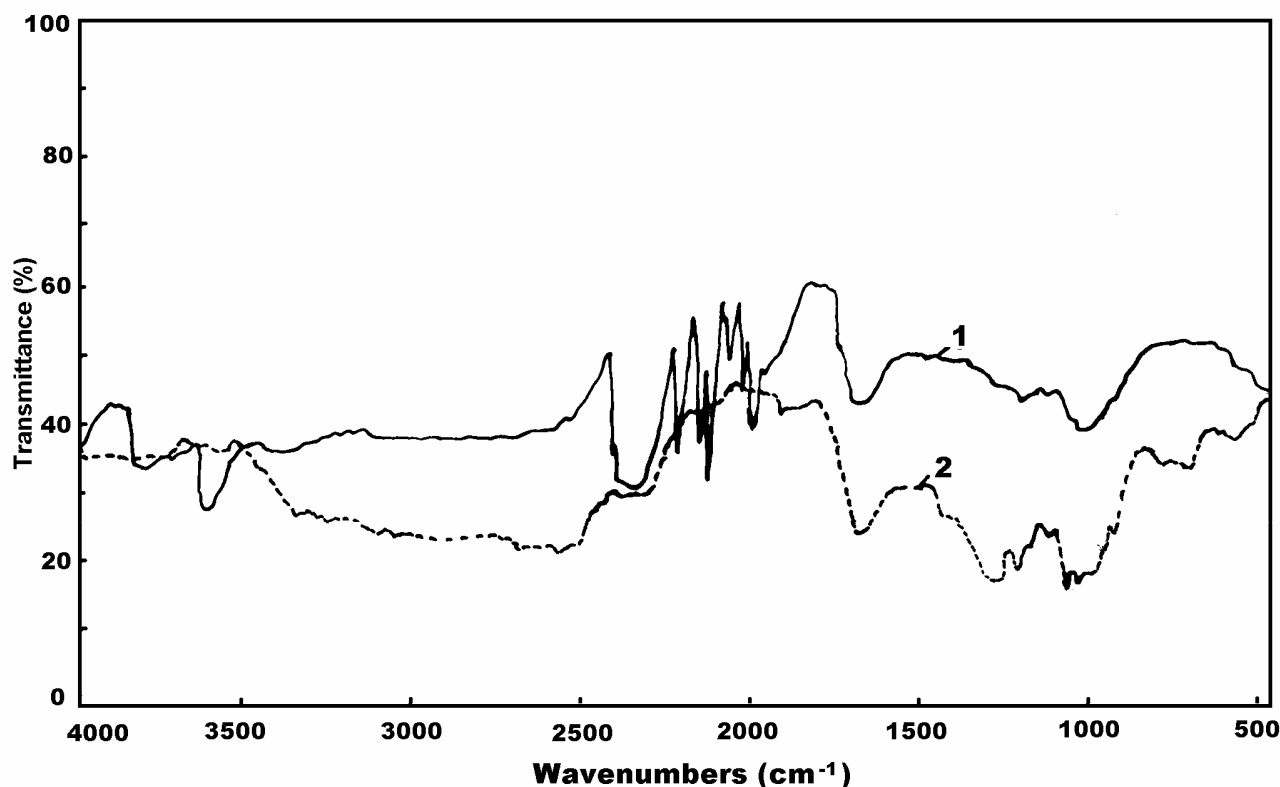**Scheme 1 – Oxidation cascade reactions of carnosic acid**

Fig.2 – IR – spectra of rosemary extraction precipitate obtained in methanol (1) and acetone (2)

Isothermal chemiluminescence measurements were performed in an Oxyluminograph OL-94, which has been previously described [8].

3.Results and discussion

Figure 2 shows a typical infra-red absorption curves obtained for the rosemary extraction precipitates. The absorption bands occurring in the region 1100-1190 cm^{-1} can be ascribed to etheric and carboxylic groups. The 3300-3600 cm^{-1} region show the content of bonded hydroxyl groups. Absorption at 1715 cm^{-1} characterizes the content of C=O groups and absorption at 1650 cm^{-1} belong to monomeric OH groups. The 2000-2300 cm^{-1} region can be attributed to diazo groups or nitrile group [9].

Figure 3 shows a typical ultra-violet absorption curves obtained for the rosemary liquid extracts. These show a maximum in the region 220-230 nm and a shoulder at 260-270 nm. The latter region must be due to the ketonic carbonyl (see [10]) also shown in the infra-red region. According to Bosch et al [11], the UV spectra (230 nm) of all phenolic diterpenes are similar to carnosic acid.

Figure 4 shows the chemiluminescence ($200^{O}C$, air) of LDPE unstabilized with rosemary extracts. The kinetic parameters of CL data are given in table 1.

As can be seen all rosemary extracts inhibited LDPE degradation in air at $200^{O}C$ by trapping the radicals formed in the polymer matrix. It is proved by the increased values of the induction periods (t_i) by comparison with the blank sample. However, the results obtained with extracts from rosemary seeds demonstrate that the type of extraction solvent strongly influences the composition of the extracts and consequently their antioxidation activity.
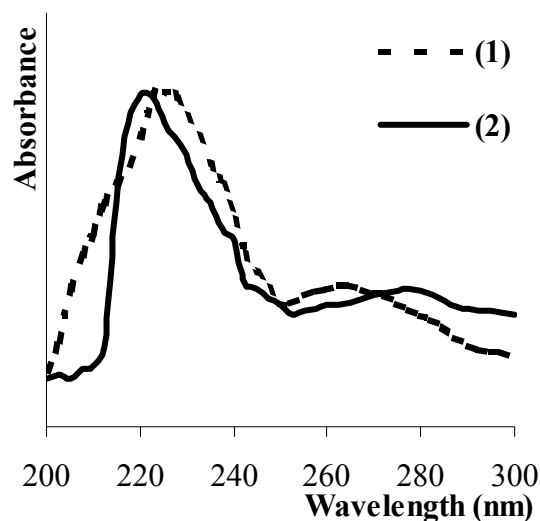

Fig.3 – UV-spectra of rosemary extraction liquids: (1) diethyl ether; (2) methanol

Methanol seems to be the most efficient solvent for the antioxidant extraction. This is proved by the lowest I_O and $\sum_{0}^{20} I_{CL}$ values. The concentration of carnosic acid in the methanolic extract would be probably situated at the highest level. The scheme 1 shown above illustrates the mechanism through which carnosic acid acts as an efficient antioxidant [12].

When carnosic acid donates a hydrogen to quench a free radical, it forms carnosol, which is also an antioxidant, which in turns forms rosmanol, another antioxidant compound. Therefore, these compounds are oxidized to other compounds that can be rearranged to produce in addition more antioxidants, capable to scavenging more free radicals.
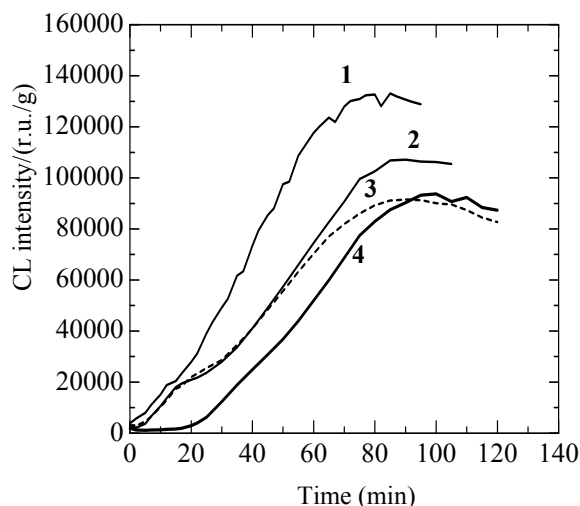
Fig.4 – Isothermal CL curves (200OC, air) for LDPE unstabilized (1) and stabilized (0,25% w/w) with rosemary extraction precipitates resulted from solutions in diethyl ether (2), acetone(3) and methanol (4)

Table 1- Kinetic parameters for thermal oxidation of LDPE in air at 200OC in the presence of studied extracts

Solvent	Induction period t_i(min)	Initial CL intensity I_O (r.u./g)	Integrated CL signal $\sum_0^{20} I_{CL}$ (r.u./g)
—	8.8	3800	134300
Acetone	12	3067	98133
Diethyl ether	14.9	3133	98301
Methanol	24	1900	14767

Figure 5 shows the effect of temperature on the chemiluminiscence of LDPE stabilized (0.25% w/w) with the rosemary extraction precipitate resulted from the methanol solution. The curves from figure 5 were used to calculate the main kinetic features as listed in table 2.Table 2 also includes the kinetic features for the unstabilized LDPE samples.

From t_i and t_{max}, E_i and E_{max} activation energies were calculated respectively. As can be seen in table 2, $E_i > E_{max}$. This difference could be due to the existence of different processes: E_i corresponds for induction period, while E_{max} corresponds to overall process (induction and acceleration of oxidation).

The stabilized LDPE presents higher values for the activation energies in comparison with the unstabilized ones.
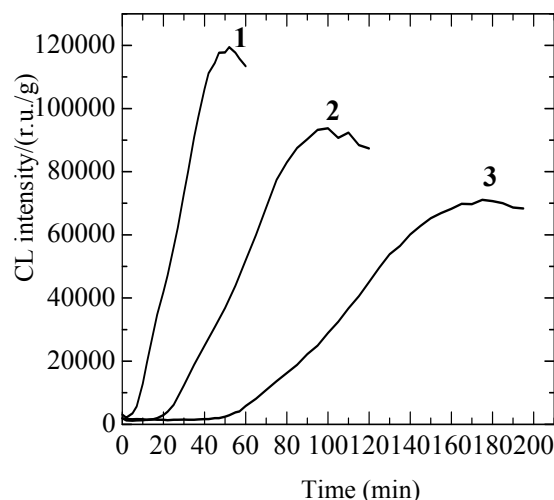
Fig.5 – CL curves for LDPE stabilized with rosemary extraction precipitate in methanol (1) 210^OC; (2) 200^OC; (3) 190^OC

Table 2- The CL kinetic parameters of the LDPE unstabilized and stabilized with rosemary extraction precipitate in methanol

Temp. (^{O}C)	Unstabilized LDPE		Stabilized LDPE	
	Induction time t_i (min)	Maximum oxidation time t_{max} (min)	Induction time t_i (min)	Maximum oxidation time t_{max} (min)
180	36	187	—	—
190	20	92	65	175
200	8.8	84	24	100
210	—	—	10	52
E(Kj/mol)	113.8	71.5	165.8	107.6
lnA	-26.6	-13.9	-38.9	-22.8
Corr. coef.	0.998	0.918	0.999	0.999

4.Conclusions

- Rosemary extracts containing carnosic acid or other phenolic compound which derives from carnosic acid, can be used as low temperature antioxidant for LDPE;
- The compounds responsible for the antioxidant activity come from a cascade of oxidation reactions starting with carnosic acid;
- Scavenging of radicals is a suitable method for inhibition of primary oxidation product formation by natural extracts in the plastic packing;
- Chemiluminiscence provides a means for quickly determining the stability of various materials in the presence of different antioxidants. The length of the induction period is a measure of stabilizer efficiency and the initial CL intensity is dependent upon the degree of oxidation.

5.References

[1] Brieskorn,C.H., Domling,J.H., *Z.Lebensm Unters Forsch.*, **141**, 10,1969;

[2] Brieskorn,C.H., Domling,J.H., *Arch. Pharm.*, **302**,641, 1969;

[3] Scwarz,K., Ternes, W., *Z.Lebensm Unters Forsch.*,**195**, 99, 1992;

[4] Wenkert, E., Fuchs,A., McChesney,J.D., *J.Org.Chem.*, **30**, 2931, 1965;

[5] Gonzales,A., Andres,L., Aguiar,Z., Luis,J., *Phytochemistry*, **31**, 1297, 1992 ;

[6] Richheimer,S.L., Bernart, M.W., King,G.A., Kent,M.C., Bailey,D.T*., J.Am.Oil Chem.Soc.*, **73**, 507, 1994 ;

[7] Cuvelier,E., Richard,H., Berset, C., *J.Am.Oil Chem.Soc.*, **73**, 645, 1996;

[8] Jipa,S., Zaharescu,T., Setnescu,R., Setnescu,T., Brites,M.J.S., Silva,A.M.G., Marcelo – Curto,M.J., Gigante,B., *Polym.Int.*, **48**, 414, 1999;

[9] Avram,M., Mateescu,Gh.D., *Spectroscopia in Infrarosu. Aplicatii in Chimia Organica*, Ed. Tehnica, Bucuresti, 1966;

[10] Black,R.M., Charlesby,A., *Int. J .Appl. Rad. Isot.*, **7**, 134, 1959;

[11] Bosch,S.M., Alegre, L., Schwarz,K*., Eur. Foods Technol.*, **210**, 263, 2000;

[12] Wekert,E., Fuchs,A., McChesney,J.D., *J.Org.Chem.*, **30**, 2931, 1965;

ANA-MARIA HOSSU
CRISTIANA RĂDULESCU
IONICA IONIȚĂ
IRINA-ELENA MOATER[1]
DUMITRA HOSSU[2]

STABILITY ANALYSIS OF VITAMIN E IN PHARMACEUTICAL PRODUCTS

[1]"Valahia" University Târgoviste, Sciences Faculty, Chemistry Department, 18-20 Avenue Unirii, Târgoviste, Romania
[2] School „Coresi", 2 Aleea Trandafirilor, Targoviste, Romania

Abstract: *Vitamins are generally sensitive to light, high temperatures and moisture. They should be kept in properly closed containers, protected from humidity and light at temperature of maximum 21^0C.The aim of this work is to analyse the stability of vitamin E. The analyzed technique used was the HPLC method for analytical characterization of these.*

Keywords: vitamin E, HPLC, stability analysis, pharmaceuticals

1. Introduction

Most of the fat-soluble vitamins present in pharmaceutical preparations or in natural products are accompanied by a number of closely related compounds. This explains why chromatographic methods are so frequently used in analysis of these compounds. HPLC is almost ideally suited for these compounds because of its simplicity, speed, selectivity and sensitivity.[1-6]

Vitamin E (formula 1) is an important biological molecule involved in fertility processes, an anti-sterility vitamin. The determination of vitamin E has gained increased significance in several areas of analytical chemistry such as pharmaceutical, clinical and food applications. A large number of methods have been reported for the determination of this compound.

1
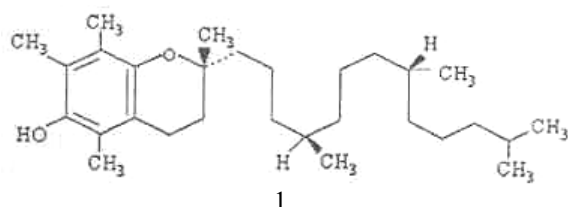
A number of HPLC modifications for the simultaneous analysis of vitamins A and E in pharmaceutical preparations and biological material have been worked out. These methods usually used UV, fluorimetric or electrochemical detection [7,8]. The two vitamins were determined on a μ-Bondapak C-18/Corasil guard column and a μ-Bondapak C-18 analytical column using elution with aqueous methanol and detection at 325 nm (retinol) or 292 nm (tocopherol).[9]

A mixture of retinol, β-carotene, α-tocopherol, retinyl palmitate, or acetate and vitamins D_2 and D_3 was separated on Zorbax ODS using the mobile phase methylene chloride with 0.001% triethylamine-acetonitrile-methanol (300:700:x; x = 0-40).[10] The solvent system without methanol separated all of the above compounds except vitamins D_2 and D_3.

The mobile phase hexane-isopropanol-methanol was used to separate α-tocopherol from vitamins A, D, H, K and another compounds in pharmaceuticals.[11]

In the experimental part of this work the influence of temperature on the stability of this vitamin fat-soluble is analyzed using the HPLC method [12], during 30 months. The stability is influenced by light, moisture and the preservation conditions, too.

2. Experimental

The investigations were carried out with a Spectra-Physics Analytical Model P 4000 liquid chromatograph with a Model 2000 UV detector (Spectra-Physics Analytical). This system was connected to a computer Pentium III 800MHz.

The pump P 4000 is conceived to reach the performances and the maximal capacities. It presents features of vanguard: four solvents, eleven files users of the names of files and solvents, and a waiting line for the link of the files.

The UV 2000 is a detecting UV/vis doubles length of wave, programmable, entirely equipped. It functions as well in simple fashion that length of wave doubles in fashion, in the UV ranges and visible. The UV 2000 also offers the spectral sweep, a file develop (for the development of the methods), the storage of several files, a waiting line (for the link of the files), and more. We place the detector to a length of wave λ = 292 nm for determination of vitamin E.

A mobile phase composed of methanol and water (98/2) allowed a very good separation of vitamin E on LC 18 column.

The vials of oral solution Biosol (Biokim Istanbul Turkey) were stored in special climate shelves. The vials were kept at temperatures of $+5^0C$, $+15^0C$, $+21^0C$ and $+37^0C$.

The following tests have been executed:
- optical appearance of the product;
- qualitative and quantitative analysis of the active ingredient (vitamin E).

3. Results and discussion

For vitamin E, the European Pharmacopoeia gives the following storage instructions: "store in a well-closed, well-filled container, protected from light, between 8^0C and 15^0C. When the container has been opened, its contents should be used as soon as possible; any part of the contents not used at once should be protected by an atmosphere of inert gas (e.g. nitrogen)".

The limits for the contain in vitamin E for each vial are 27 – 33 mg/mL.

The results of the determinations for each temperature, test period 30 months, are presented below in Tables.

Assay	Vitamin E (mg/mL)
Nominal value	30
Date of manufacture	33
6 months	33
12 months	32
18 months	32
24 months	31
30 months	31

Table 1. The results obtain at temperature $+5^0$C (refrigerator)

Assay	Vitamin E (mg/mL)
Nominal value	30
Date of manufacture	33
6 months	33
12 months	32
18 months	31
24 months	31
30 months	30

Table 2. The results obtain at temperature $+15^0$C (cool cabinet)

Assay	Vitamin E (mg/mL)
Nominal value	30
Date of manufacture	33
6 months	33
12 months	32
18 months	31
24 months	30
30 months	29

Table 3. The results obtain at temperature $+21^0$C (room temperature)

Assay	Vitamin E (mg/mL)
Nominal value	30
Date of manufacture	33
6 months	31
12 months	30
18 months	29
24 months	27
30 months	25

Table 4. The results obtain at temperature $+37^0$C (climate cabinet)

We remark from the Tables that the oral solution of Biosol in the original vial is stable and retains its activity when stored at room temperature ($18-21^0$C). Under high temperatures (37^0C climate cabinet), the solution is showing an intensifying coloring after longer storage and looses activity, which are even below the tolerances of the declared value.

4. Conclusions

The stability tests show that during a storage period of 2 years an adequate stability is provided, when the product is stored at room temperature ($< 21^0$C) and protected from light.

The choice of the storage temperature plays an important roll for the stability of the pharmaceutical products of vitamins.

References

[1] F. Pellerin, D. Dumitrescu, *Talanta*, 27, 243 (1980).

[2] J. N. Thompson, *Trace Anal.*, **2**, 1 (1982).

[3] G. O. Wachob, *Liq. Chromatogr. HPLC Mag.*, 1, 110 (1983).

[4] F. Zonta, B. Stancher, *Riv. Ital. Sostanze Grasse*, 60, 65 (1983).

[5] Y. de Roeck-Holtzhauer, E. Montel, *Ann. Falsif. Expert. Chem. Toxicol.,* 76, 331 (1983).

[6] T. Cannelle, G. Bichi, *Boll.Chim. Farm.,* 122, 205 (1983).

[7] M. Mulholland et al., *J. Chromatogr.*, **350**, 285 (1985).

[8] M. L. Huang et al., *J. Chromatogr.*, **380**, 331 (1986).

[9] J.G. Bieri et al., *Amer. J. Clin. Nutr.,* **32**, 2143 (1979).

[10] W. O. Landen, Jr. et al., *J. Chromatogr.,* **211**, 155 (1981).

[11] G. Jones, N. Edwards, D. Vriezen, C. Porteus, D.J.H. Trafford, J. Cunningham, H.L.J. Makin, *Biochemistry*, **2**, 173 (1988).

[12] ****Farmacopeea Romana*, ed X, Editura Medicala, Bucuresti, 1993.

IONICA IONIȚĂ [1]

CRISTIANA RĂDULESCU[1]

ANA-MARIA HOSSU[1]

ELENA IRINA MOATER [1]

INTERMEDIARES USED FOR SYNTHESIS OF SOME AZO PHOTOCHROMIC DYES

[1]Valahia University Târgovişte, Sciences Faculty, Chemistry Department, 18-20 Avenue Unirii, Târgovişte, România

Abstract: The paper presents the synthesis and characteristics of some photochromic dyes, derivatives of the phenylaminomethylensulfonic acid. The synthesized structures will be included on macromolecular catena to obtain some stable photochromic materials with special applications in ONL.

1. Introduction

The diazotation is the process wherewith obtained diazonium salts of primary aromatic amines, intermediaries in synthesis of azo dyes. Generally, diazonium salts are obtained by treatment of primary amines with nitrous acid (it's obtained in reaction medium from the sodium and mineral acid) in water, at cold (0-10°C) in presence of mineral acid [1].
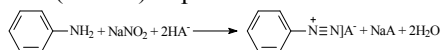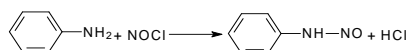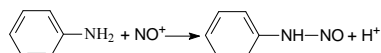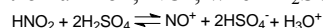

Mechanism
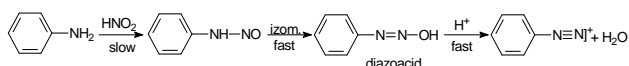
The active form of the nitrous acid, the electrophil agent which attack the primary amine depends by nature of the reaction medium:

- the nitrozil chloride or bromide at the diazotation with HCl or HBr:

$$HNO_2 + HCl \rightleftharpoons NOCl + H_2O$$

- the nitrozium ion, NO$^+$, when H$_2$SO$_4$ is used:

$$HNO_2 + 2H_2SO_4 \rightleftharpoons NO^+ + 2HSO_4^- + H_3O^+$$

The mineral acid, which is used at the diazotation process by the strength of the generated electrophil agent, therefore it's selection depends by the basicity of the used amines.

Therefore, the diazonium salts used us, were obtained in the aqueous medium with HCl (p-chloroaniline, p-bromaniline) or H$_2$SO$_4$ (p-anisidine, p-iodoaniline, p-toluidine, p-ethylaniline).

2. The general procedure of synthesis

Aniline (0.05 mole) is dissolved in acidulated water with amount of proper acid (table 1). After the cooling of this solution (max.5°C) added in drop and below agitation, with temperature control (<5°C) aqueous solution of NaNO$_3$ (3.5 g/18.5 ml water), so the molar rate amine: NaNO$_3$ = 1:1.

Therefore, the reaction mass is maintained about 30 minutes below agitation at temperatures 0-5°C and the nitrous acid in excess is destroyed by addition of the sulphamic acid and it is filtered the diazonium salt.

Table 1. *Diazotation procedure.*

Amine type	Mineral acid type	V$_{acid}$ (ml)	VH$_2$O (ml)	η %	Observation
p-anisidine	H$_2$SO$_4$ 98%	6.68	31	86	Subsequent dilution of reaction medium mass with 60 ml water
p-chloroaniline	HCl 36%	30	75	82	Subsequent dilution of reaction medium mass with 100 g ice
p-iodoaniline	H$_2$SO$_4$ 98%	26.6	-	79	Subsequent dilution of reaction medium mass with 50 ml water
p-bromaniline	HCl 36%	15	50	85	Subsequent dilution of reaction medium mass with 100 g ice
p-toluidine	H$_2$SO$_4$ 98%	5.3	40	80	Subsequent dilution of reaction medium mass with ice
p-ethylaniline	H$_2$SO$_4$ 98%	5	30	84	-

A. Coupling diazonium salt with phenylaminomethylensulphonic acid (sodium salt):
- the coupling reaction results after the model of the electrophil substitution, the diazonium group which is deficitaryed in electrons, substituting a hydrogen atom from the couples component, a position with higher electrons density (*o* and/or *p*) because is necessary the presence of a electronodonor substituent (as shown in Fig.1).

It is know the fact that in the low acid, the aromatic amines couples preferentially in the *para* position, coupling rate being determinate direct by structure of two reaction partners: diazocomponent and coupling component.

Thus, the presence of the electronoacceptor substituents in diazocomponet and of the electronodonors in coupling component will grow the reaction rate.

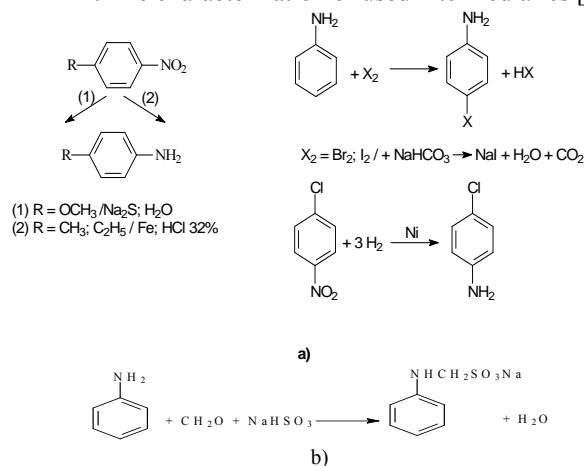Therefore, these conclusions can be explained depending by:
- the limit structure of the diazonic component is necessary because the phenyl nucleu has strong character attraction of electrons (as show in Fig.1a);
- the limit structure of the coupling component has a major contribution as well the phenyl nucleu has a higher density of electrons.

a) $X = OCH_3; Cl; I; Br; CH_3; C_2H_5$

b) $Y = \ddot{N}HCH_2SO_3Na$
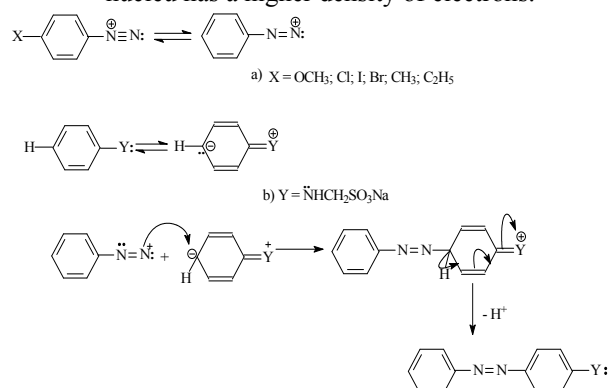
Figure 1. *The general reaction of synthesis scheme of azo dyes:*
a) The electrophil active form of the diazonium derivatives;
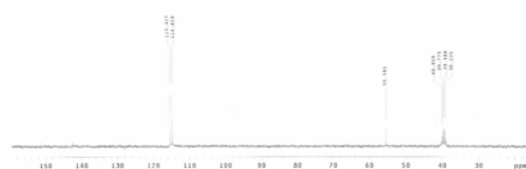*b) The active form of coupling component.*

B. The characterization of used intermediaries [2]

(1) $R = OCH_3 / Na_2S; H_2O$
(2) $R = CH_3; C_2H_5 / Fe; HCl\ 32\%$

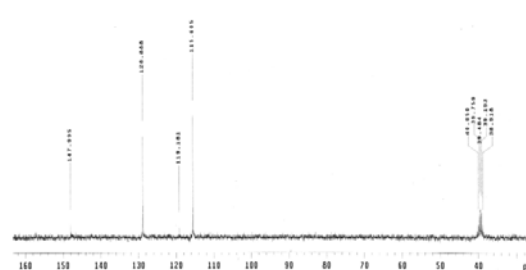$X_2 = Br_2; I_2 / + NaHCO_3 \rightarrow NaI + H_2O + CO_2$

a)

b)

Figure 2. *The synthesis of necessary intermediaries for obtained the azo derivatives:*
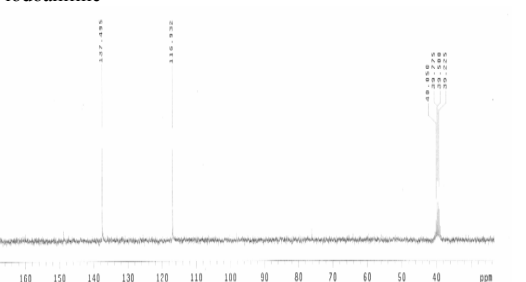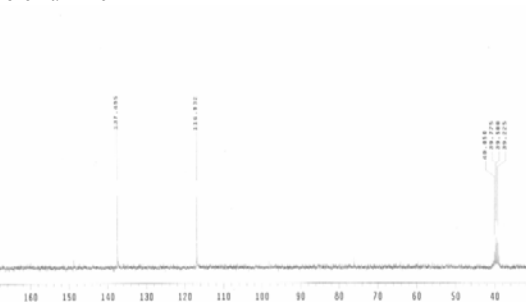*a) coupling component; b) diazotation component.*

p-anisidine

p-chloroaniline

p-iodoaniline

p-bromaniline

The ^{13}C-NMR spectra

Table 2. *The physical properties of synthesised intermediaries.*

Compound	Boiling point	η, %	Solubility	UV-Vis spectra λ_{max}, nm (extinction)
4-ethylaniline	215 – 217 ^{0}C*	85	CH$_3$COCH$_3$,C$_2$H$_5$OH, C$_6$H$_6$, DMF.	229.7 (1.662) 281.3 (0.269)
p-anisidine	58	90%	CH$_3$COCH$_3$,C$_2$H$_5$OH, C$_6$H$_6$, C$_2$H$_5$OC$_2$H$_5$, DMF.	290.4 (0.071)
p-chloroaniline	70	72	H$_2$O(at hot), C$_2$H$_5$OH, CH$_3$OH, CH$_3$COCH$_3$, CS$_2$, C$_2$H$_5$OC$_2$H$_5$, DMF.	237.2 (0.258) 292.9 (0.028)
p-iodaniline	63	80	CH$_3$COCH$_3$,C$_2$H$_5$OH, C$_6$H$_6$, DMF.	242.2 (0.457)
p-bromaniline	62	87	CH$_3$COCH$_3$,C$_6$H$_6$, DMF.	239.3 (0.282)
p-toluidine	44	85	CH$_3$COCH$_3$, C$_2$H$_5$OH, C$_6$H$_6$, DMF.	229.7 (0.103)

*:$T_t = -5 - 2^0$C
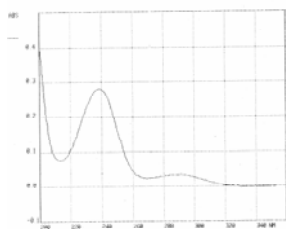
p-bromaniline | p-ethylaniline
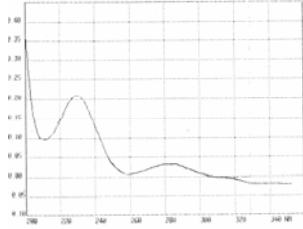
p-chloroaniline | p-iodoaniline

The UV-Vis spectra of intermediaries

3. Conclusions

The UV-Vis spectra were recorded on a SECOMAM S750 spectrophotometer, using the quartz vats, for solutions having a 2.10^{-5} mol/l in C_2H_5OH concentration. The characterisation by ^{1}H-NMR and ^{13}C-NMR spectra shown in table 3 and 4, confirm the theoretical structures of synthesised intermediaries.

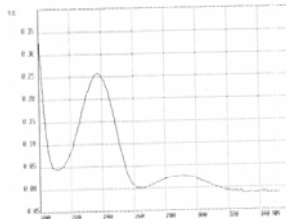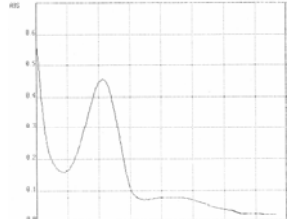The NMR spectra were made with a Varian Gemini 300BB apparatus, the frequency of registration being of 75 MHz for ^{13}C-NMR and 300 MHz for ^{1}H-NMR, using deuterated dimethyl-sulfoxide as a solvent [4].
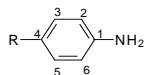

Table 3. *The ^{1}H-NMR spectra of intermediaries.*

δ(ppm) Cod	$H^2(H^6)$ exp	t	$H^3(H^5)$ exp	t	NH_2	OCH_3	CH_3
p-anisidine	6.51 $J_{2,3}$=3.06Hz $J_{2,6}$=1.55Hz	6.43	6.63 $J_{3,2}$= 8.66Hz $J_{3,5}$=1.55Hz	6.6	4.56	3.60	6.43
p-chloroaniline	6.54 $J_{2,3}$=8.49Hz $J_{2,6}$=1.58 Hz	6.46	6.99 $J_{3,2}$=8.49 Hz $J_{3,5}$=1.55 Hz	7.05	5.18	-	-
p-iodoaniline	6.41 $J_{2,3}$=8.66Hz $J_{2,6}$=3.06Hz	6.26	7.25 $J_{3,2}$=8.66Hz $J_{3,5}$=1.55Hz	7.43	5.22	-	-
p-bromaniline	6.50 $J_{2,3}$=7.68 Hz $J_{2,6}$=1.55 Hz	6.39	7.11 $J_{3,2}$=7.68Hz $J_{3,5}$=1.55 Hz	7.25	5.21	-	-
p-toluidine	6.45 $J_{2,3}$=8.17Hz $J_{2,6}$=1.55Hz	6.46	6.8 $J_{3,2}$=8.17Hz $J_{3,5}$=1.55 Hz	6.86	4.74	-	2.1

*exp = experimental; t = theoretic.

Phenylaminomethylensulphonic acid
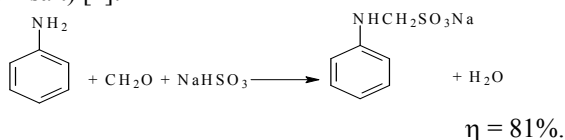(N-methilenphenylamino-ω-sulphonic acid; sodium salt) [4]:

$\eta = 81\%$.

Table 3. *The ^{13}C-NMR spectra of intermediaries.*

δ (ppm) Cod		p-anisidine	p-chloro aniline	p-iodo aniline	p-brom aniline	p-toluidine
$C^3(C^5)$	exp	115.427	128.888	137.49	131.71	129.648
	t	117.10	130.1	138.7	123.6	130.4
$C^2(C^6)$	exp	114.829	115.605	116.93	116.20	114.473
	t	115.4	117.1	117.7	118.3	116.1
–OCH_3		55.501	-	-	-	-
- CH_3		-	-	-	-	20.280

The ^{1}H-NMR spectra for phenylaminomethylensulphonic acid:
- H^4 triplet δ_H: 6.48 ppm, with the coupling constants orto J(4,3) = 7.68 Hz
- (H^2) H^6 split doublet δ_H: 6.69 ppm, with the coupling constants orto J(2,3) = 8.16 Hz
- (H^5) H^3 triplet δ_H: 6.69 ppm, with coupling constants orto J(3,4) = 7.29 Hz
- NH – triplet at 5.96 ppm, constants J = 6.61 Hz
- the signals of 3.88 ppm has been attributed the presence of group –CH_2, constants J = 6.61 Hz

The ^{13}C-NMR spectra present signals for carbon atoms: C^3, C^5 δ: 128.694 ppm, C^2, C^6 δ: 112.677 ppm, C^4 δ: 115.864 ppm, and carbon atom from CH_2- group present δ: 60.613 ppm.
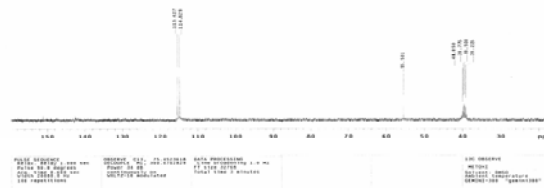
The final conclusion is that all intermediaries used to the azo dyes synthesis had maxim purity as well as all UV-Vis and NMR spectra [5].

References

[1]. Floru L., Langfeld H.W., Tărăbăşanu-Mihăilă C., *Azo dyes*, **296**, Ed. Tehnică, Bucureşti, 1981.

[2]. Sanielevici H., Urseanu F., *Synthesis of aromatic intermediaries*, Vol.II şi II, **145**, Ed. Tehnică, Bucureşti, 1983

[3]. Balaban A.T, Banciu M., Pogany I., *Application of the physic methods in organic chemistry*, Ed. Ştiinţifică şi Enciclopedică, Bucureşti, 1983

[4]. Ioniţă I, Tărăbăşanu–Mihăilă C., Rădulescu C., Annals of Ovidius University, series: Chemistry, volume XIV-lea, year 2003 – *''Azo dyes with photochromic proprieties''* , p.118-121.

[5]. Ioniţă I., Rădulescu C., Hossu A.-M., The Annals of ''Valahia'' University of Târgovişte, Session: Fundamental Science, **13**, 2003, *Azoic dyes derivatives of phenylaminomethylensulphonic acid*, p. 67-69.

S. JIPA[1]

W. KAPPEL[2]

T. ZAHARESCU[2]

R. SETNESCU[1]

R. L. OLTEANU[1]

M. BUMBAC[1]

INCREASES OF SALT SOLUBILITY IN MAGNETIC TREATED WATER AS STUDIED BY LYOLUMINESCENCE METHOD

[1] "Valahia" University of Târgovişte, Faculty of Sciences, 18-22 Unirii Bd., Târgovişte, Romania
[2] INCDIE, ICPE CA Bucharest, 313 Splaiul Unirii, P. O. Box 87, Bucharest 030138, Romania

___

Abstract: Water subjected to magnetic field was used as solvent for the dissolution of some halides, NaCl and KBr. Solubility measurements were carried out by lyoluminescence (LL). Significant differences between the dissolution rates with magnetically treated and untreated water were observed from the LL decay curves. The most important kinetic parameters (rate constant, half time and activation energy) that depict dissolution process were calculated. Reliable explanation on the magnetic treatment on water is presented regarding the scission of hydrogen bridges that are naturally formed in water.

Keywords: salt solubility, magnetic field, lyoluminescence

_____

1. Introduction

Magnetic treatment of water provides significant results in the decreasing of the amounts of deposits on pipe walls [1-4]. Permanent magnets or electromagnets are recommended to be used for magnetic treatment of domestic and industrial waters [5-8]. World-wide multidisciplinary performances have discovered the interest on magnetic treatment of water for various areas of human activities: agriculture [9], organic synthesis [10], biology [11] and so on, determining scholarly applications in the benefit of mankind. In the same time, the study concerning the effect induced by magnetic treatment on physical and chemical properties of water is of a large scientific and practical concern.

The purpose of the present work is the studying the kinetic behaviour of salt
dissolution in water upon its exposing to permanent magnetic field.

It is well known that solid alkaline halides previously subjected to the action of high energy radiation emit photons during their dissolution in water. This phenomenon is called lyoluminescence (LL). For the attending of paper purpose, we applied this method for measuring the rate of dissolution, taking into account the proportionality between the photon

emission rate and the recombination rate of the V and F centers that were formed during irradiation.

2. Experimental

In the present work analytical pollycrystaline sodium chloride and potassium bromide were used; 3g of each powder (NaCl or KBr) ground to 40 - 60 mesh were tightly sealed in glass capsules. These samples were exposed with ^{137}Cs gamma rays (dose rate 0.4 kGy/h) in air, at room temperature, in a Gammator M 38 irradiator to a total dose of 28 kGy. After irradiation, the samples were kept in a desiccator at room temperature for 24 h. After the storage period, lyoluminescence measurements were carried out.

The homemade equipment employed for studying the light emission is illustrated in Figure 1.
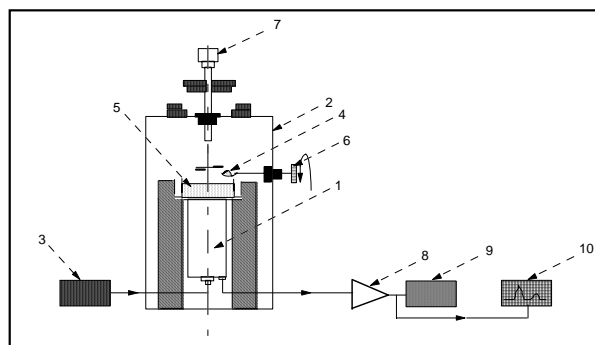
Fig. 1. Schematic diagram of the instrument for lyoluminescence measurements.
(1) light-tight box; (2) hopper; (3) sample; (4) dissolution cell; (5) photomultiplier tube; (6) EHT supply; (7) DC amplifier; (8) integrator; (9) X-Y recorder; (10) stirrer

This instrumentation consists of a photomultiplier FEU-19M enclosed in a light-tight box. The dissolution takes place in a cell on a stand placed just above the window of photomultiplier. The irradiated salt sample is allowed to drop in water from a hopper, which can be manipulated from outside. The

output of photomultiplier tube is directed to an electronic DC amplifier and this signal is then registered on a X-Y plotter.

For quantitative study on the lyoluminescence emitted by crystalline NaCl and KBr, the samples of 0.15 g were used for dissolution after dropping into 40 cm^3 of water placed previously in a transparent glass cell. The distilled water used in this experiment was checked to have a resistivity of at least 1 M $^{\sim}$
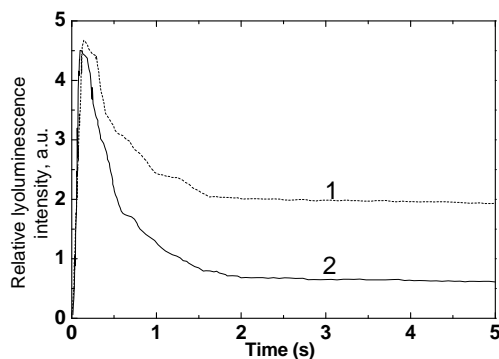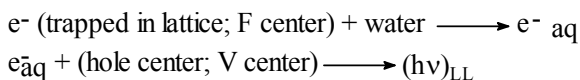
For the magnetic treatment of water, a permanent magnet with field strength in working zone of 0.4 T was employed.

3. Results and discussion

After the exposure of sodium chloride and potassium bromide crystals to the action of ionizing radiation the studied materials become coloured due to the presence of F centres that are formed: NaCl was turned to yellow and KBr was coloured in blue. In alkaline halides, some of the electrons trapped at colour centres recombine with holes, when the crystalline structure breaks down during dissolution.

The damage of irradiated crystal lattice on dissolution allows the defects to react to each other emitting a faint lyoluminescence as may be seen in Figures 2 and 3 drown for sodium chloride and potassium bromide, respectively.

Following the mechanism generally accepted for lyoluminescence is:

$$e^- \text{ (trapped in lattice; F center)} + \text{water} \longrightarrow e^-_{aq}$$

$$e^-_{aq} + \text{(hole center; V center)} \longrightarrow (h\nu)_{LL}$$

Fig. 2. Lyoluminescence decay curves of irradiated NaCl after dissolution in normal water (1) and in magnetic treated water (2). Total dose 28 kGy; applied magnetic field: 0.4 T for 1 h.
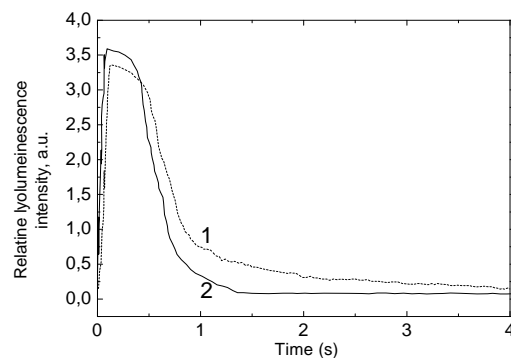
Fig. 3. Lyoluminescence decay curves of irradiated KBr after dissolution in normal water (1) and in magnetic treated water (2).Total dose 28 kGy; applied magnetic field: 0.4 T for 1 h.

The maximum intensity of emitted light begins to be detected after 0.25 s from the immersion of salt in water, while the decay time is extended to about 4-5 seconds. In the both figures, the two curves present different inclination for normal water and magnetic treated water. The two pairs of curves are beyond error limits. This aspect highlights the difference in the dissolution rates for the two types of waters. It means that the dissolution rate is influenced by the application of magnetic field before dissolution.

The dissolution rate of salt samples can be measured by watching the variation of lyoluminescence intensity in time on the descending parts of the curves.

Linear plots of $1/I_{LL}$ versus dissolution time (Figures 4 and 5) indicate that the dissolution follows a second order rate law:

$$\frac{dI}{dt} = k.I^2 \qquad (1)$$

where I is the LL intensity at time t and k is the overall dissolution constant rate.

Fig. 4. Variation of $1/I_{LL}$ on time for irradiated NaCl dissolved in normal water (●) and in magnetic treated water (○). Total dose 28 kGy; applied magnetic field: 0.4 T for 1h.
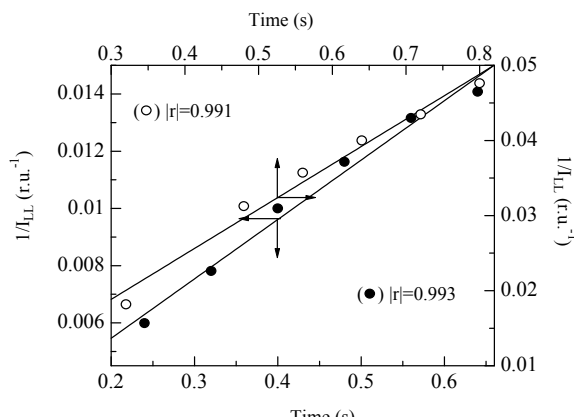
Fig. 5. Variation of $1/I_{LL}$ on time for irradiated KBr dissolved in normal water (●) and in magnetic treated water (○). Total dose 28 kGy; applied magnetic field: 0.4 T for 1 h.

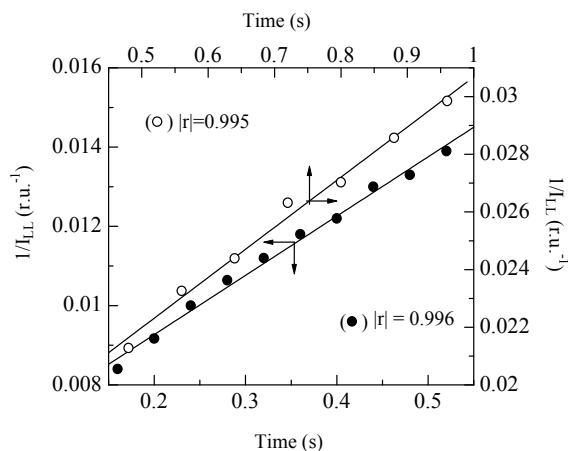The solution of rate equation (1) is

$$\frac{1}{I} - \frac{1}{I_0} = k.t \qquad (2)$$

where I_0 is the initial value of LL intensity at t=0.

Half times were calculated using the following relation:

$$t_{1/2} = \frac{1}{k.I_0} \qquad (3)$$

Table 1 shows the rate constants calculated from equation (2) and the half time values were obtained by means of equation (3).

Table 1. Rate constants for the dissolution of irradiated crystalline NaCl and KBr in the two kinds of waters

Salt	Rate constant, k [u.r.$^{-1}$.s^{-1}]		Half life, $t_{1/2}$ [s]	
	Dissolution in normal water	Dissolution in magnetic treated water	Dissolution in normal water	Dissolution in magnetic treated water
NaCl	0.0169	0.0287	0.33	0.24
KBr	0.0138	0.0456	0.35	0.17

The variation in the rate constants of sodium chloride and potassium bromide for the dissolution of irradiated samples in normal water at different temperatures has been studied.

The activation energy obtained from the Arrhenius plot of lnk vs 1/T is given in Figure 6.
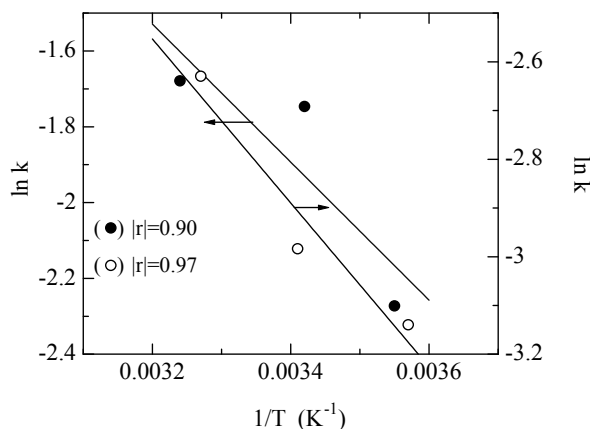
Fig. 6. Arrhenius plot for the evaluation of activation energy required in dissolution of NaCl (1) and KBr (2) in normal water

The magnetic water treatment affects the number of hydrogen bonds established between water molecules. Magnetic field would separate numerous water molecules decreasing the association degree and increasing the volume concentration of individual water dipoles. This effect influences the hydration of salt ions and, therefore, improves the salt solubility. Similar conclusion concerning the effect of magnetic field of physical properties of water was achieved by calorimetric measurements on dissolution enthalpy [12]

A reliable proof for the effect on the intermolecular interaction in magnetic-treated water is the modification in water density, as it was obtained by measurement of this physical property (Figure 7). The parameter means the ration between the densities of NaCl aqueous solutions prepared by means of magnetic-treated water and normal water at a certain time after treatment.

This behaviour demonstrates the reassociation of water molecules due to the mitigation of magnetic treatment.

From the Arrhenius representation drown for the dissolution of NaCl and KBr in water, activation energy values of 14.8 kJ/mol and 13.9 kJ/mol, respectively, were obtained. It is generally accepted that the activation energy for diffusion-controlled processes is below 20 kJ/mol [9].
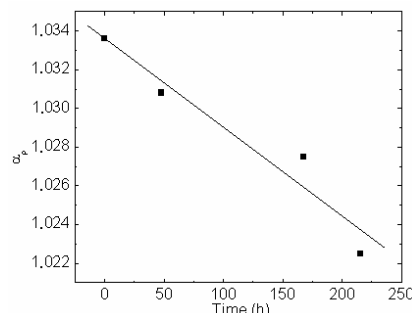
Fig. 7. Modification of density ratio for the dissolution of NaCl in magnetic-treated water.

It means that the the activation energy values obtained for the dissolution of studied halides in water correspond to this type of processes. Our results are similar to the information reported by Zdanovskii [13], but they are different in comparison with the values reported by Kulikov şi Mamaev [14].

4. Conclusion

   The magnetic treatment of water provides an accentuated increase of dissolution strength, which can be applied in various physical and chemical processes. The increase in dissolution rate may be taken into account in several applications, where high concentration of salts is required, or the dissolution of deposits must be removed. It seems that electrolytic phenomena are strongly influenced by magnetic treatment of water.

   This first paper will be followed by other investigations on the influence of magnetic field on dissolution strength of treated water.

References
[1] L. Lipus, J. Krope, L. Garbai, Hung. J. Ind. Chim. **22**, 239 (1994).
[2] R. Gehr, Z. A. Zhai, J. A. Finch, R. S. Rao, Water Res. **29**, 933 (1995).

.

[3] K. W. Busch, M. A. Busch, R. E. Darling, S. Maggard, S. W. Kubala, Trans. Inst. Chem. Eng. **75 (Part B)**, 114 (1997).
[4] G. Bikulchyus, A. Ruchinskene, V. Deninis, Protection of Metals **39**, 443 (2003).
[5] C. E. Hall, US Patent 5,944,973/Sept. 26, 1997, Int. Class. A47 J031/00.
[6] R. R. Holcomb, E. A. Arnold, A. J. Garrison, US Patent 5,113,751/May 19, 1992, Int. Class. A47J 031/00.
[7] D. J. van Gorp, US Patent 4,407,719/Oct. 4, 1983, Int. Class. C02F 001/48.
[8] C. H. Saunders, US Paternt 4,299,700/Nov. 10, 1981, Int. Class. B01D 035/06.
[9] C. H. Bamford, C. F. H. Tripper (eds), Chemical Kinetics, Elsevier, New York, 1969, p. 252.
[10] A. P. Chiriac, Rom. Rep. Phys. **56**, 503 (2004).
[11] P. Verkasalo, C. Pukkala, J. Kaprio, Scand. J. Environment Health, **22 (supl. 2)**, 7 (1998),
[12] Y. Zhao, L. A. Zhao, X. Wei, B. X. Han, H. K Yan, J. Thermal Analysis, **45**, 13 (1995).
[13]. A. B. Zdanovski, Zh. Fiz. Khim. **25**, 1951, p. 170.
[14]. B. A. Kulikov, N: A Mamaev, Zh. Fiz. Kh im. **47**, 1973, p. 91

RADU LUCIAN OLTEANU

SILVIU JIPA

RADU SETNESCU

TANȚA SETNESCU

LAURA MONICA GORGHIU

CRINELA DUMITRESCU

THERMO-OXIDATIVE STABILITY OF SOME POLYMERS RADIOCHEMICAL SYNTHETISED

[1]"Valahia" University of Târgoviste, Sciences Faculty, Chemistry Department, 18-20 Unirii Av., Târgoviste, Romania

Abstract: Several aspects regarding the influence of the monomer structure on the radiochemical polimerisation parameters – conversion rate and thermal stability – were assessed by IR spectroscopy and chemiluminescence method. The monomers – butyl acrylate (BA), butyl methacrylate (BM) and methyl methacrylate (MMA) – were exposed to gamma irradiation in air.

Keywords: polymerisation, acrylate and methacrylate monomers, γ - ray irradiation, chemiluminescence.

1. Introduction

By radio-induced polymerisation of many vinyl monomers high molecular products are obtained having almost identical properties with corresponding polymers obtained by conventional methods. Radiochemical polimerisation take place at low temperatures, no catalysts, the final products having high purity.

In most cases radiochemical polymerisation follows a chain radicalic mechanism. It was pointed out that gamma-radiation chemical action is limited to the primary events which lead to the generation of free radicals [1]. The main factors who contribute at polymerisation mechanism are: temperature, reaction medium, monomer concentration, dose rate [2,3]. Apart from radicalic polymerisation, ionizing radiations can initiate this reaction by ionic mechanism, cationic and anionic.

The vinyl monomers can be divided in two main groups based on their reactivity on radio-induced polymerisation: high reactive monomers (require low doses for polymerisation – 0,5÷2 Mrad, such as: vinyl chloride, methyl methacrylate, acrylic nitrile) and low reactive monomers (require high doses for polymerisation – 10÷20 Mrad, such as styrene).

In comparison with other initiation methods (thermal, microwave, UV radiations), radio-induced initiation of polymerization reactions has main features in the following lines:

❑ Polymerisation can be performed at low temperature due to the large amount of initiating species who can be formed in a very short time;

❑ Chemical reactions like polymerisation can be proceeded very homogenously (even in heterogenous phase) making possible a wide range of solid state polymerisation in resonable conditions.

This paper present some results on the research work performed on polymerisation of MMA, BA and BM. The thermo-oxidation stability of final products has been studied using chemiluminescence method (isothermal conditions). Also, the values of the apparent activation energy for initial thermo-oxidative degradation was calculated.

The oxidative degradation of the polymers (PMMA, PBM, PBA) is presented in scheme 1:
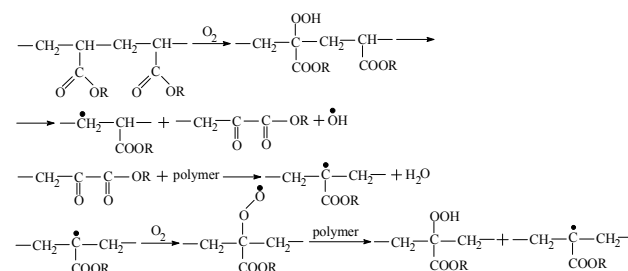
Scheme 1

Depolymerisation is the most important reaction in both thermal and themo-oxidative degradation of these polymers.

2. Experimental

For γ-irradiation (at room temperature) a 1600 Ci ^{137}Cs GAMMATOR M-38-2 equipment was employed; all monomers (Fluka) were purified prior to using by distillation and stored in the freezer in the dark.

Infrared spectra of the irradiated samples (polymers) were recorded on Specord IR-75 Carl Zeiss Jena spectrometer; the samples were dissolved in chloroform and thin films were obtained by solvent evaporation at room temperature.

The chemiluminescence mesurements were performed using a OL-94 aparatus described in a previous paper [4].

3. Results and discussion

In the IR recorded spectra the relative absorbance peak of the C=C bond of the monomer (at 1630 cm^{-1}) was measured; as internal standard to normalize the

data the carbonyl peak at 1715 cm^{-1} was used (as it remained constant during the polymerisation reaction).

Figure 1 shows the modifications of IR spectrum by gamma-irradiation for butyl methacrylate. The polymerisation reaction is accelerated at 20÷60% conversion. This phenomenon is known as gel formation or Trommmsdorf effect.
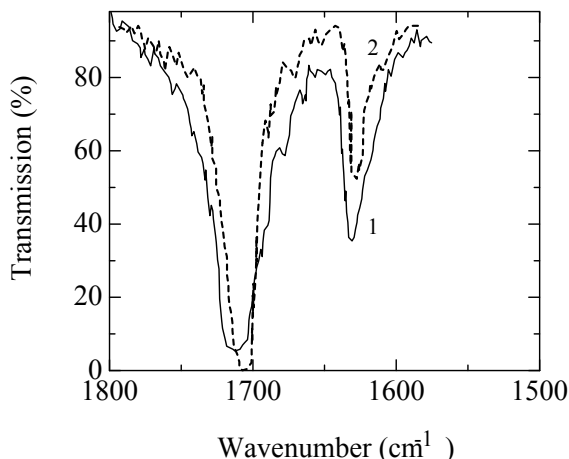
Figure 1 – Infrared spectra of butyl methacrylate samples: (1) original; (2) after 8 kGy irradiation

The percentage conversion from IR measurements was calculated using the following relation [5]:

$$\text{Conversion} = \frac{A_0 - A_t}{A_0} \cdot 100 \qquad (1)$$

where:

A_0 – absorbance peak area of C=C bond at the beginning of the reaction;

A_t – absorbance peak area of C=C bond after time t of the reaction;

The slope of the curves (figures 2-4) at inflexion point represent a kinetic parameter which is proportional with the polymerisation rate; for studied polymers this parameter follow the order:

PMMA ≅ PBA > PBM
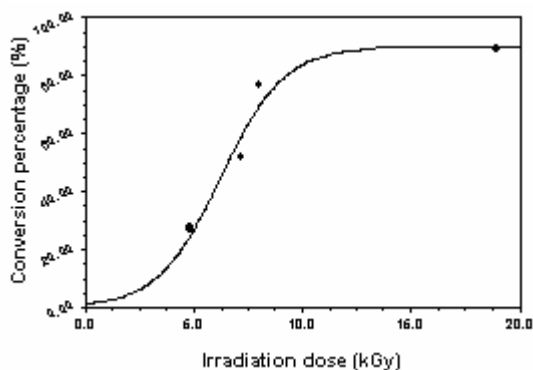
Figure 2 – Percentage conversion as function of dose for MMA polymerisation
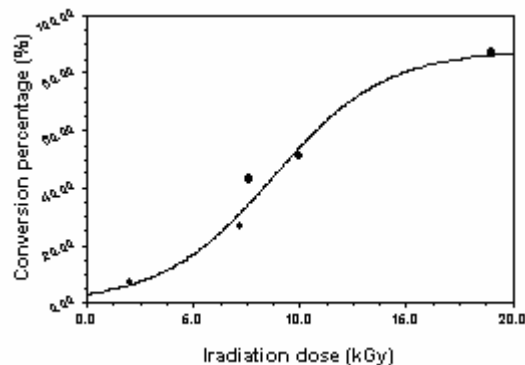
Figure 3 – Percentage conversion as function of dose for BA polymerisation
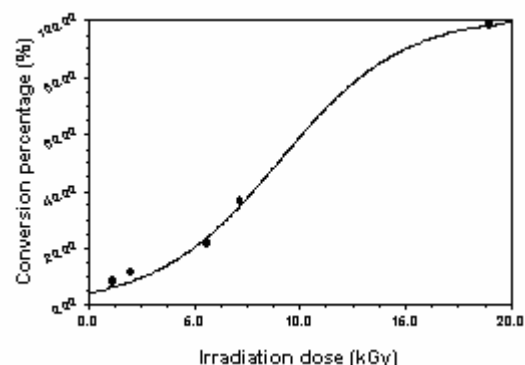
Figure 4 – Percentage conversion as function of dose for BM polymerisation

The isothermal chemiluminescence (CL) method was used to study the thermo-oxidative stability of a polymeric system. The measurement of initial CL intensity (I_0) is one of the most practical and common method for obtaining information on polymer stability and the degree of degradation (figure 5).
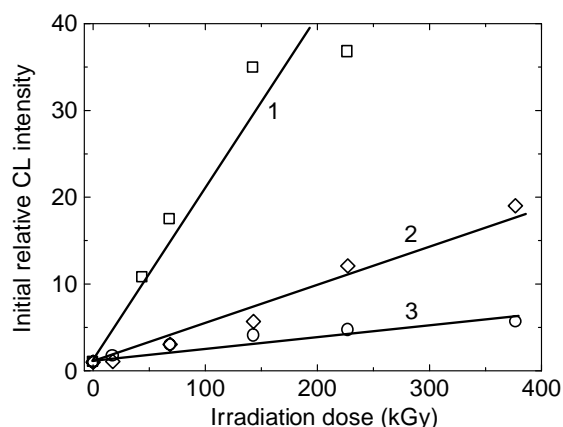
Figure 5 – Dependence of the initial relative CL (200°C, air) intensity on irradiation dose: (1) PMMA; (2) PBM; (3) PBA

The slope of the straight lines (figure 5) obtained by interpolation of I_0 values can be a parameter in the degree of polymer degradation. The slopes decrease in the following order:

PMMA >> PBM > PBA

The activation energy obtained from CL measurements are presented in table 1.

Table 1 - Activation energy for the thermo-oxidative degradation of polybutyl methacrylate (PBM)

Irradiation dose (kGy)	Activation energy for initial CL intensity (kJ/mol)
0	111,6
17,4	92,4
68,6	84,8
143	73,5
227,1	51,4
373,6	22,6

4. Conclusions

The radiation induced polymerization is a suitable alternative for the polymerisation of vinyl monomers.

Polymerisation rate, expressed by the conversion percentage, and also the thermal stability of the final products is a function of the structure of monomer.

The thermo-oxidative stability of studied polymeric systems follows the order:

PMMA << PBM < PBA

References

[1] TEODORESCU, I. E., FITI, M., *Iradierea tehnologica*, Ed. Academiei Romane, Bucuresti, 1979, 120.
[2] TABATA, Y., *Radiat. Phys. Chem.*, **9**, 32, 1977.
[3] HAYASHI, K., *Radiat. Phys. Chem.*, **18**, 183, 1981.
[4] JIPA, S., SETNESCU, T., SETNESCU, R., CAZAC, C., MIHALCEA, I., *Revista de Chimie*, **43**, 65, 1992.
[5] GOLUB, M. A., LERNER, N. R., HSU, N. S., J. *Appl. Polym. Sci.*, **34**, 383, 1990.
[6] SONG, J., FISCHER, Ch. H., SCHNABEL, W., *Polym. Degrad. Stab.*, **36**, 261, 1992.
[7] MADRAS, G., KARMORE, V., *Polym. Degrad. Stab.*, **72**, 537, 2001.
[8] CHANG, T. C., YU, P. Y., HONG, Y. S., WU, T. R., CHIU, Y. S., *Polym. Degrad. Stab.*, **77**, 29, 2002
[9] HU, Y. H., CHEN, C. Y., *Polym. Degrad. Stab.*, **82**, 81, 2003..

ELENA IRINA MOATER[1]

CRISTIANA RADULESCU[2]

IONICA IONITA[3]

ANA-MARIA HOSSU[4]

ADSORPTION OF NON-IONIC SURFACTANT AT SOLID-WATER INTERFACE

[1]"Valahia" University Targoviste, Sciences Faculty Chemistry Department, 18-22 Avenue Unirii, Targoviste Romania

Abstract: The study of adsorption of non-ionic surfactant at solid-water interface is necessary to explain the washing and cleaning processes, and dispersion of pigments. In this paper it was studied the behavior of alkyl glycosides and alkyl polyglycosides on solid-water interface through tensiometric and spectrophotometric methods.

Keywords: non-ionic surfactant, surface tension, adsorption isotherm, cotton, carbon black.

1. Introduction

Similarly of the L/G and L/L interfaces, non-ionic surfactants also influence the interface of liquid systems with solid substrates by virtue of their amphiphilic structure. This affects many applications and hence, may also can be used for numerous processes; washing and cleaning processes [1], the processing of ores [2], dispersions of solid in liquids [3].

The alkyl polyglucosides were found to possess remarkable properties which, in some cases, differ clearly from those of other non-ionic surfactant. In contrast to fatty alcohol ethoxylates (alkyl polyglycol ethers) there have been comparatively few studies of the adsorption properties of alkyl (poly)glycosides. The systematic dependence of adsorption on the structure of non-ionic surfactants was studied predominantly to non-ionic surfactant containing ethylene oxide groups [4].

There have been very few investigations into the adsorption properties of alkyl glycosides and alkyl polyglycosides to various types of solid [5]. The influence of structure of the solid was studied by the adsorption of the alkyl polyglycosides with different chain lengths on titanium dioxide [6] and hydrophilic glass surface [5].

The paper present tensiometric dates for alkyl glycosides C_8G_1, $C_{12}G_1$ and alkyl polyglucosides $C_{8\text{-}14}$ APG, $C_{12\text{-}14}$ APG.

Spectrophotometric was determined the adsorption isotherms of alkyl (poly)glycosides on different solid surfaces.

2. Materials and methods

The used non-ionic surfactants are alkyl glycosides with alkyl chain C_8 and C_{12}, abbreviated C_8G_1, $C_{12}G_1$ and alkyl polyglycosides $C_{8\text{-}14}$ APG, $C_{12\text{-}14}$ APG with an alkyl chain between 8-14 carbon atoms, abbreviated $C_{8\text{-}14}$APG and $C_{12\text{-}14}$APG, 51-53% substance active, products of Caspho-Europe.

Fig.1 Structure of alkyl polyglycosides –APG

The carbon black is produced by Cabot Corporation. He was used like an hydrophobic adsorbent with a specific surface area of $69 m^2/g$.

The cotton fibres are product of Rompel Surgical, are B-26 type corresponding to the International Calibration Cotton Standard . The cotton is cellulose material with hydrophilic sites which are negatively charged. All of the samples were conditioned at 21 ± 1^0C with $65\pm2\%$ of relative humidity for at least 24 hours (standardized conditions used for measurement of other fibre characteristics).

The mechanical preparation of cotton can affect the value of the specific surface area. The method of methylene blue adsorption for measuring the specific surface area of cotton fibre, as established here, can provide a common reference method for cotton fibre characterization in quality control. The specific surface area for these fibres cotton is $31.71 m^2/g$ [7].

The equilibrium concentration of the surfactants was determined by the surface tension method and by the UV-VIS spectrophotometry.

The surface tension was determined by the Du Nŏuy method. The Pt-Ir ring was attached to a torsion balance (Spiralfederwaage Germany) with an accuracy of 0.1 mN/m and a reproducibility of 0.05 mN/m. [8].

Spectrophotometric, the equilibrium concentration was determined by measuring UV and VIS absorbance at maxim wavelengths using Spectrophotometer Secomam S 760.

3. Results and discussion

The tensiometric results are shown in fig. 2.

Fig. 2 Static tension of alkyl (poly)glycosides with different alkyl chain lengths as a function of the concentration in water at 25^0C.

From the tensiometric date was determined the values of critical micellar concentration (CMC)(Table 1)

Table 1. The values CMC from surface tension measurements.

Surfactant	CMC mole/l
C_8G_1	1.8×10^{-2}
$C_{12}G_1$	4.5×10^{-4}
$C_{8-14}APG$	2.5×10^{-4}
$C_{12-14}APG$	5×10^{-5}

The CMC values of alkyl glycosides and alkyl polyglycoside are comparable with those of typical non-ionic surfactants and decrease distinctly with increasing alkyl chain length. The alkyl chain length has a far stronger influence on the CMC by comparison with the number of glycoside groups of the alkyl polyglycosides.

The adsorption of non-ionic surfactant is dependent upon the surface structure.

The amount of surfactant adsorbed per unit of adsorbent "a", was calculated using the following formula:

$$a = \frac{(C_0 - C)V}{m} \ (mole \ / \ g) \qquad (1)$$

where C_0 is the initial concentration of surfactant (moles/l), C is the equilibrium concentration of surfactant in solution (moles/l), m is the mass of the cotton (g) and V is the volume of solution (l)

The adsorption isotherms of C_8G_1 and $C_{12}G_1$ on carbon black at 22^0C are presented in fig.3.
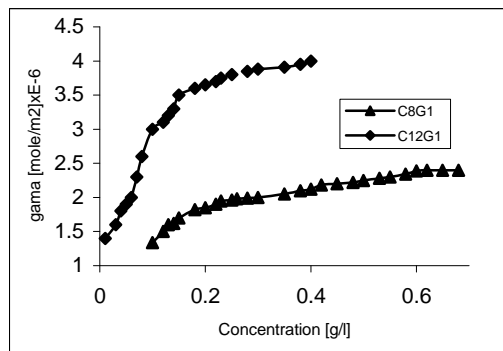
Fig.3 Adsorbed amounts Γ of C_8G_1 and $C_{12}G_1$ on carbon black as a function of the surfactant concentration at 22^0C.

The adsorption isotherms are characterized by a very steep initial slope which did not enable adsorption to be measured at low concentration of surfactants. This behavior indicates the high affinity of the alkyl glycosides for this solid surface. The alkyl glycoside C_8G_1 present a flat arrangement of the molecules, the maximum monolayer concentration is 2.4×10^{-6} moles/m^2 and $C_{12}G_1$ have a vertical arrangement, the monolayer concentration is 4×10^{-6} moles/m^2.

The adsorption isotherms of $C_{8-14}APG$ and $C_{12-14}APG$ on cotton are present in fig. 4.
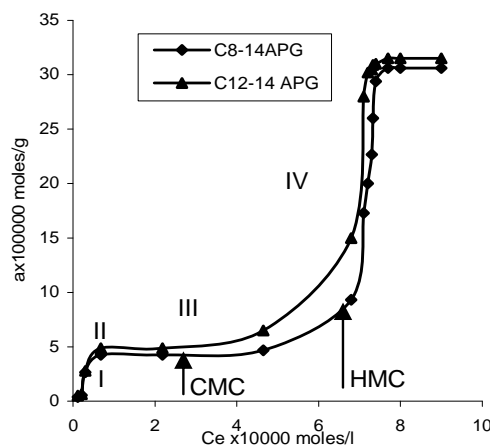
Fig. 4. Adsorption isotherms of APG on cotton from spectrophotometric data at21^0C:
1. $C_{8-14}APG$; 2. $C_{12-14}APG$

Alkyl polyglycosides show the same behavior on this polar solid surfaces. Depending of chain length, the adsorption increase with the hydrophobicity. The adsorption isotherm is characterized by two flat regions.

Theoretical, the monolayer can have an flat or vertical arrangement.

For a flat arrangement of the molecule, from our data, the maximum monolayer concentration is 1.34×10^{-6} moles m^{-2} which corresponds for a flat arrangement, compared with literature data (1.6×10^{-6} moles m^{-2}). If only the alkyl chains are adsorbed with the ether oxygen, which corresponds to a vertical arrangement, the monolayer concentration is 8.2×10^{-6} moles m^{-2}.

This thing suggests that the alkyl polyglycoside molecules at low concentration are adsorbed as isolated individual molecules. If the solution concentration of the surfactants is increased, two-dimensional aggregates named as "hemimicelles' are formed by a hydrophobic interaction of the alkyl chains.

This type of isotherm can be described by Fowler-Guggenheim equation (adsorbed film with lateral interaction):

$$-\log\left(c \cdot \frac{\Gamma_m}{\Gamma} - 1\right) = \log K - \frac{2 \cdot \omega}{2.303} \cdot \frac{\Gamma}{\Gamma_m} \qquad (2)$$

where Γ- the adsorption coefficient at the equilibrium concentration of the surfactant in solution c; Γ_m - the maximum adsorption coefficient; K - the characteristic

constant of the interaction between the adsorbed molecules and the solid surface sites, ω a parameter due to interaction between two neighboring adsorbed molecules. From the Fowler-Guggenheim equation one can obtain the free energy of adsorption ΔG_{ads} and the free energy of interaction ΔG_{int} from the following relations:

$$\Delta G_{ads} = -RT \ln K \quad \text{and} \quad \Delta G_{int} = RT\omega \quad (3)$$

The results obtained from the equations (2) and (3) for the whole adsorption isotherm (regions I-IV) is presented in Table 2.
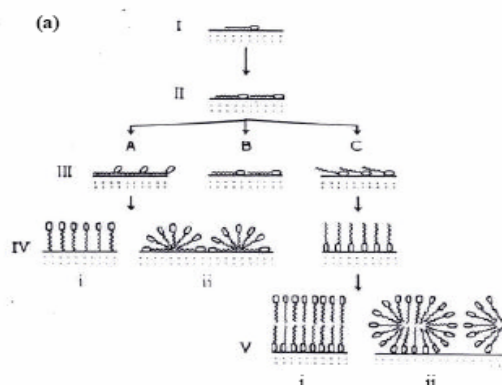
Table 2. Data for adsorption of nonionic surfactants APG on cotton at 21^0C and pH=7 (the Fowler – Guggenheim model).

APG	lnK	ω	F_{ads}	F_{int}	R^2
C_{8-14}	-4.89	-2.50	2.934	-1.50	0.935
C_{12-14}	-5.27	-2.74	3.162	-1.64	0.925

(F_{ads} –Kcal/moles; F_{int}-kcal/moles)

The Fowler-Guggenheim equation fits the results obtained at adsorption of nonionic surfactant APG on cotton.

The alkyl (poly)glycosides are physically adsorbed by adsorbate-adsorbate and adsorbate-solvent interaction which lead at surfactants aggregation and the orientation of surfactants on surface.

Fig.5 Adsorption of non-ionic surfactant, alkyl (poly)glycosides, showing the orientation of surfactant molecules on the surface [9]

The adsorbate-adsorbate interaction depends on the nature of the adsorbent and from the hydrophilic-lipophilic balance (HLB) in the surfactant.

The surfactant molecules orientation at surface depends of the surface and surfactant nature:IIIA- hydrophobic adsorbent-hydrophilic surfactant,IIIB- hydrophobic adsorbent-hidrophobic surfactant,IIIC- hydrophilic adsorbent-hidrophobic surfactant.

4. Conclusion

The alkyl chain length has a far stronger influence on the CMC by comparison with the number of glycoside groups of the alkyl polyglycosides.

The adsorption isotherms of alky glycosides C_8G_1 and $C_{12}G_1$ on hydrophobic surface are characterized by a very steep initial slope which did not enable adsorption to be measured at low concentration of surfactants. This behavior indicates the high affinity of the alkyl glycosides for this solid surface.

For alkyl polyglycosides C_{8-14}APG and C_{12-14} APG the adsorption depends of chain length and increase with the hydrophobicity.

The adsorption isotherm of alkyl polyglycosides on cotton is characterized by two flat regions. This suggests that the alkyl polyglycoside molecules at low concentration are adsorbed as isolated individual molecules, and at concentration above CMC, two-dimensional aggregates named as "hemimicelles' are formed by a hydrophobic interaction of the alkyl chains.

The forming of hemimicelles was verified by application of the Fowler-Guggenheim equation.

5. References

[1] Schwuger M.J., J.*Am. Oil Chem. Soc.* **59** ; 258. 1982.

[2] Leja, J. *Surface Chemistry of Froth Flotation, Plenum Press*, New York, 1982.

[3] McKay,R.B.,*Technological Applications of Dispersions*, Marcel Dekker, New York,1994.

[4] Rybinski von W., Schwuger M.J. ,in *Nonionic Surfactants Physical Chemistry* (M. J. Schick, cd.), Marcel Dekker, New York, 45, 1987.

[5] Nickel D., Rybinski von W., Kutschmann E. M., C. Stubenrauch, G.H. in press. Findenegg, *Procecdings 4th World Surfactant Congress*, Barcelona, June, Vol **2**, 371, 1996.

[6] Smith G.A., Zulli A.L. Grieser M.D., Counts M.C., *Colloids Surf. A* **88,** 67, 1994.

[7] Moater E.I., Olteanu M., *Buletinul Universitatii Petrol-Gaze,*vol.LVII, Seria Tehnica nr.2/2005, 170, 2005.

[8] Jones M.N. *J. Colloid Interface Sci* , **23**, 36, 1967.

[9]Clunie,J.S.and Ingram B.T. *Adsorption of non-ionic surfactant, in Adsorbtion from solution at the Solid/Liquid Interface* , Ed.Academic Press, New York, **3**, 105, 1983.

CRISTIANA RĂDULESCU[1]
IONICA IONIȚĂ[1]
ANA-MARIA HOSSU
ELENA IRINA MOATER

KINETICS OF DYEING OF SYNTHETIC FIBRES BY DISPERSE DYES DERIVATIVES FROM HETEROCYCLIC SYSTEM 2-AMINOTHIAZOLO[4,5-F]INDAZOLE

[1]"Valahia" University Târgoviste, Sciences Faculty, Chemistry Department, 18-20 Avenue Unirii, Târgoviste, Romania

Abstract: In this article a study of the colour properties of synthetic fibres is presented. The diffusion coefficient and dyeing rate constant of the synthetic fibres at the exhaust dyeing process by red disperse dyes derivatives from 2-aminothiazolo-indazole system were measured.

Keywords: disperse dye, 2-aminothiazolo[4,5-f] indazole, polypropylene, polyethylene terephthalate, dyeing rate

1. Introduction

The branch of the disperse dyes for dyeing of polyester fibres is important, because the production of polyester fibres grows rapidly. This production was increased by 155% for last 20 years. It caused larger usage of the disperse dyes.

Modification of polypropylene (PP) fibres is often oriented to the improvement of their electric properties, hydrophility and dye affinity. Production of blend from commonly accessible polymers is an effective way to prepare the new fibres with advanced properties for textile and technical application. Modification of polypropylene fibres with polyester exhibits the dye affinity from bath and printability by the disperse dyes obtained by synthesis [1-4].

The significant improvement of the dye affinity by the exhaust process was observed for blend polypropylene/poly(ethylene terephthalate) (PP/PET) fibres [2]. Disperse dyes diffuse primarily into the amorphous regions of blend fibres, mainly at the interface. This corresponds with a decrease of total crystallinity of blend fibres in comparison with total crystallinity of original PP and PET components.

The kinetics of the dyeing of polyester fibres by disperse dyes have been studied by several authors [5,6]. The various mathematical models were used for the description of the kinetics of the dyeing exhaustion process.

This paper presents a study of the colour properties of the synthetic fibres. The diffusion coefficient and dyeing rate constant of the synthetic fibres were measured at the exhaust dyeing process by disperse dyes. The new group of the disperse dyes was developed to decrease costs. These dyes used for dyeing synthetic fibres present a good stability of the dispersion on fibers, good levelness or fast diffusion into the fibres.

2. Experimental

2.1. Materials

Synthetic fibres

The following polymers were used for preparation of the fibres:
- Polypropylene Tartren TG 920 (PP)
- Polyethylene Terephthalate PET LFK (PET)

The blend PP/PET fibre was prepared in two steps – preparation of PP/PET concentrates and preparation of PP/PET blend fibres. The characteristics of the used synthetic fibres are presented in Table 1.

Table 1. Characteristics of the used fibres

Samples	A composition of	fibres
	PP TG 920 [%]	PET LFK [%]
A	100	-
B	92	8
C	-	100

Disperse dyes

- Red disperse dyes derivatives of heterocyclic systems 2-aminothiazolo[4,5-f]indazole, obtained by synthesis from authors [7-10], with structure presented in figure 1.
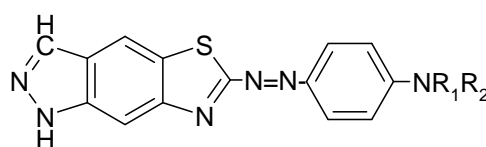
Red disperse dyes 1-9

Fig. 1. The red disperse dyes obtained by synthesis, with $R_1 = H$, CH_3, C
$R_2 = CH_3$, C_2H_5, C_2H_4OH

2.2. Dyeing

From fibres a preparation was removed in the bath (1,5g/l auxiliaries a 1 g/l Na_3PO_4) at 75^0C during 20 minutes. The fibres were dyed at temperatures 98^0C and 120^0C. The dyeing bath contained: 1 g/l dispersant, 2 g/l $(NH_4)_2SO_4$, formic acid pH=5, disperse dyes 2% and dyeing regime for PET fibres was used.

Colour characteristics

Colour characteristics of dyed fibres were calculated by CIE lab [11]. Colour parameters were estimated by measurement of reflectance curves by spectrofotometer Jasco V 550.

K/S values from Kubelka-Munk equation were calculated with the relation:

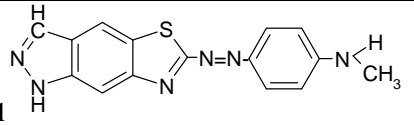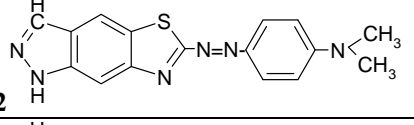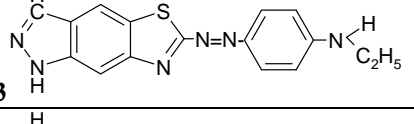$$K/S = (1-R^2)/2R \qquad (1)$$
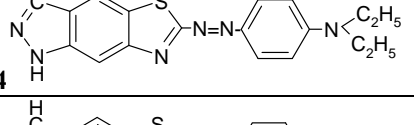
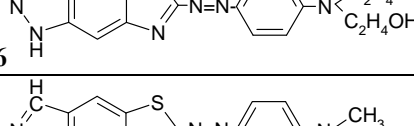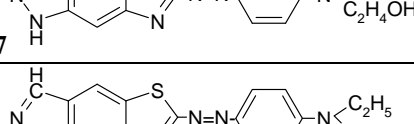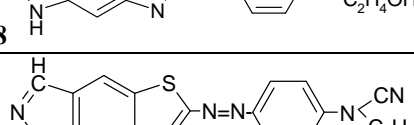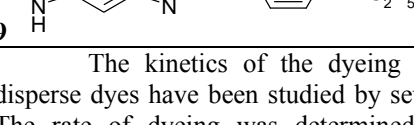where   K – absorbtion coefficient;
S – scattering coefficient;
R – reflectance value.
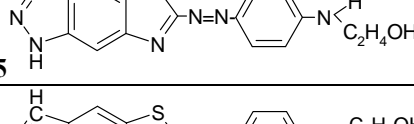
Kinetics of the dyeing

By the evaluation of the kinetics of the dyed exhaustion process of PP, PET and PP/PET fibres is regarded increase (decrease) concentration of disperse dye on fibre (in bath) in dependence from time. The process of dyeing was finished at certain time intervals (5, 10, 15, 20, 30 and 50 min). After removal of fibre from dyebath, a dyebath was completed by ethanol half and half. The quantity of exhausted dye on fibre was estimated from absorbtion of dye solution measured at its λ_{max} (Table 2) on Secoman S750 spectrofotometer. The dependence of exhaustion of dye from time was used for calculation of dyeing rate constant (K) and diffusion coefficient (D).

Table 2. The red disperse dyes used for dyeing of fibres

Disperse dye	Color, λ_{max}(nm) ε_{max}
1	Red dark 519.1 28200
2	Red dark 524.0 29800
3	Light red 531.1 31100
4	Light red 540.3 34200
5	Red-orange 529.0 30400
6	Red-orange 531.1 31800
7	Red-orange 550.2 32100
8	Red-orange 543.0 32900
9	Red 536.0 26200

The kinetics of the dyeing of polyester with disperse dyes have been studied by several authors [12]. The rate of dyeing was determined from hyperbolic Vickerstaff's equation [13]:

$$c_t = \frac{K \cdot t \cdot c_\infty^2}{K \cdot t \cdot c_\infty + 1} \qquad (2)$$

where K – dyeing rate constant, s^{-1};

c_t – concentration of dye in fibre after time t, mg/g;

c_∞ - concentration of dye at the moment of state of equilibrium,, mg/g;

t – time, s.

The diffusion coefficient (D) was determined from the following equation:

$$\frac{c_t}{c_\infty} = 4\left(\frac{D \cdot t}{\pi \cdot r^2}\right)^{1,2} \qquad (3)$$

where r – radius of fibre, m

D – diffusion coefficient, m^2/s.

and K, c_t, c_∞ and t are the some above mentioned.

3. Results and discussion

The objective of this work was to find, how PP fibres modified by PET are dyed by disperse dyes and to evaluate of kinetics of their dyeing.

A dependence of K/S and exhaustion of dyes on type of dyeing fibres (PP, PET and PP/PET) at 98^0C and 120^0C are given on the figures 2 and 3.

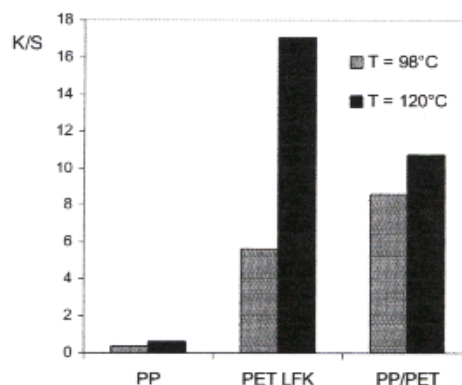

Fig. 2. The dependence of K/S of red disperse dyes on the type of fibre and temperature
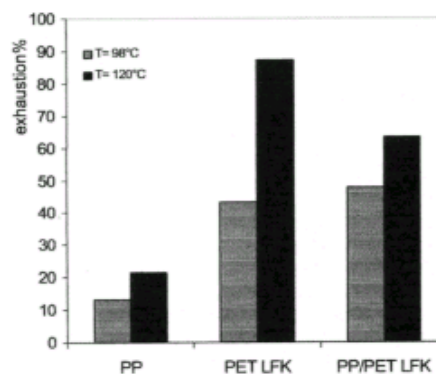

Fig. 3. The dye exhaustion of disperse dyes on fibres at 98^0C and 120^0C

of dyes is the highest for PP/PET fibres dyed at temperature 98^0C. The increase of dyed temperature on 120^0C causes a change of dyeing ability of these fibres.

At the temperature 120^0C, PET fibre is dyed the best and PP fibre is dyed the worst; the blend PP/PET fibres are dyed better as respond to 8% additives in PP fibres.

For exhaust dyeing of PP/PET fibres by red disperse dyes it is assumption, that disperse dye diffuse mainly into the amorphous areas and affinity of these dyes to PP/PET fibres depends on their chemical structure and conditions of dyeing. On the base of experimental results (figures 2 and 3) it is possible to state, that PET additive dispersed in PP matrix is able to change a supermolecular structure of PP. The dyes diffuse in the place where supermolecular structure is disturbed. The improvement of dye diffusion leads to increased of colour strength a few time at 98 and 120^0C. The comparison of dyeing ability of PP/PET fibre with PET fibre is more interesting; PP/PET fibre achieves better dye exhaustion at 98^0C and lower 120^0C as PET fibre. It is possible predict that PET additives change a stable crystalline structure of PP and it is allowed a higher diffusion of disperse dyes into fibre.

The kinetics of the dyeing of PP, PET and PP/PET were measured at 98^0C by evaluation of red disperse dye on the fibre as a dependence on time dyeing. The dependence of disperse dyes on time of dyeing (figure 4) confirms previous results that temperature (98^0C) and time of dyeing (50 min) are not satisfactory on the ideal colouring of PET fibre. The curve of the exhaustion of dye on fibre does not reach state of equilibrium dyeing in full time interval. The disperse dyes used for PP fibre is not satisfactory (exhaustion of dye on fibre is very low). The exhaustion curve confirms a well-known theory. From aspect of kinetics of dyeing, in spite of low dyeing ability of PP fibres, the equilibrium of dyeing PP fibre is achieved earlier as by PET and PP/PET fibres. From the view of kinetics of dyeing, the dyeing process of the blend PP/PET fibre can by described as additive process of dyed PP and PET fibres (figure 3). The diffusion of into PP/PET fibres is essentially lower in compared with PET fibre as well as the equilibrium state of dyed PP/PET fibre at 98^0C occurs essentially early (about 30 minutes).
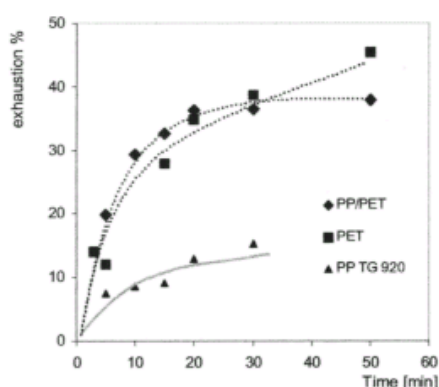

Fig.4. The dependence of the exhaustion of red dye **2** on the dyeing time, at 98^0C

Dyeing rate (K) and diffusion coefficient (D) for PP, PET and PP/PET fibres coloured at 98^0C was calculated with equations (1), (2) and (3). The results are presented in Table 3.

Table 3. Diffusion coefficient (D) and rate dyeing constant (K) for PP, PET and PP/PET fibres at 98^0C

Samples	K [s^{-1}]	D [m^2/s]
PP TG 920	3,019E-04	1,359E-14
PET	3,324E-05	2,155E-15
PP/PET	2,321E-04	2,316E-14

4. Conclusions

This paper presents next results:
- The exhaustion of red disperse dye at dyeing of PP, PET and PP/PET from dyebath was higher at 120^0C as 98^0C.
- At temperature 98^0C PP/PET fibre reached the highest of dye from all fibres.
- The kinetics of dyeing of synthetic fibres by disperse dyes is possible described by the equation (2) and (3) presented in literature.

References

[1] Ruys, L., *Chem. Fibres Intern.*, 47, 376, 1997

[2] Marcincin, A. et all, *Fibres and Textile*, 6, 119, 1999

[3] Teters, R. H., *Textile Chem.*, 3, Elsevier, Scientific Publishing, 1975

[4] Cegarra, J., Puente, P., *Textile Research Journal*, 37, 343, 1967

[5] Etters, J.N., *Textile Chem and Colorist*, 26, 17, 1994

[6] Wang, P. Y., Ma, J.F., *Dyes and Pigments*, 37, 121, 1998

[7] Rădulescu, C., Tărăbăşanu-Mihăilă, C., Hossu, A.M., Ioniţă, I., *Revista de Chimie*, 55(12), 1006, 2004,

[8] Rădulescu, C., Hossu, A.M., Ioniţă, I., *Valahia University Annals of Târgovişte - section Fundamental Science,* 13, 70, 2003

[9] Rădulescu, C., Ioniţă, I., Hossu, A.M., *Valahia University Annals of Târgovişte – section Fundamental Science*, 13, 77, 2003

[10] Rădulescu, C., Ioniţă, I., Hossu, A.M., Tărăbăşanu, C.M., Moater E. I., *Ovidius University Annals of Chemistry*, 16, 211, 2005

[11] Wright, W.D., *The Measurement of Color*, Ed. 4., Adam Higler Ltd. London, 1969

[12] Paterson, D., Sheldon, R.P., *Dyes and Pigments*, 55, 125, 2001

[13] Rosen, C. A. *Textile Chem.*, Unites States Patent, 4,985,258, 2000

C. MATHEMATICS SECTION

ALINA CONSTANTINESCU

A CLASSIFICATION OF THE ESTIMATION METHODS FOR THE NONLINEAR MODELS PARAMETERS

Valahia University of Targoviste, Dept. of Mathematics, Str. G. Enescu No.1, Romania

Abstract: In this paper we present a syntesis and a classification of the estimation methods which usses maximum likelihood function. The nonlinear models with random parameters allows as to model a set of nonlinear shape which ressults from the repeated measurements. This models describe both the inter-individual and the intra-individual variability.

1. Introduction (Headings –10 pt bold)

In the further exposition we deal with the nonlinear model in the clasical parametricaly aproach. We consider that the parameters are gaussian.
Thus, the model is:

$$\begin{cases} \mathbf{Y}_i = f\left(\mathbf{t},\boldsymbol{\beta}_i\right)+\boldsymbol{\varepsilon}_i \\ \boldsymbol{\beta}_i = \boldsymbol{\beta} + \mathbf{B}_i \\ \mathbf{B}_i \sim N_p\left(0,\boldsymbol{\Gamma}\right) \ \text{i.i.d.} \\ \boldsymbol{\varepsilon}_i \sim N_p\left(0,\sigma_\varepsilon^2 Id_j\right) \ \text{i.i.d.} \end{cases} \tag{1}$$

Where i is into the individuals set I; j is into the observations set J.

This model consist in the regresion ecuation which describes the intra-individual variability. The residual terms ε_i have the covariance gived by $\sigma_\varepsilon^2 Id_j$.

The expresion of the random parameters shows the inter-individual variability. This variability is gived by the random effects distribution.

The random parameters β_i have one commune parth for all the individs (β) and one particular parth for the I th individ. This second parth describes the deviation from the mean β.

$\theta = \left(\beta,\Gamma,\sigma_\varepsilon^2\right)$ is the parameter vector and must be estimated.

Its components are the model parameters mean β, the random parameters variance-covariance matrix $\Gamma = diag\left(\sigma_\beta^2\right)$ and the residual variance σ_ε^2.

If we deal with the maximum likelihood method for the parameters estimations, then is needful to maximise the likelihood function. For our model, this function and the log-likelihood function are:

$$V\left(\mathbf{Y}\,|\,\boldsymbol{\beta},\boldsymbol{\Gamma},\sigma_\varepsilon^2\right) = \left(2\pi\right)^{-\frac{IJ+I_p}{2}} \sigma_\varepsilon^{-IJ} \left|\boldsymbol{\Gamma}\right|^{-\frac{I}{2}}$$

$$\int \exp\left[\sum_{i=1}^{I}\left(-\frac{1}{2\sigma_\varepsilon^2}\sum_{j=1}^{J}\left[y_{ij}-f\left(t_j,\boldsymbol{\beta}+\mathbf{B}_i\right)\right]^2 -\frac{1}{2}\mathbf{B}_i^T\boldsymbol{\Gamma}^{-1}\mathbf{B}_i\right)\right]d\mathbf{B} \tag{2}$$

$$l\left(\mathbf{Y}\,|\,\boldsymbol{\beta},\boldsymbol{\Gamma},\sigma_\varepsilon^2\right) = \frac{IJ+I_p}{2}\log\left(2\pi\right)-\frac{IJ}{2}\log\sigma_\varepsilon^2 -\frac{I}{2}\log\left|\boldsymbol{\Gamma}\right|+$$

$$\sum_{i=1}^{I}\left\{\log\left[\int\exp\left(-\frac{1}{2\sigma_\varepsilon^2}\sum_{j=1}^{j}\left[y_{ij}-f\left(t_j,\boldsymbol{\beta}+\mathbf{B}_i\right)\right]^2 -\frac{1}{2}\mathbf{B}_i^T\boldsymbol{\Gamma}^{-1}\mathbf{B}_i\right)d\mathbf{B}_i\right]\right\} \tag{3}$$

In this two previous formulas apear an multiple integral of vector B_i dimension. This fact imply the calculation difficulty for the classical method. In this sens we can

simplify the problem appling one of the existent strategies.

In the furter we present the method which exist in the specialised literature.

2. The classification of the likelihood methods

We propose the following classification for the estimation method which usses the maximum likelihood criterion:

Tab.1 The classification of the likelihood methods

Straight likelihood	Straight approximate kikelihood	Nonstraight likelihood
EM	Laplacean approximation	Pseudo-likelihood
	Monte Carlo	Linearisation
	Gaussian Quadrature	

The Expectation Maximization algorithm (EM) is the only one method which work out the maximum likelihood of the initial model. The general principle of the EM algorithm (Dempster et al. [6]) consists in calculation of the maximum of the a posteori density. This algorithm usses an iterative sgheme and yields an estimator sequence. The yielded estimators sequence converge to the maximum likelihood solution.

The second class contains the methods which maximises an aproximation of the initial model likelihood. We named this class "straight approximate likelihood methods". In this methods are applied the classical numerical integration technics (Dahlquist G., Bjorck A. et Andersen [3], Davis, P. J. et Rabinowitz P. [4]) for the integral approximation. Thus, the estimators is those who maximises an approximated initial model likelihood.

The log-likelihood functions have the following expresions:

$$l_{lap}\left(\theta \mid Y\right)=-\frac{IJ}{2}\log\left(2\pi\sigma_{\varepsilon}^{2}\right)-\frac{I}{2}\log\left|\mathbf{\Gamma}\right|+\sum_{i=1}^{I}F\left(\mathbf{\beta},\mathbf{\theta},\mathbf{Y}_{i},\hat{\mathbf{B}}_{i}\right)-\frac{1}{2}\sum_{i=1}^{I}\log\left|F_{**}''\left(\hat{\mathbf{B}}_{i}\right)\right|$$

$$l_{MC}\left(\mathbf{\theta} \mid \mathbf{Y}\right)=-\frac{IJ}{2}\log\left(2\pi\sigma_{\varepsilon}^{2}\right)-\frac{1}{2}\sum_{i=1}^{I}\log\left|F''\left(\hat{\mathbf{B}}_{i}\right)\right|+\sum_{i=1}^{I}\log\left\{\frac{1}{N_{MC}}\sum_{k=1}^{N_{MC}}\exp\left[F\left(\mathbf{\theta},\mathbf{Y}_{i},\mathbf{B}_{i}^{*}\right)+\frac{1}{2}\mathbf{z}_{k}^{*T}\mathbf{z}_{k}^{*}\right]\right\}$$

$$l_{QG}\left(\theta \mid Y\right)=-\frac{IJ}{2}\log\left(2\pi\sigma_{\varepsilon}^{2}\right)+\sum_{i=1}^{I}\left\{\sum_{k_{1}=1}^{N_{QG}}...\sum_{k_{p}=1}^{N_{QG}}\exp\left(-\frac{1}{2\sigma_{\varepsilon}^{2}}\sum_{j=1}^{J}\left[Y_{ij}-f\left(t_{j},\mathbf{\beta}+\mathbf{\Gamma}^{\frac{1}{2}}\mathbf{z}_{k_{1},...,k_{p}}\right)\right]^{2}\right)\prod_{l=1}^{p}\omega_{jl}\right\}$$

The laplacean approximation consists in a Taylor series development for F on the $\hat{B}$ neighbourhood and keeping the first and second terms.

The Monte Carlo method consist in application of the Monte Carlo tehnic for the integral calcul.

For the Gaussian quadrature method is applied the quadrature formula for the integral.

The therd class contains the methods for who the initial model was modified into a model with the likelihood function more issely.

The estimators are calculated maximises the new model likelihood. We named those methods "nonstraight likelihood methods".

The pseudo-likelihood was proposed by Concordet and Nunez [2]. The linearisation method principle consists in approximation of the nonlinear model with one linear model. Thus the linear model tehnics are applicable (Searle et al. [9], Gaybill [7].

The liniarisation is efected by Taylor series development and keeping the first term.

Beal and Sheiner [1] propose liniarisation in the neighbourhood of the theoretical mean of the B_i. This method is developed in Davidian and Giltinian [5].

Lindstrom and Bates [8] make the Taylor development in the neighbourhood of the some prediction $\hat{B}_i$ (this prediction was modified at each step of the iterative algorithm).

References

[1] Beal, S.L. et Sheiner, L.B., Estimating population kinetics. *CRC Critical Reviews in Biomedical Engineering*, vol. 8, pp. 195-222, 1982.

[2] Concordet, D. et Nunez, O., A simulated pseudo-maximum likelihood estimator for nonlinear mixed models. *Computational Statistics and Data Analysis*, 2002.

[3] Dahlquist, G., Bjorck, A. et Andersen, N., *Numerical Methods*. Prentice-Hall, Prentice-Hall series in automatic computation, 1974.

[4] Davis, P.J. et Rabinowitz, P., Methods of Numerical Integration. *Computer Science and Applied Mathematics,* Academic Press, 1984.

[5] Davidian, M. Et Giltinian, D.M., Nonlinear Models for Repeated Measurement Data., *Monographs on Statistics and Applied Probability*, Chapman & Hall, 1995.

[6] Dempster, A.P., Laird, N.M. et Rubin, D.B., Maximum likelihood from incomplete data via the EM algorithm. *Journal of the Royal Statistical Society B*, vol. 39, pp.1-38, 1977.

[7] Graybill, F.A., *Theory and application of the linear model*, Duxbury press, 1976.

[8] Lindstrom, M.J. et Bates, D.M., Nonlinear mixed effects models for repeated measures data, *Biometrics*, vol. 46, pp.673-870, 1990.

[9] Searle, S., Casella, G. Et McCulloch, C., *Variance Components*, Wiley, New York, 1992.

DINU TEODORESCU

A REPRESENTATION RESULT FOR LIPSCHITZ OPERATORS IN NORMED SPACES

Department of Mathematics, Valahia University of Targoviste

Abstract: In this paper we will prove that every Lipschitz operator from a normed space into yorself can be decomposed in a sum of two Lipschitz injective operators.

1. Introduction

The representation of an operator as a sum of two operators with more convenable properties is a used method in the study of abstract operator equations. In this note we obtain a representation result for a Lipschitz operator from a normed space into yourself.

2. The Result

Let E be a normed space with the norm $\|\bullet\|$ and $T : E \rightarrow E$ a Lipschitz operator with constant $M > 0$, i.e.

$$\|T(x) - T(y)\| \leq M\|x - y\|, \text{ for all } x, y \in E .$$

In this note we will prove that the operator T can be written as a sum of two Lipschitz injective operators. We have:

$$T = T - (M + \varepsilon)I + (M + \varepsilon)I ,$$

with $\varepsilon > 0$, where I is the identity of E.

It is clear that the operator $T_1 = T - (M + \varepsilon)I$ is a Lipschitz operator with constant $2M + \varepsilon$, the operator $T_2 = (M + \varepsilon)I$ is a Lipschitz operator with constant $M + \varepsilon$ and T_2 is an injection.
For all $x, y \in E$ we have so

$$(M + \varepsilon)\|x - y\| = \|T_2(x) - T_2(y)\| =$$
$$\|T(x) - T_1(x) - T(y) + T_1(y)\| \leq$$
$$\leq \|T(x) - T(y)\| + \|T_1(x) - T_1(y)\| \leq$$
$$\leq M\|x - y\| + \|T_1(x) - T_1(y)\| .$$

Cosequently we obtain:

$$\|T_1(x) - T_1(y)\| \geq \varepsilon\|x - y\| \text{ for all } x, y \in E .$$

It results now that the operator T_1 is injective and our assertion is proved.
In fact, the present result shows that every Lipschitz operator T with constant M can be representeted as $T = \alpha(I + F)$, where $\alpha > M$ and F is a Lipschitz injective operator with constant $\dfrac{M + \alpha}{\alpha}$.

6. References

[1] Teodorescu, D., Asupra uniform continuitatii functiilor reale de o variabila reala, *A III-a Conf.Anuala a SSMR,* Craiova 1999, vol. 3, pp, 345-350.
[2] Teoderescu, D., O clasa de functii inversabile. Aplicatii., *Didactica Matematicii*, Univ. Babes-Bolyai Cluj-Napoca, vol. 18 (2002), pp. 163-166.

.

DUMITRU FANACHE

THE JACOBI METHOD OF SOLVING LINEAR EQUATIONS SYSTEMS ON A PARALLEL CALCUL SYSTEM

"Valahia" University of Târgovişte, Faculty of Science , Department of Mathematics

d_fanache@yahoo.ro

Abstract.*This paper present Jacobi method of solving linear equations systems, because of its strong parallelism character. Leaving from an equation with partials derivatives as elliptic type (Poisson equation) with initials conditions on the border of curve C (which limits the integration domain Ω) of an unknown function with two variables $\phi(x, y)$, in order to apply the methods with finite differencess, integration domain is divided in rectanglular small regions which form a lattice parallel to the axes of coordinates. The derivations are replaced with differences which deppend on the size of the rectangular element of the lattice. If the lattice has p^2 points, we'll have a linear system with p^2 equations with p^2 unncknown values. Try to represent the coordinates of the lattice, we'll write the equations of aproximation as finite differences form. Gauss-Seidel method represents an improvement of Jacobi method. The numeric results obtained by running the parallel algorithm show we can get a calcuation time better than sequential calculation time.*

Key words: parallel system, speedup (S), parallel execution time (T_p), sequential execution time(T_s), granularity.

1. The change of equations with partial derivates into equations with finite differences

Equations with partial derivates are frequently used for modelling physical phenomena. Consider the particular case of an equation with partial derivates of second order on a subset of two-dimensional space

$$a\frac{\partial^2\phi}{\partial x^2}+b\frac{\partial\phi}{\partial x\partial y}+c\frac{\partial^2\phi}{\partial y^2}+d\frac{\partial\phi}{\partial x}+e\frac{\partial\phi}{\partial y}+f\phi+g=0$$

(1)

where a, b, c, d, e, f si g are reals continous functions depending on variables x and y, and ϕ is unknown function. We distinguish three types of equations with partial derivates: elliptical equations when $b^2 - 4ac < 0$, parabolic equations when $b^2 - 4ac = 0$ and hyperbolic equations when $b^2 - 4ac > 0$.

Consider the case of an elliptic equation. The integration domain Ω of the elliptic equation, is bound of curve C, along which are defined certain boundary conditions of the unknown function $\phi(x, y)$ or of its derivat. For the use of methods with finite differences, integration domain is divided in small rectangular regions which form a set of lines parallel to axes xx' respectively yy', equaly remote. The approximate solution is supplied in the crossing points of these lines, in two-dimensional grid. The solution is obtained by approximating partiale derivates of ϕ in each point of two-dimensional grid (i, j) with linear functions depending on the values of ϕ in point (i, j) and in certain points situated in its neighborhood in the lattice. Using certains techniques of values interpolation in the points of the lattice we have the numeric solution which covers the whole domain.

The derivates are replaced by the ratios of differeces depending on the dimensions of the rectangular element of the lattice. Thus, $\frac{\partial\phi}{\partial x}$ is replaced in the ecuation with $\frac{\delta\phi}{\delta x}$, where δx is the step on axis xx' of the lattice, so that for a finer lattice can be reaqed a certain accuracy of the numeric solution. If the lattice includes p^2 points, then we have a linear system with p^2 equations having p^2 unknown values.

Let, the Poisson equation,

$$\frac{\partial^2 u}{\partial x^2} + \frac{\partial^2 u}{\partial y^2} = q$$

(2)

and the boundary conditions:
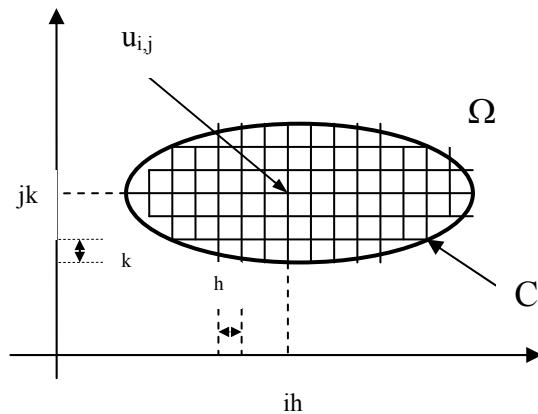
$$u(x, y) = u_0(x, y) \text{ pe } C \qquad (3)$$

Fig 1. Disintegrate of domain

If the integration domain is dividing in rectangles of size $\delta x = h$ şi $\delta y = k$ and we represent the coordinates of the lattice by $x = ih$ and $y = jk$, then we can approximate:

(7)
$$\frac{\partial^2 u}{\partial x^2} = \frac{u_{i+1,j} - 2u_{i,j} + u_{i-1,j}}{h^2}$$

where $u_{i,j} = u(ih, jk)$, and

$$\frac{\partial^2 u}{\partial y^2} = \frac{u_{i,j+1} - 2u_{i,j} + u_{i,j-1}}{k^2}$$

(8)   (8)

Using Taylor formula in two dimensions we have

$$u(x + h, y) = u(x,y) + \frac{\partial u}{\partial x} h + \frac{1}{2} \frac{\partial^2 u}{\partial x^2} h^2 + \dots \qquad (4)$$

$$u(x - h, y) = u(x, y) - \frac{\partial u}{\partial x} h + \frac{1}{2} \frac{\partial^2 u}{\partial x^2} h^2 - \dots \qquad (5)$$

From (4) and (5), ignoring terms of order $O(h^4)$ we have:

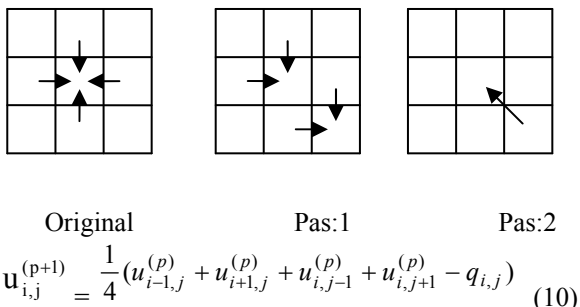$$\frac{\partial^2 u}{\partial x^2} \approx \frac{u(x+h, y) - 2u(x, y) + u(x - h, y)}{h^2}$$

(6)

When $h = k$ (and marking $q_{i,j} = h^2 q(ih,jh)$) the equation of the approximation with finite differences for Poisson equation can by written like:

$$u_{i,j} = \frac{1}{4}(u_{i-1,j} + u_{i+1,j} + u_{i,j-1} + u_{i,j+1} - q_{i,j})$$

(9)

2. Solving an equations system by Jacobi method

Assum we use a SIMD parallel system, with interconnecting processors in the shape of a lattice (each processor is connected to four adjacent neighbours).

Punctual Jacobi method has a strong character of parallelism. The schema is define by iterative process:

Original   Pas:1   Pas:2

$$u_{i,j}^{(p+1)} = \frac{1}{4}(u_{i-1,j}^{(p)} + u_{i+1,j}^{(p)} + u_{i,j-1}^{(p)} + u_{i,j+1}^{(p)} - q_{i,j}) \quad (10)$$

At each step, $u_{i,j}$ is replaced with the average of the values of the four adjacent neighbours less the quantity $\frac{q_{i,j}}{4}$ (fig 2).

Eeach point of the lattice is given a processor. Thus all points can be updated simultaneously. The memorization of a copy of the previous status of the lattice is necessary. If the number of processors is sufficient to cover the entire lattice, they update is made by only four operations of addition and substraction. The parallel calculation, can be reorganised (fig 3) in two steps:

(1) step 1 : we add the values of the neighbours from North and West;

(2) in 2 : we add to the matrix have from step 1, the values of the neighbours from South end East and then we substract $q_{i,j}$.

Fig 2. Updating the approximations in Jacobi method

During the iterative process only the internal points of the lattice are updated. Boundary conditions are in principle of two types:

-the values of function u(x, y) on the border of the integration domain are specified(Dirichlet);

-the values of derivatives of the function u(x, y) on the border of the domain are specified (Neumann).

An natural extension of Jacobi method is Gauss-Seidel algorithm, which uses the most recently determined values for u, from the right side of the current point of the lattice. Its advantage consist of the necessity of memorising only the last value of $u_{i,j}$.

Gauss-Seidel iteration is define by :

$$u_{i,j}^{(p+1)} = \frac{1}{4}\left(u_{i,j-1}^{(p+1)} + u_{i-1,j}^{(p+1)} + u_{i,j+1}^{(p)} + u_{i+1,j}^{(p)} - q_{i,j}\right) \quad (11)$$

Fig 3. The organisation of the calculation in Jacobi method

Schematicly, the process is represented in fig 4. The method requires a certain order and a diagonal working front (fig 5). At the first step, the point "1" is updated on boundary conditions and on initial estimations for points "2". A step two, points "2" are updated simultaneously by using the estimations for points "3" and determined value for point "1". A third step, points "3" are updated and point "1" can be updated
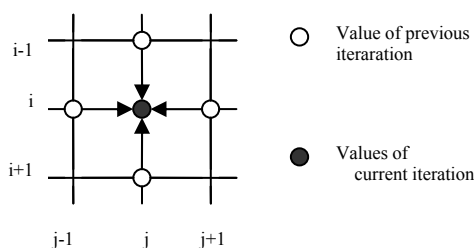
simultaneously for the second time, because the information on this current approximation is no longer necessary. The first iteration evolves like a wave in the lattice; the next waves are the iterations which follow it.

Instead of several levels now being calculated we prefer to operate with only two levels (white-black or red-black method). "Black" points are the first to be updated, using the previous "white" points, and the "white" points are updated using the latest values of the "black" points (fig 6).
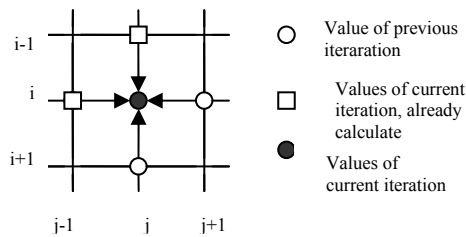
Fig 4. Updating information in Gauss-Seidel method

"Black" points are updated at one level of iteration, and "white" points are updated at next level of iteration. After one iteration, "black" points are at level 1 like in Jacobi method, and "white" points have been already updated and they are at level 2.

At one iteration Jacobi method updates all the points, and Gauss-Seidel method only half of them. Thus, for one matrix with $n \times n$ processors, one problem of $2n \times n$ dimensions can be solved using Gauss-Seidel method in the same time in which one problem $n \times n$ is solved by Jacobi method, by attaching a $n \times n$ matrixes for "black" and "white" points separately and by updating them simultaneously.

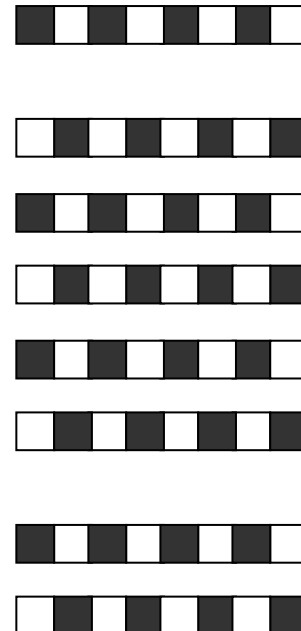Fig 5. Advanced front of aproximation

in Gauss-Seidel method

Fig 6. The levels of iteration a Gauss-Seidel method

Succesive overrelaxation method is a generalization of Gauss-Seidel and it improves a rate of convergence at the function $u(x, y)$ by adding a value $\omega u(x, y)$. The factor ω is called speeding factor (or relaxation factor). So, a $p+1$,

1	2	3	4	5	6	7	8
2	3	4	5	6	7	8	
3	4	5	6	7	8		
4	5	6	7	8			
5	6	7	8				
6	7	8					
7	8						
8							

step

$$u^{(p+1)} = u^{(p)} + \omega \delta u, \ \delta u = u_{GS}^{(p+1)} - u^{(p)} \qquad (12)$$

where .GS shows one iteration Gauss-Seidel. The iteration scheme is

$$u_{i,j}^{(p+1)} = (1-\omega)u_{i,j}^{(p)} + \frac{1}{4}\omega \begin{pmatrix} u_{i,j-1}^{(p+1)} + u_{i-1,j}^{(p+1)} + \\ u_{i,j+1}^{(p)} + u_{i+1,j}^{(p)} - q_{i,j} \end{pmatrix} \qquad (13)$$

At first step, $u_{i,j}^{(p+1)}$ is updated for all black points, that is for i + j even and at the second step, for all white points, that is for i + j odd. Each step consists of independent calculations which are performed simultaneously. The process is repeated until a certain accuracy is satisfied, which we can express through an inequality of the following type :

$$\left| u_{i,j}^{(p+1)} - u_{i,j}^{(p)} \right| < \varepsilon, (\forall) i, j, u_{i,j} \in \Omega \qquad (14)$$

In the next method, an entire row of points can be updated simultaneously. The points on row j are updated according to the relation

$$u_{i+1,j}^{(p+1)} + 4u_{i,j}^{(p+1)} + u_{i+1,j}^{(p+1)} = q_{i,j} - u_{i,j+1}^{(p)} - u_{i,j-1}^{(p)} \qquad (15)$$

as in fig 7.

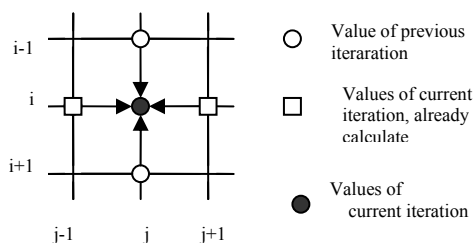
Figura 7. Update of approximations in Gauss-Seidel method

For each column j is necessary the solution of a tridiagonal linear system. The problema can be solved in parallel using odd-even cyclic reduction method. If we use updated values of the previous column, we have

Gauss-Seidel method in line. We can adopt the iteration on two levels by updating the columns alternatively, just like punctual Gauss-Seidel method (fig 8).
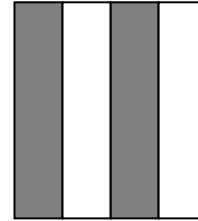

Fig 8. Gauss-Seidel method in line, on two levels

Black columns are updated by using the white values given at the previous step. White columns are updated by using the black values from the current step. This way, black columns are updated at a certain iteration level and white columns are updated at the next level.

Introducing a speeding factor ω in order to improve the convergence leads to overrelaxation method succesive in line. One step of iteration requires the following:

(1) the calculation of values

$$r_{i,j}^{(p)} \leftarrow q_{i,j} - u_{i,j+1}^{(p)} - u_{i,j-1}^{(p)}$$

(16)

for each column j;

(2) in order to obtain the value of $u_{i,j}^{(p+1)}$, the tridiagonal system is solved exactly for each black column j :

$$u_{i,j}^{(p+1)} - 4u_{i,j}^{(p+1)} + u_{i+1,j}^{(p+1)} = r_{i,j}^{(p)}$$

(17)

(3) the relaxation is included

$$u_{i,j}^{(p+1)} \leftarrow (1-\omega)u_{i,j}^{(p)} + \omega u_{i,j}^{9p+1)} \qquad (18)$$

in the black columns;

(4) each stage from (1) to (3) is repeated for white columns .

In order to obtain the convergence the relaxation factor ω must be between 0 and 2. For solving the Poisson equation on a rectangular domain divided in n × n points, the optimal value of ω from the viewpoint of convergence rate is [1]

$$\omega_{\text{opt}} = \frac{2}{1 + \sin \pi / n} \tag{19}$$

On an asynchronous MIMD system is recommended the use of explicite block iterative scheme, in which groups of points from the lattice are valued by using a direct method. Let equation:

$$u_{i,j} = \frac{1}{4}(u_{i-1,j} + u_{i+1,j} + u_{i,j-1} + u_{i,j+1} - q_{i,j}) \tag{20}$$

$$u_{i+1,j} = \frac{1}{4}(u_{i,j} + u_{i+2,j} + u_{i+1,j-1} + u_{i+1,j+1} - q_{i+1,j})$$

By rearranging these equations we get [7] :

$$u_{i,j} = \frac{1}{15}\left[\begin{array}{l} 4\left(u_{i-1,j} + u_{i,j+1} + u_{i,j-1} - q_{i,j}\right) + u_{i+1,j+1} \\ + u_{i+2,j} + u_{i+1,j-1} - q_{i+1,j} \end{array}\right] \tag{21}$$

$$u_{i+1,j} = \frac{1}{15}\left[\begin{array}{l} 4(u_{i+1,j} + u_{i+2,j+1} + u_{i+1,j-1} - q_{i+1,j}) \\ + u_{i-1,j} + u_{i,j+1} + u_{i,j-1} - q_{i,j} \end{array}\right]$$

These equations are independent, so that they can be solved simultaneously. The lattice can be divided in blocks of 2 × 2 dimension and its points can be updated simultaneously by using two processors. Using a table of processors, several blocks can be solved simultaneously by using black and white technique (a chess-board table), in which every square of a certain colour represents a block of 2 × 1 dimension. In a

first stage, all the black squares are updated simultaneously using the white squares . In the second stage, the white squares are updated using values from the black squares .

The algorithm can be accelerated by introducing the relaxation factor ω. The step p+1 consists of two stages :

we determinate the values

$$r_{i,j}^{(p)} \leftarrow u_{i-1,j}^{(p)} + u_{i,j+1}^{(p)} + u_{i,j-1}^{(p)} - q_{i,j} \tag{22}$$

$$r_{i+1,j}^{(p)} \leftarrow u_{i+1,j+1}^{(p)} u_{i+2,j}^{(p)} + u_{i+1,j-1}^{(p)} - q_{i+1,j}$$

and then the aproximations for the black squares.

$$u_{i,j}^{(p+1)} = u_{i,j}^{(p)} + \frac{1}{15}\omega\left(4r_{i,j}^{(p)} + r_{i+1,j}^{(p)} - 15u_{i,j}^{(p)}\right) \tag{23}$$

$$u_{i+1,j}^{(p+1)} = u_{i+1,j}^{(p)} + \frac{1}{15}\omega\left(4r_{i+1,j}^{(p)} + r_{i,j}^{(p)} - 15u_{i,j}^{(p)}\right)$$

(2) we determinate the values for the white squares

$$u_{i,j}^{(p+1)} = u_{i,j}^{(p)} + \frac{1}{15}\omega\left(4r_{i,j}^{(p+1)} + r_{i+1,j}^{(p+1)} - 15u_{i,j}^{(p)}\right) \tag{24}$$

$$u_{i+1,j}^{(p+1)} = u_{i+1,j}^{(p)} + \frac{1}{15}\omega\left(4r_{i+1,j}^{(p+1)} + r_{i,j}^{(p+1)} - 15u_{i+1,j}^{(p)}\right)$$

Similar formulae can be built for bigger blocks, such as blocks of dimension 3 × 3. By enlarging the size of the block, the number of iterations necessary for reaching a certain accuracy of a numeric solution decreases.

The black-white method can be extended for different multi-colour methods. Thus, in 1978, Hackbush introduced three colours formulae based on schemes with finite differences with 9 points.

For solving equations of aproximation with finite differences corresponding to the Poisson equation, we can also use the alternative directions method, whose step consists of two stages [7],

$$(H + \alpha_k I)x^{k+1/2} = (\alpha_k I - V)x^k + b$$

$$(V + \alpha_k)x^{k+1/2} = (\alpha_k I - H)x^k + b$$

where linear system is $Ax = b$, $A = H + V$

For the approximations of Poisson equation, the first stage is solving n tridiagonal systems, corresponding to the vertical lines. These triangular systems can be solved in parallel, successively for the two stages, using a matrix of processors, for example Gauss method of elimination.

Most of the considerations and methods mentioned in solving elliptical equations can be used for parabolic and hyperbolic equations .

3. Conclusions

Numeric algorithm consists in dividing the matrix obtained by the division of the equation and the distribution of blocks from the matrix on several processors which will make calculations and will exchange information corresponding to commun domains.

Finding the solution of the Poisson equation is necessary in many practical applications wich require the solution of the same equation but having different boundary conditions or different functions as "free term". This requires are substantial time for

calculation. Such situations appear, for example when problems depend on time and we want the solution for distinct moments of time.

The use of parallel systems generated an intense study of parallel implementation of known sequential algorithms and of making the algorithms which take count of new architectures of computers.

The following table shows the use of (10) for different sizes of the linear systems and granularity of a MIMD virtual parallel system, using MULTIPASCAL ver 2.0.

4.References

[1] Andersen L.,Brotherton R.; The equity option volatility smile: An implicit finite difference approach, Journal of Computational Finance 1(2),5-37, 1998

[2] Bunnin F.O., Guo Y, Ren Y., Darlington J.;Parallel Pseudospectral Solution of Financial PDE; Parallel Algorithms and Applications 14(7),1-11,2000

[3] Dodescu Gh., Toma M.; Metode de calcul numeric; Editura Didactică şi Pedagogică, Bucureşti, 1976

[4] Dodescu Gh.; Metode numerice în algebră; Editura Tehnică, Bucureşti, 1979

[5] Iftimie V.;Ecuaţii cu derivate parţiale; Tipografia Universităţii Bucureşti, 1980

[6] Modi J. J.; Parallel algorithms and matrix computation; Clarendon Press, 1988

[7] Petcu D.; Calcul paralel; Editura de Vest, Timişoara, 1994

ANDREI VERNESCU

ABOUT THE CONSTRUCTION OF APPROXIMATION OPERATORS USING THE FINITE OPERATIONAL CALCULUS

Valahia University, Târgovişte, Faculty of Science
Department of Mathematics, 118. Bd. Unirii, Târgovişte

Abstract: We present here some principal modalities to construct approximation operators by the mean of the Umbral Calculus. We emphasize the romanian contributions.

1. Introduction

We consider a sequence of operators $(L_n)_n$ where every operator L_n is defined from $C[0,1]$ to $C[0,1]$ and has the following properties (similar to the *Bernstein* operator).

(i) L_n is linear for every $n \in \square$;

(ii) L_n is positive for every $n \in \square$, i.e.
$$f \geq 0 \Rightarrow L_n f \geq 0 ;$$

(iii) L_n is interpolator in 0 and 1, i.e.
$$(L_n f)(0) = f(0) \text{ and } (L_n f)(1) = f(1);$$

(iv) $L_n f$ converges uniformly to f on $[0;1]$ for any $f \in C[0,1]$.

These operators are of *Bernstein* type. The operator of *Bernstein* B_n, is defined by the formula:

$$(B_n f)(x) = \sum_{k=0}^{n} \binom{n}{k} x^k (1-x)^k f\left(\frac{k}{n}\right); \quad n = 0,1,2,...$$

The Romanian School of Numerical Analysis and Approximation Theory had and has an important contribution in the construction of the approximation operators.

This School was founded by the great romanian mathematicians *Tiberiu Popoviciu* (1906-1975) and *Dumitru V. Ionescu* (1901-1985). Now the School is conducted by Professor *Dimitrie D. Stancu* (born in 1927), Ph.d., Dr. Honoris Causa, a Honorary Member of Romanian Academy.

Important works in this domain also are realized by *Grigor Moldovan, Alexandru Lupaş, Gheorghe Coman, Gheorghe Micula, Constantin Manole, Ioan A. Rus, Ioan Mihoc, Ioan Gavrea, Luciana Lupaş, Octavian Agratini, Radu Păltănea* and others.

Generally speaking, the approximation operators can be constructed by three kind of methods:

    a) algebraic methods;
    b) probabilistic methods;
    c) methods based on the finite operatorial calculus.

2. Some Elements of Umbral Calculus

The finite operatorial calculus (or umbral calculus) has the origin in the so – called Heaviside calculus, invented by *G. Boole* and developed by *A. Cayley, P. Appell, S. Pincherle, J. Blissard* and, after 1900, by *N. Nielsen, N. E. Nörlund, I. M. Sheffer, J. F. Steffensen, F. B. Hildebrand* and others. A work of *E. T. Bell* (from 1940) made to give certain axiomatic bases for the finite operatorial calculus was no sufficiently efficient.

The first rigorous version of the finite operatorial calculus was the version of *Gian-Carlo Rota* and his collaborators *Ronald Mullin, Steven Roman, Andrei Odlyzko* and others. This version was created in the years 1970.

The umbral calculus presents an *unified theory of the development of certain polynomials in terms of others*, using the duality between x and $\dfrac{d}{dx}$.

A sequence of polynomials with real coefficients $(p_n)_n$ with $\deg(p_n) = n$, for any $n \in \square$, is called of binomial type if it satisfies identically the equalities:

$$p_n(x+y) = \sum_{k=0}^{n} \binom{n}{k} p_k(x) p_{n-k}(y), \quad n = 0,1,2,...$$

Of course, these identities generalize the classical formula for $(x+y)^n$, of Newton.

We denote by E^a the shift operator, defined by the formula $(E^a p)(x) = p(x+a)$ for any polynomial p and for any $x \in \square$.

We denote by $\prod$ the set of all polynomials with real coefficients. Let $e_k(x) = x^k$ be, $k = 0,1,2,...$

A linear operator $T : \prod \rightarrow \prod$ is said to be shift invariant if $TE^a = E^a T$ for any $a \in \square$ (where, if U and V are two operators from $\prod$ to $\prod$, we denote, for more simplicity, UV in place of $U \circ V$).

An operator $Q : \prod \rightarrow \prod$ is called to be a delta operator if:

    (i) Q is shift invariant

    (ii) It exists a constant $c \neq 0$ such that $Qe_1 = c$, (i.e. $(Qe_1)(x) = c$ for any $x \in \square$).

Let Q be a delta operator. A sequence of polynomials $(p_n)_n$ (with $\deg(p_n) = n$ for any $n \in \square$) is called to be a sequence of basic polynomials for Q if it satisfies the following conditions:

    (i) $p_0 = 1$ (i.e. $p_0(x) = 1$ for every $x \in \square$);

(ii) $p_n(0) = 0$, for any $n \geq 1$;

(iii) $Qp_n = np_{n-1}$, for any $n \geq 1$ (i.e.

$(Qp_n)(x) = np_{n-1}(x)$ for every $x \in \square$).

Every delta operator Q possesses an unique basic sequence $(p_n)_n$, which is of binomial type.

Conversely, every polynomial sequence of binomial type $(p_n)_n$ is the sequence of basic polynomials for a certain delta operator Q.

A sequence of polynomials $(s_n)_{n \geq 0}$ is called a Sheffer sequence for a delta operator Q if it satisfies the following conditions:

(i) It exists a constant $c \neq 0$ such that $s_0 = c$ (i.e. $s_0(x) = c$ for any $x \in \square$);

(ii) $Qs_n = ns_{n-1}$ for any $n \geq 1$ (i.e.

$(Qs_n)(x) = ns_{n-1}(x)$ for every $x \in \square$).

It is known [7] a connection between a *Sheffer* sequence for Q and basic sequence: if $(s_n)_n$ is a *Sheffer* sequence for a delta operator Q, with the basic sequence $(p_n)_n$, then it exists a shift invariant and invertible operator $S : \prod \rightarrow \prod$, such that $s_n = S^{-1}p_n$ for every $n \in \square$.

A Sheffer sequence satisfies identically the equalities:

$$s_n(x+y) = \sum_{k=0}^{n} \binom{n}{k} p_k(x) s_{n-k}(y); \quad n = 0,1,2,...$$

A Sheffer sequence for the usual operator of derivation D is an *Appell* sequence.

The Umbral Calculus allows an unified study of binomial, *Appell* and *Sheffer* sequences.

3. The Main Constructions

The Umbral Calculus is able to construct different approximation operators.

First, in an old paper, from 1932, *Tiberiu Popoviciu* has constructed in [6] the sequence of operators $T_n : C[0,1] \rightarrow C[0,1]$ defined by the equalities

$$(T_nf)(x) = \frac{1}{p_n(1)} \sum_{k=0}^{n} \binom{n}{k} p_k(x) p_{n-k}(1-x) f\left(\frac{k}{n}\right)$$

$n = 0,1,2,...$, where $(p_n)_n$ is a sequence of binomial type with the natural supplementary property that $p_n(1) \neq 0$ for any $n \in \square$ and $p_n(x) \geq 0$ on $[0.1]$.

This operator and their generalization were intensively studied; it is linear, positive, it is interpolator in 0 and 1 and preserves the polynomials of first degree.

The operator T_n of *Tiberiu Popoviciu* was revisited by *Constantin Manole* [5] by Umbral Calculus and by *P. Sablonnière* [8] using the generating functions.

An important result of Approximation Theory is the theorem of *Bohman-Popoviciu-Korovkin*, which affirms that $(L_n)_n$ is a sequence of linear operators $L_n : C[0,1] \rightarrow C[0,1]$ with the property that L_ne_k converges uniformly to e_k, for $k = 0,1,2$, then L_nf converges uniformly to f, for any $f \in C[0,1]$.

Using the *Bohman-Popoviciu-Korovkin* theorem it is easy to obtain that T_nf converges uniformly to f, for any $f \in C[0,1]$.

In 1968, in an important work [9], *D. D. Stancu* has constructed, by a probabilistic way, the operator $S_n : C[0,1] \rightarrow C[0,1]$, defined by the equality:

$$(S_nf)(x) = \frac{1}{p_n^{\langle \alpha \rangle}(1)} \sum_{k=0}^{n} \binom{n}{k} p_k^{\langle \alpha \rangle}(x) p_{n-k}^{\langle \alpha \rangle}(1-x) f\left(\frac{k}{n}\right)$$

where the polynomials $p_n^{\langle \alpha \rangle}$ are $p_0^{\langle \alpha \rangle} = 1$, and

$p_n^{\langle \alpha \rangle}(x) = x(x+\alpha)(x+2\alpha) \cdot ... \cdot (x+(x-1)\alpha)$.

For $\alpha = 0$ we obtain the operator of *Bernstein*.

In [4] *L.Lupaş* and *A. Lupaş* has defined the operators $L_n^Q : C[0,1] \rightarrow C[0,1]$

$$(L_n^Qf)(x) = \frac{1}{p_n(1)} \sum_{k=0}^{n} \binom{n}{k} p_k(nx) p_{n-k}(n-nx) f\left(\frac{k}{n}\right),$$

where Q is a delta operator and $(p_n)_n$ is its basic sequence. Later I have generalized it.

Recently, a young researcher from Cluj-Napoca, *Maria Crăciun*, has defined in [2] approximation operators using the *Sheffer* sequences.

6. References

[1] Agratini, O., *Binomial polynomials and their applications in approximation theory*.

[2] Crăciun, M.. *Approximation operators constructed by means of Sheffer sequences*, Rev. Anal. Num. et Th. Approx. 30 no.**2** (2001), 135-150.

[3] Hildebrand, F., *Introduction to Numerical Analysis*, Mac Grow-Hill, New York, 1974.

[4] Lupaş, L., Lupaş., A.: *Polynomials of binomial type and approximation operators,* Studia Univ. Babeş-Bolyai, Mathematica, 32, no.4 (1987), 40-44.

[5] Manole C., *Expansions in series of generalized Appell polynomials with applications in the approximation of functions,* Ph.D.Thesis, 1984.

[6] Popoviciu, T., *Remarques sur les polynomes binomiaux*, Bul. Soc. Şt. Cluj, 6, 1931, 146-148.

[7] Rota, G.C., *Finite Operator Calculus*, Academic Press, New York-London, 1975.

[8] Sablonnière: *Positive Bernstein-Sheffer Operators*, J. Approx. Theory **83** (1995), 330-341.

[9] D.D.Stancu: *Approximation of functions by means of a new generalized Bernstein Operator*, Calcolo, 20 (1983) no.**20**, 211-229.

[10] Steffensen, *J.F., Interpolation*, Chelsea, New York, 1927.

INGRID NASTASIA

THE KANTOROVICH-STANCU OPERATORS FROM THE UMBRAL CALCULUS PERSPECTIVE

University of Valahia Targoviste, Unirii Avenue

Abstract: In this paper, we construct a linear positive operator of Kantorovich-Stancu type
$$\widetilde{K}_m^Q : L_1([0,1]) \to C([0,1]) \text{ where Q is a delta-operator.}$$

1. Preliminaries

A sequence of polynomials $\left(p_n\right)_{n \in N}$ is said to be polynomial sequence of binomial type if it satisfies the following conditions:

1. $grad\left(p_n\right) = n, (\forall)n \in N$

2. $p_n(x+y) = \sum_{k=0}^{n} \binom{n}{k} p_k(x) p_{n-k}(y), (\forall)x, y \in R$

If Π is the comutative algebra of polynomials with coefficients real numbers then an operator $T : \Pi \to \Pi$ which commutes with all shift operators $E^a : \Pi \to \Pi, E^a p(x) = p(x+a)$ is called shift-invariant operator.

A shift-invariant operator Q is called delta-operator if Qx is a nonzero constant.

A polynomial sequence $p = (p_n)_{n \geq 0}$ is called the sequence of bazic polynomials for the delta-operator Q if for any $x \in R$ and $n \in N$ we have:

1. $p_0(x) = 1$

2. $p_n(0) = 0$

3. $\left(Qp_n\right)(x) = np_{n-1}(x)$.

(see [4]).

2. Main result

For two given real parameters $0 \leq \alpha \leq \beta$ we construct a linear operator $\widetilde{K}_m^Q : L_1([0,1]) \to C([0,1])$ defined for any function $f \in L_1([0,1])$ by:

$$\left(\widetilde{K}_m^Q f\right)(x) = \frac{m+\beta+1}{p_m(1)} \sum_{k=0}^{m} \binom{m}{k} p_k(x) p_{m-k}(1-x) \int_{\frac{k+\alpha}{m+\beta+1}}^{\frac{k+\alpha+1}{m+\beta+1}} f(t)dt$$

where Q is a delta-operator and $p = (p_n)_{n \geq 0}$ is the basic polynomials sequence.

It is well known that there is an isomorphism between the ring of formal power series in the variable t over the same field and the ring of shift-invarinat operators, which carries

$$f(t) = \sum_{k \geq 0} \frac{a_k}{k!} t^k \text{ into } T = \sum_{k \geq 0} \frac{a_k}{k!} Q^k$$

If $\phi(t)$ is the formal power series that corresponds to Q we know that its inverse, which we denote by $\varphi(t)$ can be written as

$$\varphi(t) = \sum_{k \geq 1} c_k t^k$$

If $c_1 > 0$ and $c_j \geq 0$, $j \geq 2$ then the operator $\widetilde{K}_m^Q$ becomes positive.

Theorem: The operators $\widetilde{K}_m^Q$ have the following properties:

1. $\left(\widetilde{K}_m^Q e_0\right)(x) = 1$

2. $\left(\widetilde{K}_m^Q e_1\right)(x) = x + \frac{2\alpha - 2\beta - 1}{2(m+\beta+1)}$

3.
$$\left(\widetilde{K}_m^Q e_2\right)(x) = \frac{m^2}{(m+\beta+1)^2}\left(x^2 + \left(x - x^2\right)a_m\right) +$$

$$+ \frac{2\alpha + 1}{(m+\beta+1)^2} mx + \frac{3\alpha^2 + 3\alpha + 1}{3(m+\beta+1)^2}$$

where

$$a_m = \frac{1}{m}\left(1 + (m-1)\frac{r_{m-2}(1)}{p_m(1)}\right)$$

the sequence $\left(r_m(x)\right)_{m \geq 0}$ being generated by

$$\varphi''(t)e^{x\varphi(t)} = \sum_{m \geq 0} r_m(x)\frac{t^m}{m!}$$

4. $\lim_{m \to \infty}\left(\widetilde{K}_m^Q f\right) = f$ uniformly on $[0,1]$ if and only if

$$\lim_{m \to \infty} \frac{r_{m-2}(1)}{p_m(1)} = 0.$$

Proof:

1. We know that $(p_n)_{n \geq 0}$ is the basic polynomials sequence for the delta-operator Q, so it is a polynomial sequence of binomial type, therefore:

$$\left(\widetilde{K}_m^Q e_0\right)(x) = \frac{m+\beta+1}{p_m(1)} \sum_{k=0}^m \binom{m}{k} p_k(x) p_{m-k}(1-x) \int_{\frac{k+\alpha}{m+\beta+1}}^{\frac{k+\alpha+1}{m+\beta+1}} dt =$$

$$= \frac{1}{p_m(1)} \sum_{k=0}^m \binom{m}{k} p_k(x) p_{m-k}(1-x) = \frac{1}{p_m(1)} p_m(x+1-x) = 1$$

2.

$$\left(\widetilde{K}_m^Q e_1\right)(x) = \frac{m+\beta+1}{p_m(1)} \sum_{k=0}^m \binom{m}{k} p_k(x) p_{m-k}(1-x) \int_{\frac{k+\alpha}{m+\beta+1}}^{\frac{k+\alpha+1}{m+\beta+1}} t\, dt =$$

$$= \frac{m+\beta+1}{p_m(1)} \sum_{k=0}^m \binom{m}{k} p_k(x) p_{m-k}(1-x) \frac{1}{2} \frac{(k+\alpha+1)^2 - (k+\alpha)^2}{(m+\beta+1)^2} =$$

$$= \frac{1}{2(m+\beta+1)p_m(1)} \sum_{k=0}^m \binom{m}{k} p_k(x) p_{m-k}(1-x)(2k+2\alpha+1) =$$

$$= \frac{1}{(m+\beta+1)p_m(1)} \sum_{k=0}^m \binom{m}{k} p_k(x) p_{m-k}(1-x)k +$$

$$+ \frac{2\alpha+1}{2(m+\beta+1)p_m(1)} \sum_{k=0}^m \binom{m}{k} p_k(x) p_{m-k}(1-x) =$$

$$= \frac{1}{(m+\beta+1)p_m(1)} m p_m(1)x + \frac{2\alpha+1}{2(m+\beta+1)p_m(1)} p_m(1) =$$

$$= \frac{m}{m+\beta+1} x + \frac{2\alpha+1}{2(m+\beta+1)} = x + \frac{2\alpha-2\beta-1}{2(m+\beta+1)}$$

3.

$$\left(\widetilde{K}_m^Q e_2\right)(x) = \frac{m+\beta+1}{p_m(1)} \sum_{k=0}^m \binom{m}{k} p_k(x) p_{m-k}(1-x) \int_{\frac{k+\alpha}{m+\beta+1}}^{\frac{k+\alpha+1}{m+\beta+1}} t^2\, dt =$$

$$= \frac{m+\beta+1}{p_m(1)} \sum_{k=0}^m \binom{m}{k} p_k(x) p_{m-k}(1-x) \frac{1}{3} \frac{(k+\alpha+1)^3 - (k+\alpha)^3}{(m+\beta+1)^3} =$$

$$= \frac{1}{3(m+\beta+1)^2 p_m(1)} \sum_{k=0}^m \binom{m}{k} p_k(x) p_{m-k}(1-x) \cdot$$

$$\cdot \left(3k^2 + 3k(2\alpha+1) + 3\alpha^2 + 3\alpha + 1\right) =$$

$$= \frac{1}{(m+\beta+1)^2 p_m(1)} \sum_{k=0}^m \binom{m}{k} p_k(x) p_{m-k}(1-x)k^2 +$$

$$+ \frac{2\alpha+1}{(m+\beta+1)^2 p_m(1)} \sum_{k=0}^m \binom{m}{k} p_k(x) p_{m-k}(1-x)k +$$

$$+ \frac{3\alpha^2 + 3\alpha + 1}{3(m+\beta+1)^2 p_m(1)} \sum_{k=0}^m \binom{m}{k} p_k(x) p_{m-k}(1-x) =$$

$$= \frac{1}{(m+\beta+1)^2 p_m(1)} p_m(1) m^2 \left(x^2 + (x - x^2)a_m\right) +$$

$$+ \frac{2\alpha+1}{(m+\beta+1)^2 p_m(1)} p_m(1) mx + \frac{3\alpha^2 + 3\alpha + 1}{3(m+\beta+1)^2 p_m(1)} p_m(1) =$$

$$= \frac{m^2}{(m+\beta+1)^2} \left(x^2 + (x - x^2)a_m\right) + \frac{2\alpha+1}{(m+\beta+1)^2} mx +$$

$$+ \frac{3\alpha^2 + 3\alpha + 1}{3(m+\beta+1)^2}$$

4. From 1 and 2 we can easily conclude that

$$\lim_{m \to \infty} \left(\widetilde{K}_m^Q e_0\right)(x) = 1$$

$$\lim_{m \to \infty} \left(\widetilde{K}_m^Q e_1\right)(x) = x$$

uniformly on [0,1].

If $\lim\limits_{m \to \infty} \dfrac{r_{m-2}(1)}{p_m(1)} = 0$ then

$$\lim_{m \to \infty} a_m = \lim_{m \to \infty} \left(\frac{1}{m} + \frac{m-1}{m} \frac{r_{m-2}(1)}{p_m(1)}\right) = 0$$

and using the $\left(\widetilde{K}_m^Q e_2\right)(x)$ expression we have:

$$\lim_{m \to \infty} \left(\widetilde{K}_m^Q e_2\right)(x) = x^2$$

Applying the Bohman-Korovkin theorem ([2]-[3]) we reach the desired result.

References:

[1] O. Agratini, *Approximation by linear operators* (Romanian), Presa Universitara Clujeana, Cluj-Napoca, 2000

[2] H. Bohman, *On approximation of continuous and analytic functions*, Ark. Mat., **2** (1952), 43–56.

[3] P.P. Korovkin, *On convergence of linear operators in the space of continuous functions* (Russian), Dokl. Akad. Nauk. SSSR (N.S.), **90** (1953), 961–964.

[4] S. M. Roman, G. C. Rota, *The Umbral Calculus*, Advances in Mathematics 27, 2, 1978, 95-188

[5] D.D. Stancu, Gh. Coman, O. Agratini, R. Trimbitas, *Numerical Analysis and Approximation Theory*, Vol.I (Romanian), Presa Universitara Clujeana, Cluj-Napoca, 2001.

D.G. Ghiţă[1]
H. Mach[2]
B. Fogelberg[2]
G. Căta-Danil[1]

SUBNANOSECOND LIFETIME MEASUREMENTS IN ^{124}Sn

[1]National Institute of Physics and Nuclear Engineering, P.O.~Box MG-6, R-077125 Bucharest - Magurele, Romania

[2]Department of Radiation Sciences, Uppsala University, S-61182 Nyköping, Sweden

Abstract: *We have applied the Advanced Time-Delayed βγγ method to investigate the subnanosecond level lifetimes in ^{124}Sn populated in the β decay of ^{124}In. From the γγ coincidence measurements a number of new levels have been identified and several γ transitions have been placed in the level scheme for the first time. The half-lives of the 8^+ 2578.4 keV level has been measured as $T_{1/2}$ = 1079(54) ps, while the following lifetime limits were determined for the 6^- 2568.1, 3011.1, and the 0^+ 2192.2 keV levels as $T_{1/2}$ < 20 ps, <50 ps and <20 ps, respectively.*

1. Introduction

The long chain of the tin isotopes for a long time has attracted a strong experimental and theoretical interest. This chain of the medium-heavy nuclei has a unique property that at it both ends are two doubly magic and very exotic nuclei of 100Sn and 132Sn representing the very light proton-rich and the very neutron rich cases, respectively. Moreover the N=Z 100Sn nucleus is at the proton drip-line. Thus Z=50 tin nuclei represent a perfect testing ground for the shell model. The present study is focussed on 124Sn, which has 24 neutron particles outside of the doubly magic 100Sn or 8 neutron-holes below 132Sn. It is the heaviest stable tin isotope. Despite many experimental studies the information on the low-lying states in 124Sn is incomplete. The nuclear states in 124Sn, predominantly at low-spin, have been studied by a variety of probes. The results are summarized in [1]. The high spin states have been observed in the decay of 124In [2] and from the 45 s isomer produced in the heavy ion induced reaction [3]. Recently the low-lying states have been studied via the (n,n') reaction and members of the two- and three-phonon quadrupole excitations have been identified [4]. The low-lying states in 124Sn have been interpreted within the shell model [5], [6], [7] and IBM model [8], while the intruder 0+ states have been discussed in [9]. Strong B(E1) transition rates were observed in 124Sn for the E1 transitions de-exciting the collective 3^-_1 state and the 1^- member of the two-phonon $2^-_1 \otimes 3^-_1$ multiplet [10], [11], [12]; for systematics and model interpretation see [13], [14] and [15], [16], respectively.

A broad range of low-lying excited states in 124Sn is populated in the decay of two isomers of 124In of spin J = 3+ and (8-) [2], respectively. The populated levels include the 0^+_2 state at 2192.1 keV [4] and the 8+ and 6-states at 2578.4 and 2568.1 keV, respectively. The aim of the present study is to measure the subnanosecond lifetimes of low-lying states in 124Sn populated in the decay of In.

1. Experimental details

The experiment was performed at the OSIRIS fission-product mass separator located at Studsvik in Sweden [17]. The radioactive products of Cd and In were produced by the thermal-neutron induced fission of the 235U target. The mass-separated beam of A=124 was

continuously deposited onto aluminized Mylar tape in an experimental station where detectors were positioned in a close geometry.

The activities included 124Cd and both isomers of 124In. The fast timing (t) detection system [18], [19], [20], consisted of a thin 3 mm NE111A plastic scintillator for detection and and 47 mm long BaF2 crystal as detector. The lifetime information was derived from the time-delayed (t) coincidences in the fast-response scintillator detectors, while a coincidence with a high purity germanium detector allows for a judicious selection of the decay path and a strong simplification of the energy spectrum in the BaF2 detector characterized by poor energy resolution of ~9.2% at 661 keV. A second Ge detector was incorporated in the set-up which provided increased detection efficiency and allowed to collect Ge-Ge coincidences.

Triple coincident (t) events have been collected using the -Ge-BaF2 and -Ge-Ge detectors and analysed off-line. Time-response calibrations of the BaF2 detector was made using the A=140 sources.

Fig 1

Fig. 2
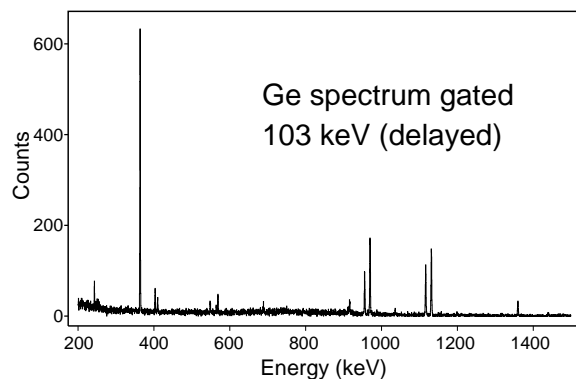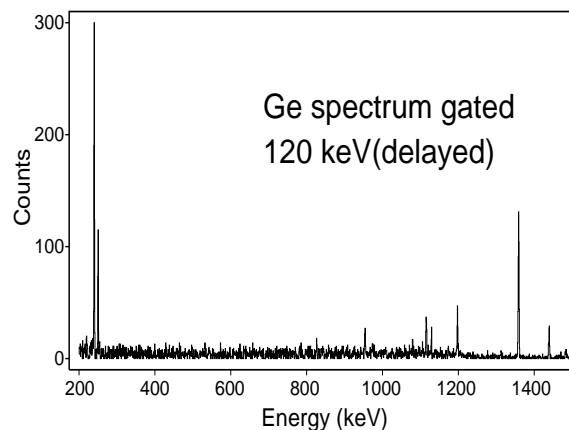

About 2.4x106 (t) coincidences involving two Ge detectors have been collected. The energy range was set from about 20 to 3000 keV for each of the detectors. The coincidence multiplet involved five collected parameters: the energies of the and each of the Ge detectors and two time differences. The time difference was measured in a Time-to-Amplitude-Converter unit (TAC) started by a event and stopped by a signal from an individual Ge detector delayed by about 1 s. The range for the TAC unit was set at 2 s. The time-difference spectrum has shown a semi-prompt peak in the center, a flat randoms background to the left of the peak and a delay slope to the right due to the transitions de-exciting the known isomeric states at 2204.6 keV, T1/2=0.27 s, and at 2325.1, T1/2=3.1 s.

About 78 gates have been set on all -ray peaks observed in the spectra and sorted onto the other Ge with a broad gate set on the energy spectrum. In the first sorting in both TAC's, we accepted only those events, which were in the semi-prompt coincidence peak with the flat random background subtracted.

In addition, two energy gates set on the 102.9 and 120.4 keV peaks were sorted out by selecting the delayed section of TAC spectrum with randoms subtracted, while for the coincident events in the other Ge detector the TAC gate was set on the semi-prompt peak as in the first sorting.

This sorting allowed to select only those coincidence -rays, which fed the isomeric states directly from above. These spectra are shown in Figures 1 and 2.

The purpose of the Ge-Ge coincidences was to verify the previously reported decay schemes for the decay of the In isomers and to provide detailed information on the content of the BaF2 energy spectra in the (t) coincidences involving the -Ge-BaF2

detectors. In the latter case identical gates were selected in the Ge detector but projected onto the BaF2 detector.

Our coincidences generally confirmed the previously reported decay schemes [2] with a few modifications. We also observe the 403.0-916.4 keV cascade, but we find it feeding the 2204.6 keV level as seen by the presence of a strong line at 916.4 keV in Figure 1, but not in Figure 2. Our energy determination for the second transition is slightly different than previously reported (915.4 keV). This cascade de-excites a know level at 3524.0 keV and proceeds via a new state at 3121.0 keV. At the same time one must eliminate two levels at 3240.4 and 3643.4 keV as no evidence for their existence come from the   decay of In. The 916.4 keV transition is also in coincidence with a 564.4 keV line, which then de-excites a known state at 3684.9 keV and provides a further support for the new location of the 916.4 keV transition in the decay scheme.

Another change involves the previously reported 569.1 and 1037.3 keV transitions. We observe a cascade of 1036.4-568.9 keV transitions feeding the 2204.6 keV state. Both transitions are seen in the 103 keV gate, see Fig.~1, but not in the 120 keV gate in Fig.~2. The cascade de-excites the known level at 3809.7 keV and defines a new state at 2773.5 keV. The sequence of   -rays in the cascade is defined by the intensities of these lines observed in the spectrum gated by the 103 keV transition and shown in Fig.~1. This placement is further confirmed by the coincidence of the 568.9 keV transition with the 911.6 keV line, which then feeds the 2773.5 keV state from the known level at 3684.9 keV. The 784.0 keV line has not been observed in our experiment, and in particular is not observed in the coincidence gates involving the 568.9, 253.4, 120.4 nor 102.9 keV transitions, where it should have been observed if present in the decay scheme with suggested intensity. Therefore we find no evidence for the existence of energy levels at 3362.3 and 3931.5 keV populated in the   decay of In. In the coincidence spectrum gated by the 102.9 keV transition we observe the 410.0 and 548.9 keV transition, see Fig. 1, which most likely represent the 409.6 and 549.0 keV   -rays reported before [2] but unplaced in the decay scheme. We find them de-exciting the known 4- states at 2614.5 and 2753.0 keV, respectively. Other changes are related to the decay of the 3+ isomer of In. We find no evidence for the placement of the weak 1234.8 keV transition, although it should have

been observed in coincidence with the 1131.7 keV line if it directly feeds the 1131.7 keV level. Most likely it is located much higher in the decay scheme.

2. Fast timing   (t) measurements

We have applied the Advanced Time-Delayed   (t) method to determine the lifetimes in 124Sn in the subnanosecond range. Measurements in the low-picosecond range were performed by the centroid shift technique, while longer lifetimes were measured by fitting the slope on the time-delayed side of the time distribution. The centroid shift technique [18] allows to measure short lifetimes, down to a few ps. Here, the mean life   =T1/2/ln 2 of a level directly   fed is given by the difference between the centroid of the delayed time spectrum and the prompt centroid of the same E   . When the level of interest is fed by a   -ray from a higher-lying level the mean life of interest is given by the difference between the centroid shift of the spectrum gated by the de-exciting   -ray and the centroid shift of the spectrum gated by the feeding   transition (the latter represents a "reference point". If the energies of these transitions are different one uses the prompt curve to correct for energy dependence of the time response of the BaF2 detector. Essential to the method is that the prompt/reference and delayed time spectra are measured concurrently in order to maintain identical conditions in the face of small but persistent drifts of the electronics. This is assured if the spectra belong to the same decay under study.

Lifetimes long enough to be observed as slopes on the time-delayed side of the time spectra (in the present case it is about T1/2 $\geq$ 60 ps at E   ~ 100 keV) are measured by the slope deconvolution technique [18]. Important to the shape fitting at low transition energies is the determination of unwanted asymmetries of prompt time spectra occasionally caused by electronics at low energies.

Centroid Shift Analysis

The prompt positions for the full energy peaks at 363 and 525 keV were obtained in two steps. First we define as the prompt positions internal to the decay of 231Fr to 231Ra, the Compton events from   transitions in 231Ra with energies in the range from 1.0 to 2.4 MeV. These lines de-excite states, which have predominantly low-spin and decay mainly by

moderately fast M1 transitions. Even if the M1's are slow, the lifetimes of the de-exciting states will be well below 1 ps and would give a negligible uncertainty to the final results. Due to the large density of states at ~ 2 MeV, no single -ray dominates the spectrum. A functional dependence between the prompt centroids of the time spectra gated on the high-energy Comptons, and the prompt positions for the full energy peaks at 363 and 525 keV is carried by the time calibration curves and includes one small correction. Namely, since the average energy of transitions contributing to the Comptons, weighted by the intensity contribution, was 1.47 MeV, a Compton to Compton correction of CC = 1.03(26) ps (estimated from the "Compton correction curv") has been applied to the calibration curves. This accounts for the difference between this energy and the energy of 1.60 MeV for the calibration transition in the A = 140 source.

Shape fitting analysis

By inverting the gates used in the centroid shift analysis, and selecting the 363.4 or 525.2~keV lines in Ge and the 95.5~keV peak in the BaF2 (while keeping the same gate on the spectrum), one gets a time-delayed -BaF2 spectrum with a long slope due to the lifetime of the level de-excited by the 95.5 keV transition. From the shape fitting of the spectrum, one obtains T1/2 = 4.35(44) ns in agreement with the more precise value obtained from the analysis of -BaF2(t) coincidences discussed below.

Bibliography

1. H. Iimura, J. Katakura and K. Kitao, Nuclear Data Sheets 80, 895(1997).
2. B. Fogelberg, T. Nagarajan and B. Grapengiesser, Nucl. Phys A230, 214 (1974).
3. R. Broda et al., Phys. Rev. Lett. 68, 1671 (1992).
4. D. Bandyopadhyay et al., Nucl. Phys. A747, 206 (2005).
5. A. Insolia and N. Sandulescu, Nucl. Phys. A550, 34 (1992).
6. F. Andreozzi, L. Corragio, A. Covello, A. Gargano, A. Porrino, Z. Phys. A 354, 253 (1996).
7. A. Holt, T. Engeland, M. Hjort-Jensen, E. Osnes. Nucl. Phys. A 634, 41 (1998).
8. M. Hasegawa, Nucl. Phys. A440, 1 (1985).
9. K. Heyde, J. Jolie, J. Moreau, J. Ryckebusch and M. Waroquier, Nucl. Phys, A466, 189 (1987).
10. K. Govaert, F. Bauwens, J. Bryssnick, D. De Frenne, E. Jacobs, and W. Mondelaers, Phys. Rev. C, Vol. 57, No. 5 (1998).
11. J. Bryssinck et al., Phys. Rev. C, Vol. 59, No. 4 (1999).
12. J. Bryssinck et al., Phys. Rev. C, Vol. 61, 024309-1 (2000).
13. W. Andrejtscheff, C. Kohstall, P. von Brentano, C. Fransen, U. Kneissl, N. Pietralla, H.H. Pitz, Phys. Lett. B 506, 239 (2001)
14. N. Pietralla, Phys. Rev. C, Vol. 59, No. 5 (1999).
15. R.V. Jolos and W. Scheid, Phys. Rev. C {\bf 66}, 044303 (2002).
16. R.V. Jolos, N. Yu. Shirikova and V. V. Voronov, Phys. Rev. C{\bf 70}, 054303 (2004).
17. B. Fogelberg, M. Hellström, L. Jacobsson, D. Jerrestam, L. Spanier, and G. Rudstam, Nucl. Instr. Meth. Phys. Res. B 70, 137 (1992).
18. H. Mach, R.L. Gill, and M. Moszynski, Nucl. Inst. Meth. Phys. Res. A 280, 49 (1989).
19. M. Moszynski and H. Mach, Nucl. Inst. Meth. Phys. Res. A 277, 407 (1989).
20. H. Mach, F.K. Wohn, G. Molnar, K. Sistemich, John C. Hill, M. Moszynski, R.L. Gill, W. Krips, and D.S. Brenner, Nucl. Phys. A523,197(1991).